UNIVERSITI SAINS MALAYSIA

Laporan Akhir Projek Penyelidikan Jangka Pendek

First Principles Density Functional Theory Calculations On Zinc Oxide Growth Mechanism

by
Assoc. Prof. Dr. Ahmad Azmin Mohamad
Mr. Oskar Hasdinor Hassan
Mr. Mohd Asri Teridi
Mr. Zainal Arifin Ahmad
Miss Kausar Harun

2015

F0790 2/2013

BORANG FRGS – P3(R)

KEMENTERIAN PENDIDIKAN MALAYSIA

FINAL REPORT
FUNDAMENTAL RESEARCH GRANT SCHEME (FRGS)

Laporan Akhir Skim Geran Penyelidikan Fundamental (FRGS)
Pindaan 1/2015

A **RESEARCH TITLE: First Principles Density Functional Theory Calculations on Zinc Oxide Growth Mechanism**

PHASE & YEAR: 2/2013

START DATE: 01/12/2013
END DATE: 30/11/2015
EXTENSION PERIOD (DATE): RMC LEVEL: N/A
KPM LEVEL: N/A

PROJECT LEADER: PROF MADYA DR. AHMAD AZMIN MOHAMAD
I/C / PASSPORT NUMBER: 750621035445

PROJECT MEMBERS: (including GRA)
1. **Oskar Hasdinor Bin Hassan**
2. **Mohd Asri Mat Teridi**
3. **Zainal Arifin bin Ahmad**
4. **Kausar binti Harun**

PROJECT ACHIEVEMENT *(Prestasi Projek)*

B

ACHIEVEMENT PERCENTAGE			
Project progress according to milestones achieved up to this period	**0 - 50%**	**51 - 75%**	**76 - 100%**
Percentage (please state #%)			100%
RESEARCH OUTPUT			
Number of articles/ manuscripts/ books *(Please attach the First Page of Publication)*	**Indexed Journal**		***Non-Indexed Journal***
	4 (2 accepted, 2 draft manuscript)		
Conference Proceeding *(Please attach the First Page of Publication)*	**International**		***National***
	1		
Intellectual Property *(Please specify)*	N/A		

HUMAN CAPITAL DEVELOPMENT

Human Capital	Number				Others (please specify)
	On-going		Graduated		
Citizen	Malaysian	Non Malaysian	Malaysian	Non Malaysian	
No. PHD STUDENT					
Student Fullname: IC / Passport No: Student ID:					
No. MASTER STUDENT					
Student Fullname: IC / Passport No: Student ID:	KAUSAR BINTI HARUN 890810075272 52317				
No. UNDERGRADUATE STUDENT					
Student Fullname: IC / Passport No: Student ID:			NUR SAKINAH MANSOR 910926075616 -		
Total	1		1		

EXPENDITURE *(Perbelanjaan) as Borang K1(RMC)*

C

Budget Approved *(Peruntukan diluluskan)* : **RM148,000.00**
Amount Spent *(Jumlah Perbelanjaan)* : **RM147,917.22**

Balance *(Baki)* : **RM82.78**
Percentage of Amount Spent : 99.94 %
(Peratusan Belanja)

ADDITIONAL RESEARCH ACTIVITIES THAT CONTRIBUTE TOWARDS DEVELOPING SOFT AND HARD SKILLS
(Aktiviti Penyelidikan Sampingan yang menyumbang kepada pembangunan kemahiran insaniah)

D

International		
Activity	Date (Month, Year)	Organizer
(e.g : Course/ Seminar/ Symposium/ Conference/ Workshop/ Site Visit)	5th International Conference on Recent Advances in Materials, Minerals and Environment (August, 2015)	School of Materials and Mineral Resources Engineering, Universiti Sains Malaysia, Engineering Campus, Penang

National		
Activity	Date (Month, Year)	Organizer
(e.g : Course/ Seminar/ Symposium/ Conference/ Workshop/ Site Visit)	1- Material Studio **Visualizer** training course (August, 2014) 2- Material Studio **CASTEP** training course (October, 2014)	Amista Technologies Sdn Bhd & UiTM Shah Alam

E **PROBLEMS / CONSTRAINTS IF ANY** *(Masalah/ Kekangan sekiranya ada)*

1)Challenge to obtain well aligned and uniform hexagonal shape under microscopic examination.
2)Small deviation well-fitted Rietveld-refinement data must be obtained in order to get structural parameter close to standard.
3)Challenge to obtain an exact value of energy band gap. However, the energy band gap obtained in this work are within 0.02 tolerance.

F **RECOMMENDATION** (*Cadangan Penambahbaikan*)

1) The simulation work could be further investigated, involving material with havier system such as doped-ZnO. From that, the fundamental explanation and exploration can be studied to a greater extend.
2) More exhibition/conferences need to be participitated to further enhanced and collaborate with other national and international researchers.

G. **RESEARCH ABSTRACT – Not More Than 200 Words** (*Abstrak Penyelidikan – Tidak Melebihi 200 patah perkataan*)

The ZnO nanoparticles was synthesized by sol-gel method with varied aging time. The structural analysis proved the formation of pure ZnO phase for all parameters and the crystallinity improved after heat-treatment process. Sample with 36 hour aging gave the highest crystallinity and nearly hexagonal shape nanoparticles. Structural Rietveld analysis shows that the synthesized ZnO belonged to space group P63mc and the refined structural data fit well with a goodness of fit value approaching 1. Further investigation on optical responses revealed a strong absorption in UV region with energy gap 3.10 eV. This findings was supported by great photoluminescence characteristic at about 380 nm. Surface chemical analysis was used to explain the origin of electronic transition which were dominated by valence electron from Zn-3d and O-2p state. To provide a bridge to experimental results, the ZnO unit cell was built based on the lattice parameters and atomic coordination using first principles approach. The calculated electronic properties of synthesized ZnO using LDA+U gave Eg = 3.08 eV while GGA+U gave Eg = 3.10 eV, which are comparable with experimental value. The optical properties also show similar characteristic to the one determined by laboratory testing and the validity was confirmed with reported literature.

Date : **21 Jan 2016**
Tarikh

Project Leader's Signature:
Tandatangan Ketua Projek

AHMAD AZMIN MOHAMAD
B.Sc Hons (Malaya), PhD (Malaya), CEng (MIMechE)
Associate Professor
School of Materials & Mineral Resources Engineering
Universiti Sains Malaysia,
14300 Nibong Tebal, Penang, Malaysia.
Email : aam@usm.my

H **COMMENTS, IF ANY/ ENDORSEMENT BY RESEARCH MANAGEMENT CENTER (RMC)**
(Komen, sekiranya ada/ Pengesahan oleh Pusat Pengurusan Penyelidikan)

.....

.....

.....

Name:
Nama:

PROF. DR LEE KEAT TEONG
Director
Research Creativity & Management Office
Universiti Sains Malaysia

Signature:
Tandatangan:

Date:
Tarikh:

6/2/16

UNIVERSITI SAINS MALAYSIA

JABATAN BENDAHARI
PENYATA PERBELANJAAN SEHINGGA 18 JANUARI 2016

Projek :

No. Akaun : 203.PBAHAN.6071262.

Vot	Nama Vot	Peruntukan Projek	Perbelanjaan Terkumpul Sehingga Thn Lalu	Baki Peruntukan Tahun Lalu	Peruntukan Thn Semasa	Jumlah Peruntukan Thn Semasa	Tanggungan Semasa	Bayaran Thn Semasa	Jum Belanja Thn Semasa	Baki Projek
111	GAJI	35,150.00	0.00	35,150.00	0.00	35,150.00	0.00	0.00	0.00	35,150.00
221	PERJALANAN DAN SARA HIDUP	23,474.32	0.00	23,474.32	0.00	23,474.32	0.00	0.00	0.00	23,474.32
223	PERHUBUNGAN DAN UTILITI	-87.50	0.00	-87.50	0.00	-87.50	0.00	0.00	0.00	-87.50
224	SEWAAN	1,944.00	0.00	1,944.00	0.00	1,944.00	0.00	0.00	0.00	1,944.00
227	BEKALAN DAN BAHAN LAIN	-49,108.40	0.00	-49,108.40	0.00	-49,108.40	8,654.59	0.00	8,654.59	-57,762.99
228	PENYELENGGARAN & PEMBAIKAN KECIL	5,000.00	0.00	5,000.00	0.00	5,000.00	0.00	0.00	0.00	5,000.00
229	PERKHIDMATAN IKTISAS & HOSPITALITI	-3,436.05	0.00	-3,436.05	0.00	-3,436.05	0.00	0.00	0.00	-3,436.05
335	HARTA MODAL	-4,199.00	0.00	-4,199.00	0.00	-4,199.00	0.00	0.00	0.00	-4,199.00
	Jumlah	**8,737.37**	**0.00**	**8,737.37**	**0.00**	**8,737.37**	**8,654.59**	**0.00**	**8,654.59**	**82.78**

Penyata ini adalah cetakan komputer tiada tandatangan diperlukan

Penyata ini adalah dianggap tepat jika tiada maklumbalas dalam tempoh masa 14 hari dari tarikh penyata

UNIVERSITI SAINS MALAYSIA

BORANG PENYERAHAN ASET / INVENTORI

A. BUTIR PENYELIDIK

1. NAMA PENYELIDIK :...PROF. MADYA DR. AHMAD AZMIN MOHAMAD
2. NO STAF :...AE50276.....
3. PTJ :...PP KEJURUTERAAN BAHAN & SUMBER MINERAL
4. KOD PROJEK :...203.PBAHAN.6071262.....
5. TARIKH TAMAT PENYELIDIKAN :...30 NOVEMBER 2015.....

B. MAKLUMAT ASET / INVENTORI

BIL	KETERANGAN ASET	NO HARTA	NO. SIRI	HARGA (RM)
1	ACCELRYS MATERIAL STUDIO SOFTWARE	AK00007442	CD INSTALLER	28000
2	HP ENVY DESKTOP 700-275D PC	AK00007479	4CE4110B1Q	4198
3	HP PAVILION 20fi MONITOR	AK00007480	3CM4040K3CR	1

C. PERAKUAN PENYERAHAN

Saya dengan ini menyerahkan aset/ inventori seperti butiran B di atas kepada pihak Universiti:

.....

(AHMAD AZMIN MOHAMAD) Tarikh: 21 Jan 2016

BSc Hons (Malaya), PhD (Malaya), CEng (MIMechE)
Associate Professor
School of Materials & Mineral Resources Engineering.
Universiti Sains Malaysia,
14300 Nibong Tebal, Penang, Malaysia.
Email : azmin@usm.my

D. PERAKUAN PENERIMAAN

Saya telah memeriksa dan menyemak setiap alatan dan didapati :

- ☐ Lengkap
- ☐ Rosak
- ☐ Hilang : Nyatakan.....
- ☒ Lain-lain : Nyatakan TAMAT PENYELIDIKAN

Diperakukan Oleh :

.....
Mohd Saiful Azman.....
Penolong Jurutera
Pusat Pengajian Kejuruteraan Bahan & Sumber Mineral
USM Kampus Kejuruteraan
Pegawai Aset PTJ

Tarikh: 21/1/2016

*Nota :

Satu salinan borang yang telah dilengkapkan perlulah dikemukakan kepada Unit Pengurusan Harta, Jabatan Bendari dan RCMO untuk rekod

Journal of King Saud University – Engineering Sciences (2015) xxx, xxx–xxx

King Saud University

Journal of King Saud University – Engineering Sciences

www.ksu.edu.sa
www.sciencedirect.com

ORIGINAL ARTICLE

First-principles calculation on electronic properties of zinc oxide by zinc–air system

Ahmad Azmin Mohamad [a,*], Muhammad Syafiq Hassan [a], Muhamad Kamil Yaakob [b], Mohamad Fariz Mohamad Taib [b], Fadhlul Wafi Badrudin [c], Oskar Hasdinor Hassan [b], Muhd Zu Azhan Yahya [c]

[a] *School of Materials and Mineral Resources Engineering, Universiti Sains Malaysia, 14300 Nibong Tebal, Pulau Pinang, Malaysia*
[b] *Ionics Materials & Devices (iMADE) Research Laboratory, Faculty of Applied Sciences, Universiti Teknologi MARA, 40450 Shah Alam, Malaysia*
[c] *Faculty of Defence Science & Technology, Universiti Pertahanan Nasional Malaysia, 57000 Kuala Lumpur, Malaysia*

Received 21 October 2014; accepted 27 August 2015

KEYWORDS

Zinc oxide;
Rietveld refinement;
First-principles calculation;
Density functional theory

Abstract First-principles calculations are performed to study the electronic properties of zinc oxide (ZnO) formed on an anode after discharging a Zn–air system. Prior to calculation, the ZnO is characterised by X-ray diffraction using Rietveld refinement. Diffracted patterns proved the formation of single phase ZnO, while Rietveld analysis shows that the ZnO has a hexagonal wurtzite structure with lattice parameters, a = 3.244 and c = 5.199 Å. Geometry optimisation of the hexagonal wurtzite structure of the ZnO is performed using various exchange–correlation energy functionals. The local density approximation functional method is used to explain the structure, electronic band structure and density of state properties of hexagonal ZnO. The calculated energy band gap was 0.75 eV while the density of states reveals that the O 2p (the top valence band) and Zn 4s (the bottom conduction band) states domination.

1. Introduction

Zinc oxide (ZnO) is an interesting material due to its low cost, chemical inert-ness, photo-stability, and excellent charge transport, and has received considerable attention as a potential solar cell material (Alias and Mohamad, 2014b, 2013). Synthesis of ZnO has been done by various techniques, such as, sputtering (Gabas et al., 2011), sol–gel (de la L Olvera et al., 2002; Alias et al., 2010), vapour–liquid–solid growth (Huang et al., 2001), physical vapour deposition (Kato et al., 2002) and zinc–air (Zn–air) system (Yap et al., 2009). X-ray diffraction (XRD) is still the main tool to characterise the formation of ZnO. Other characterisation methods, such as scanning/transmission electron microscopy and photoluminescence spectroscopy, have also been used to support observations; however, these supporting methods are costly and time

* Corresponding author. Tel.: +60 4 599 6118; fax: +60 4 594 1011.
E-mail address: aam@usm.my (A.A. Mohamad).
Peer review under responsibility of King Saud University.

ELSEVIER Production and hosting by Elsevier

http://dx.doi.org/10.1016/j.jksues.2015.08.002

consuming. Hence, no theoretical investigation of the ZnO obtained from Zn–air system has been reported. Simulation of ZnO properties can be utilised to predict the properties of the material, and an interesting method of simulation is first-principles calculation, which is based on density functional theory (DFT).

Scattered reports of first-principles calculations on pure ZnO and dopants are available (Wang et al., 2013; Xie et al., 2012; Yao et al., 2012; Guan et al., 2011; Li et al., 2009; Osuch et al., 2006; Ren et al., 2004). However, very little effort has been exerted to use experimental data of ZnO produced by the electrochemical system as crystal inputs for these calculations. The inputs from XRD can be used to predict material properties by first-principles calculations. XRD data of the crystal structure, such as its lattice parameters, volume and atomic positions, are the main inputs for simulation. If the values of the crystal structure are satisfied, the simulation proper will be a success.

The aim of the present work is to characterise the ZnO produced from the end product of a Zn–air system using the first-principles calculation. The data obtained from the first-principles calculation are compared with those of standard ZnO to validate the formation of ZnO from the Zn–air system. This study begins with XRD and Rietveld refinement of ZnO to obtain the relevant crystal structure properties. Prior to examining the electronic properties of the ZnO, structural (lattice) optimisation is initially performed using various exchange–correlation energy functions, namely, local density approximation (LDA), generalised-gradient approximation functional with Perdew–Burke–Ernzerhof (GGA-PBE), and GGA-PBE function for solids (GGA-PBESol). Structural optimisation is implemented to determine the best functional approximation to perform in examining the electronic properties of ZnO.

2. Experimental

2.1. Zinc–air system assembly

Cell components consisted of a Zn foil, air–cathode and electrolyte. The Zn foil (1×1 cm^2, 99.98% purity, Alfa Aesar) was used as an anode, while fibre-carbon-MnO_x (MEET Co. LTD, Korea) was used as an air–cathode. A mixture of 1.5 M potassium hydroxide pellets (KOH) and 0.04 M ZnO powder was used as an electrolyte. The cell was discharged using Neware BTS with a constant current of 10 mA at room temperature (27 °C).

2.2. Material characterisation

After discharging, the Zn anode was characterised by XRD (Bruker AXS D9) over 2θ ranging from 10° to 90°. The data were then analysed by Rietveld refinement using X'pert High Score Plus software. The morphology of the Zn anode was observed by a field emission scanning electron microscope (FESEM, Zeiss Supra 35VP) to support the findings during the anode characterisation.

2.3. First-principles calculation

First-principles calculation based on DFT with the plane-wave pseudo-potential method was performed as implemented in the Cambridge Serial Total Energy Package (CASTEP) program code (Segall et al., 2002). Exchange-correlation functional of LDA, GGA-PBE and GGA-PBESol were used to compare the ZnO lattice properties.

To obtain a stable structure, geometry optimisation was performed to refine the geometry of the 3D periodic system. All of the first-principles calculation areas were determined according to the softer ultrasoft pseudopotential method (Vanderbilt, 1997) in which only valence electrons are considered. A ($5 \times 5 \times 4$) k-point grid generated using the Monkhorst–Pack method for Brillouin zone sampling with an energy cut-off of 340 eV was obtained. For energy minimisation calculation, convergence thresholds were set to 1×10^{-6} eV per unit atom for maximum energy change. The electrons of Zn ($3d$, $4s$) and O ($2s$, $2p$) were treated as valence states.

3. Results and discussion

3.1. Synthesis of ZnO

The Zn–air cell produced the open circuit potential of 1.28 V and flat discharge plateau at 1.10 V (Fig. 1). After 6.4 h, the cell stopped. Upon complete discharge, the Zn anode foil was cleaned by immediately rinsing in deionized water and then dried. The surface of Zn anode that exposed to the electrolyte was characterised by FESEM. Long needle-like ZnO structures covered the surface of the Zn anode (Fig. 2). These structures were scattered in different directions and formed rosette-like agglomerations. The formation of these structures on the surface of the anode separated the active Zn from the electrolyte and inhibited the discharge.

3.2. Structural and Rietveld analysis

The comparison of the Zn foil obtained before and after discharge was made by reference to the XRD patterns. The diffraction pattern was perfectly matched with the respective Zn (ICSD: 98-009-1553) and ZnO (ICSD: 98-002-7791) patterns. Pure Zn showed high crystallinity and intensity at

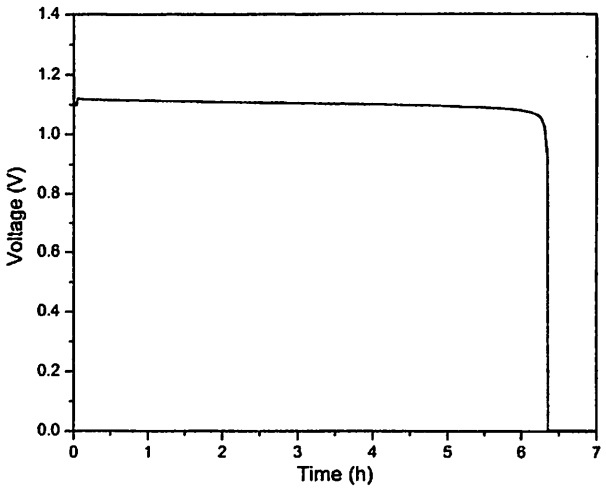

Figure 1 Discharge profile of Zn–air system at a constant current of 10 mA.

Please cite this article in press as: Mohamad, A.A. et al., First-principles calculation on electronic properties of zinc oxide by zinc-air system. Journal of King Saud University – Engineering Sciences (2015), http://dx.doi.org/10.1016/j.jksues.2015.08.002

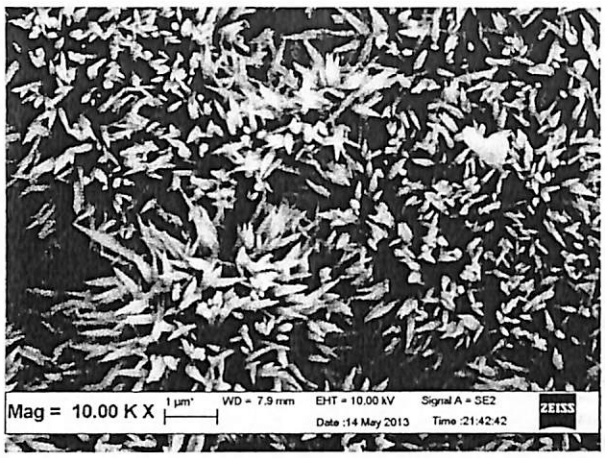

Figure 2 FESEM of ZnO as the end product of a Zn–air system after discharge at a constant current of 10 mA.

the orientation (0 1 1) and $2\theta = 42.5°$ (Fig. 3a). After being discharged (Fig. 3b), the phase present was clearly ZnO. Based on this initial identification (i.e., pattern matching identification), ZnO was proven to be the end product of the discharged Zn–air cell. As well as the presence of ZnO, a small peak of Zn ($2\theta = 42.5°$) was also evident; this Zn peak resulted from the Zn foil beneath the ZnO. A similar observation was previously observed in a study on a Zn foil and the electrochemical formation of ZnO (Pai and Lin, 2011). To confirm the presence of the ZnO and Zn phases in the anode after being discharged, quantitative XRD analysis was carried out using the Rietveld analysis method. The patterns obtained showed that the anode was made of 97.9% ZnO and 2.1% Zn.

To determine the lattice constants and coordinates of the atomic positions of the Zn and O for the first-principles calculation, the identified phases were matched between the diffracted and reference patterns, and the calculated pattern was proposed. Numerous residual (R) values, such as the weighted R profile (R_{wp}) and expected R (R_{exp}) values, can be generated from the refinement process (Table 1); however, the main value always refers to R_{wp}. The reliability of the calculated pattern during refinement was verified by the R and goodness of fit (GOF = R_{wp}/R_{exp}) values.

For acceptable refinement, $R_{wp} < 10$ and GOF < 2 (Guinebretière, 2007; Alias and Mohamad, 2014a). However, the values obtained were slightly higher than expected ($R_{wp} = 11.45$; GOF = 2.34). It is believed that the small peak of Zn at $2\theta = 42.5°$ (with composition of 2.1%) contributed to these slightly higher values. The R_{wp} and GOF values obtained in this work are still valid as ZnO is naturally formed by electrochemical reaction, compared with the calcined ZnO that produces higher crystallinity (Pola-Albores et al., 2011).

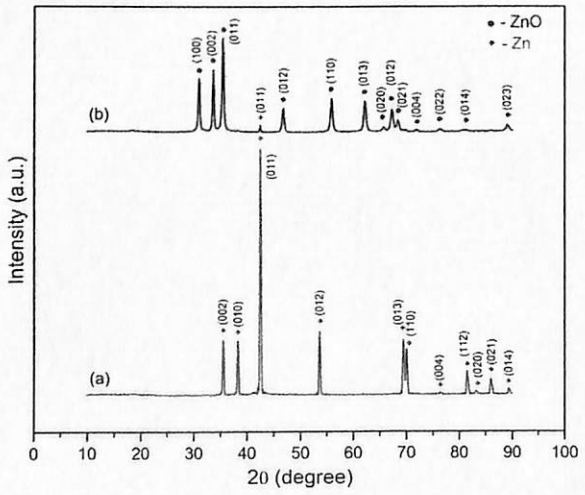

Figure 3 XRD patterns of Zn anode (a) before and (b) after discharge at a constant current of 10 mA.

3.3. First-principles calculation of ZnO materials: structure and optimisation

Based on the ZnO unit cell, a 2 × 2 × 2 supercell containing 32 atoms was adopted for the ZnO and examined using DFT implemented in CASTEP computer code. The unit cell lattice parameters were set as 3.244 Å (a) and 5.199 Å (c) obtained from Rietveld analysis. The supercell has been used to study the effect of doping concentration on the electronic structure of ZnO (Li et al., 2009). However, in the present work, this cell was used to show the unit cell comprising O–Zn–O bonds (Fig. 4a) and to provide a crystal structural-perspective polyhedral view (Fig. 4b). The primitive unit cell was used for structural optimisation. The ICSD 98-002-7791 revealed that the ZnO had a hexagonal wurtzite structure with space group symmetry of P63 mc (Table 1). Each ZnO primitive cell contained two O atoms and two Zn atoms, whereby each Zn atom was located at the centre of a tetrahedron made up of four O atoms; that is, the ZnO formed a $Zn–O_4$ tetrahedron in which the arrangement of the O atom was similar to that of the Zn.

Table 1 The lattice parameters and crystal data of ZnO ICSD and after Rietveld analysis obtained from XRD.

Parameter	ICSD (98-002-7791)			Rietveld-analysis (this work)		
Refinement indexes						
Crystal system	Hexagonal			Hexagonal		
Space group	P63mc, 186			P63mc, 186		
R_{exp}	–			4.89		
R_{wp}	–			11.45		
GOF	–			2.34		
Unit cell parameters						
a (Å)	3.254			3.244		
b (Å)	3.254			3.244		
c (Å)	5.215			5.199		
Alpha (°)	90			90		
Beta (°)	90			90		
Gamma (°)	120			120		
Volume (Å^3)	47.82			47.392		
Crystallite size (Å)	–			298.8		
Atomic position	x	y	z	x	y	z
Zn	0.3333	0.6667	0	0.3333	0.6667	0
O	0.3333	0.6667	0.3824	0.3333	0.6667	0.3824

Please cite this article in press as: Mohamad, A.A. et al., First-principles calculation on electronic properties of zinc oxide by zinc–air system. Journal of King Saud University – Engineering Sciences (2015), http://dx.doi.org/10.1016/j.jksues.2015.08.002

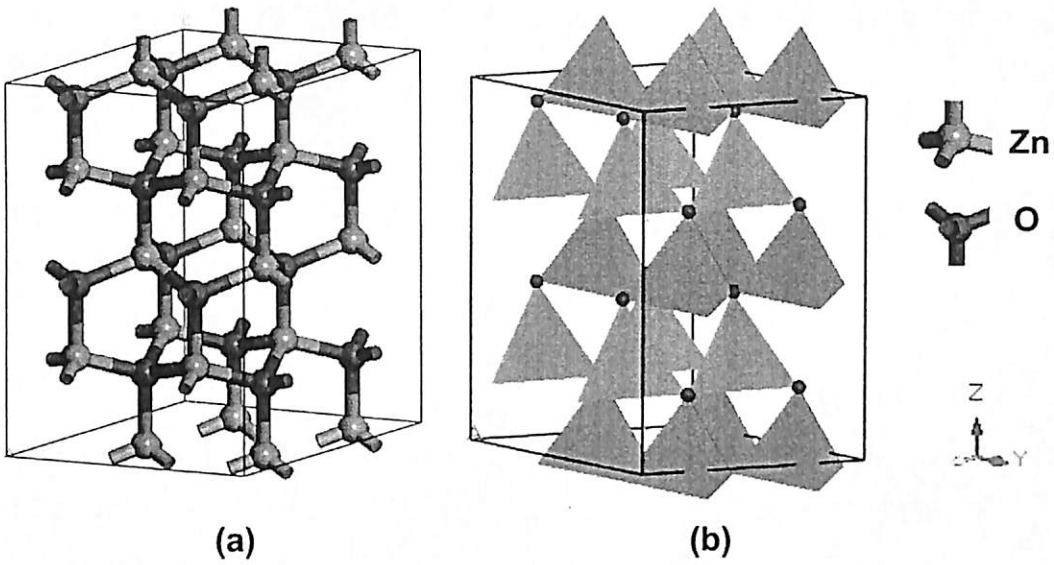

Figure 4 Optimised structure of ZnO with a (2 × 2 × 2) supercell: (a) atom bonding and (b) polyhedron generated from CASTEP.

Data obtained from Rietveld analysis (lattice constants and coordinates) were used in geometrical optimisation by LDA, GGA-PBE and the GGA-PBESol functional. To calculate the relative deviation, the experimental results obtained from the Rietveld analysis were used as a standard reference. Compared with GGA-PBE and the GGA-PBESol functional, the relative deviation values of the lattice parameters and atomic position of the ZnO calculated using LDA were the most accurate (Table 2). It is noted that the accuracy of the lattice calculation is very important; even a 2–3% change in lattice will consequently affect the stability and other structural calculations. Xu and Chen (2010) studied the doping of $LiFePO_4$ and mentioned that the significant consistency between the calculated and experimental values must be lower than 5%. In this work, the deviation of the LDA function was the lowest (less than 3%) and agreed well with the experimental results (Rietveld analysis). Thus, it could be concluded that LDA was the best functional approximation at this point; this function was next used to calculate the electronic properties of the ZnO.

Table 2 Comparison of lattice constants and volume of ZnO by Rietveld analysis obtained from XRD with geometrical optimisation by LDA, GGA-PBE and GGA-PBESol functional.

Parameter	Rietveld-analysis (this work)	Functional (relative deviation, %)		
		LDA	GGA-PBE	GGA-PBESol
a (Å)	3.244	3.189 (−1.69)	3.326 (+2.53)	3.257 (+0.40)
c (Å)	5.199	5.237 (+0.73)	5.418 (+4.21)	5.337 (+2.65)
V (Å^3)	47.392	46.141 (−2.64)	51.900 (+9.51)	49.024 (+3.44)

+ = overestimate, − = underestimate.

3.4. First-principles calculation of ZnO materials: electronic properties

The calculated band structure of pure ZnO using LDA functional approximation with the absence of spin orbit interaction is presented along the various symmetry lines [G (0.0, 0.0, 0.0), A (0.0, 0.0, 0.5), H (−0.3, 0.7, 0.5), K (−0.3, 0.7, 0.0), G (0.0, 0.0, 0.0), M (0.0, 0.5, 0.0), L (0.0, 0.5, 0.5) and H (−0.3, 0.7, 0.5)] in the Brillouin zone (Fig. 5). The Fermi level was set to zero; above and below this level were the conduction and valence bands, respectively. The bottom of the conduction band and the top of the valence band were at the same k-point (G–G), indicating that the ZnO was a direct band gap semiconductor. The calculated band gap of the ZnO was about 0.75 eV; this value was obtained from the highest valence band to the lowest conduction band and was in good agreement with the data from other calculations (0.73–0.76 eV) based on DFT (Li et al., 2009; Xie et al., 2012; Osuch et al., 2006; Chunying et al., 2012). Compared with the experimental value (3.26 eV) (Tan and Mohamad, 2010), the calculated band gap was much

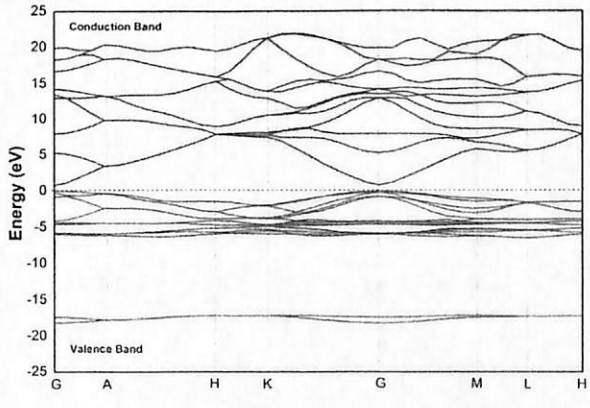

Figure 5 Band structure of ZnO representing conduction and valance bands.

Please cite this article in press as: Mohamad, A.A. et al., First-principles calculation on electronic properties of zinc oxide by zinc–air system. Journal of King Saud University – Engineering Sciences (2015), http://dx.doi.org/10.1016/j.jksues.2015.08.002

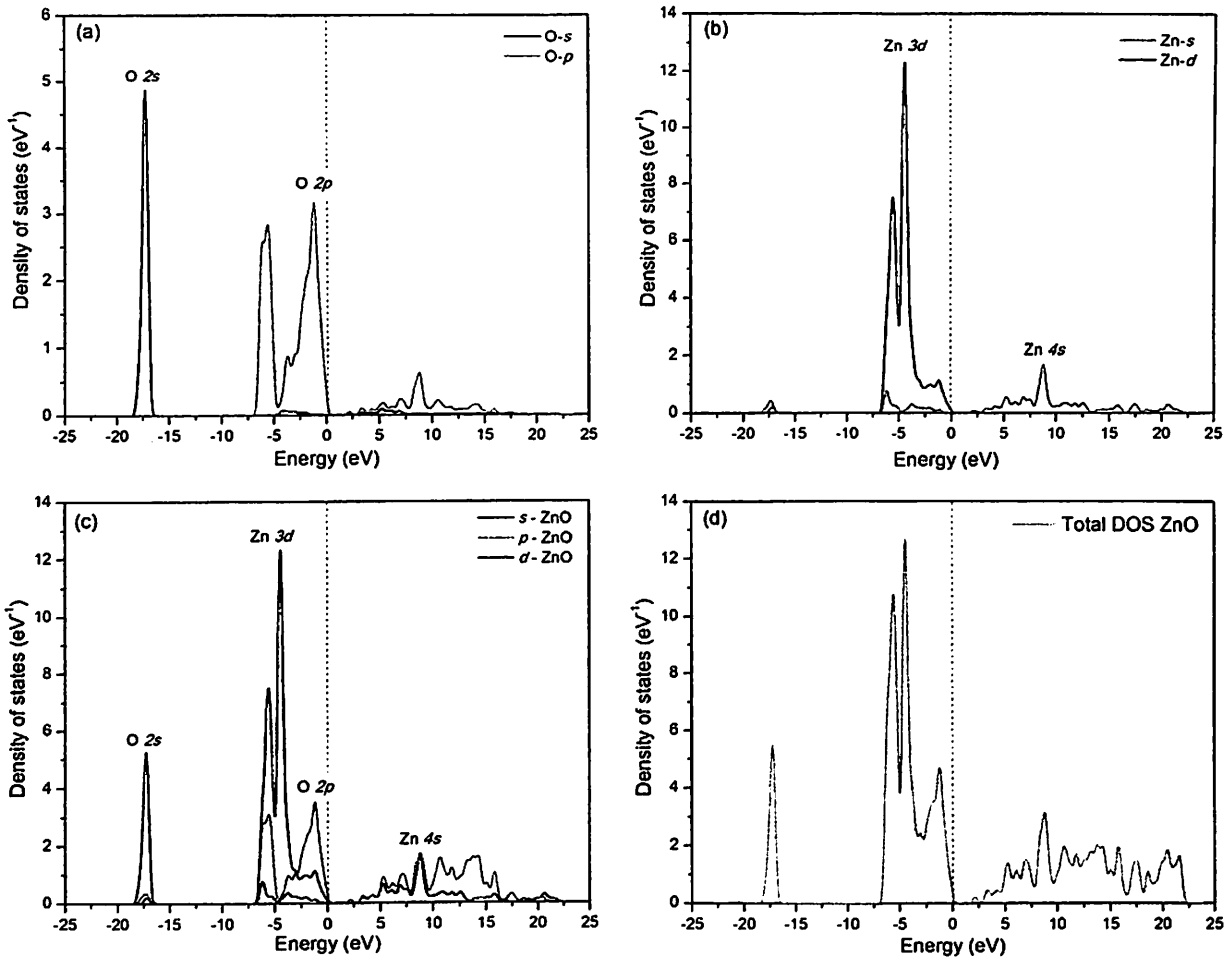

Figure 6 (a) Partial DOS of O, (b) partial DOS of Zn, (c) combined partial DOS of ZnO, and (d) total DOS of ZnO.

smaller because of the well-known calculation error of Kohn–Sham DFT for the conduction band. However, these results did not affect the accuracy of the comparison of the related properties of the crystals (e.g., band structure and density of state properties).

Point (G-G) showed the lowest energy band gap of 0.75 eV, whereas point (K–K) showed the highest value of 9.42 eV (Table 3). The excitation of electrons (from the highest valence band to the lowest conduction band) will occur at the lowest energy band gap. Thus, point (G–G) was the point where electron excitation most probably occurred because it had the lowest energy gap from the valence band to the conduction band.

The electron distribution in an energy spectrum is represented by the density of state (DOS). To elucidate the chemical bonding of ZnO, an individual atom is calculated by the partial DOS (PDOS) and all atoms by the total DOS (TDOS). In this work, the calculated DOS of the ZnO materials was within the energy interval from −25 eV up to +25 eV and the Fermi level was specified to be zero. The calculated PDOS of the O atom was contributed by O 2*p* and O 2*s* states (Fig. 6a). Considering that the O 2*p* was located at ~−1.26 eV, which was closer to the Fermi level than O 2*s* (~17.25 eV), the valence band of O was then mainly contributed by the O 2*p* rather than the O 2*s* state. On the other hand, the calculated PDOS of the Zn atom was dominated by Zn 3*d* and Zn 4*s* (Fig. 6b). The contribution of Zn 3*d* to the valence band was located at ~−4.47 eV, while that of Zn 4*s* was located at ~8.64 eV above the Fermi level. The PDOS of the ZnO, combining the contribution of all the atoms in the conduction and valence bands, showed that the lowest state in the ZnO was O 2*s*, followed by Zn 3*d*; O 2*p* was dominant in the valence band because of the highest states or upper valence states in ZnO (Fig. 6c). In the conduction band, the lowest and most dominant state was Zn 4*s*, followed by O 2*p*. The TDOS, which included O 2*s*, Zn 3*d*, O 2*p* and Zn 4*s* states, was plotted in a single curve (Fig. 6d). These results also agreed with other reports that characterised pure ZnO using DFT (Li et al., 2009; Xie et al., 2012; Osuch et al., 2006; Chunying et al., 2012).

Table 3 Direct band gap of electronic band structure of ZnO.

Direct band gap	Energy band gap (eV)
G–G	0.75
A–A	3.77
H–H	9.29
K–K	9.42
M–M	6.78
L–L	7.13

Please cite this article in press as: Mohamad, A.A. et al., First-principles calculation on electronic properties of zinc oxide by zinc–air system. Journal of King Saud University – Engineering Sciences (2015), http://dx.doi.org/10.1016/j.jksues.2015.08.002

4. Conclusion

ZnO is obtained from the discharge of the Zn anode in a Zn–air system. Numerous methods or machines can be used to prove the formation of ZnO through experimentation. However, some properties of ZnO can be presented without further experimentation and using only the data from XRD (Rietveld analysis). In the present study, the electronic properties of ZnO were predicted by first-principles calculation. Compared with GGA-PBE and the GGA-PBESol functionals, the exchange–correlation energy based on LDA functional yielded smallest lattice deviation and closest to the experimental results. The electronic band structure of hexagonal ZnO was calculated to determine the energy band gap of ZnO, which was determined to be 0.75 eV. DOS calculation was used to investigate the composition that determined the band structure of the ZnO, and the top valance band was dominated by the O $2p$ state, whereas the bottom conduction band was dominated by the Zn $4s$ state. First-principles calculation of the ZnO properties indicated that all the results were comparable with the data reported in the literature. Therefore, XRD data and first-principles calculations can be used to verify the properties of ZnO from Zn–air system.

Acknowledgement

This research was supported by the Ministry of Education Malaysia through FRGS (203/PBAHAN/6071262 and FRGS/2/2013/TK04/USM/02/1).

References

Alias, N., Mohamad, A.A., 2014a. Synthesis and electrochemical behavior of $LiFePO_4C$ with an air–electrode in an aqueous lithium ion battery. Ceram. Int. 40, 13089–13096.

Alias, S.S., Ismail, A.B., Mohamad, A.A., 2010. Effect of pH on ZnO nanoparticle properties synthesized by sol gel centrifugation. J. Alloy Compd. 499, 231–237.

Alias, S.S., Mohamad, A.A., 2013. Effect of NH_4I and I_2 concentration on agar gel polymer electrolyte properties for a dye-sensitized solar cell. Ionics 19, 1185–1194.

Alias, S.S., Mohamad, A.A., 2014b. Synthesis of Zinc Oxide by Sol-Gel Method for Photoelectrochemical Cells. Springer, Singapore.

Chunying, Z., Jing, W., Cheng, Z., 2012. First-principles study of the electronic structures and optical properties of Cl-Be doped wurtzite ZnO. J. Semicond. 33, 072001.

De La L Olvera, M., Maldonado, A., Asomoza, R., Melendez-Lira, M., 2002. Effect of the substrate temperature and acidity of the spray solution on the physical properties of F-doped ZnO thin films deposited by chemical spray. Sol. Energy Mater. Sol. Cells 71, 61–71.

Gabas, M., Díaz-Carrasco, P., Agulló-Rueda, F., Herrero, P., Landa-Cánovas, A., Ramos-Barrado, J., 2011. High quality ZnO and Ga: ZnO thin films grown onto crystalline Si (100) by RF magnetron sputtering. Sol. Energy Mater. Sol. Cells 95, 2327–2334.

Guan, L., Liu, B., Li, Q., Zhou, Y., Guo, J., Jia, G., Zhao, Q., Wang, Y., Fu, G., 2011. Electronic structure and optical properties of substitutional and interstitial phosphor-doped ZnO. Phys. Lett. A 375, 939–945.

Guinebretière, R., 2007. X-ray Diffraction by Polycrystalline Materials. ISTE Ltd., London.

Huang, M.H., Mao, S., Feick, H., Yan, H., Wu, Y., Kind, H., Weber, E., Russo, R., Yang, P., 2001. Room-temperature ultraviolet nanowire nanolasers. Science 292, 1897–1899.

Kato, H., Sano, M., Miyamoto, K., Yao, T., 2002. Growth and characterization of Ga-doped ZnO layers on a-plane sapphire substrates grown by molecular beam epitaxy. J. Cryst. Growth 237, 538–543.

Li, L., Wang, W., Liu, H., Liu, X., Song, Q., Ren, S., 2009. First principles calculations of electronic band structure and optical properties of Cr-doped ZnO. J. Phys. Chem. C 113, 8460–8464.

Osuch, K., Lombardi, E.B., Gebicki, W., 2006. First principles study of ferromagnetism in $Ti_{0.0625}Zn_{0.9375}O$. Phys. Rev. B 73, 075202-1-075202-5.

Pai, Y.-H., Lin, G.-R., 2011. Spontaneous electrochemical synthesis of morphologically controlled 1D ZnO structure with O/Zn composition ratio dependent photoluminescences. J. Electrochem. Soc. 158, E27–E31.

Pola-Albores, F., Paraguay-Delgado, F., Antúnez-Flores, W., Amézaga-Madrid, P., Rios-Valdovinos, E., Miki-Yoshida, M., 2011. Microstructural study of ZnO nanostructures by Rietveld analysis. J. Nanomater. 2011, 1–11.

Ren, C.-Y., Chiou, S.-H., Hsue, C.-S., 2004. Ga-doping effects on electronic and structural properties of wurtzite ZnO. Physica B 349, 136–142.

Segall, M.D., Lindan, P.J.D., Probert, M.J., Pickard, C.J., Hasnip, P. J., Clark, S.J., Payne, M.C., 2002. First-principles simulation: ideas, illustrations and the CASTEP code. J. Phys.: Condens. Matter 14, 2717.

Tan, W.C., Mohamad, A.A., 2010. A study on the effects of the discharge current and ambient temperature on the formation of zinc oxide synthesized via the zinc air system. J. Electrochem. Soc. 157, E184–E190.

Vanderbilt, D., 1997. First-principles based modelling of ferroelectrics. Curr. Opin. Solid State Mater. Sci. 2, 701–705.

Wang, Q.-B., Zhou, C., Wu, J., Lü, T., 2013. A GGA + U study of the optical properties of vanadium doped ZnO with and without single intrinsic vacancy. Opt. Commun. 297, 79–84.

Xie, F.-W., Yang, P., Li, P., Zhang, L.-Q., 2012. First-principle study of optical properties of (N, Ga) Co doped ZnO. Opt. Commun. 285, 2660–2664.

Xu, J., Chen, G., 2010. Effects of doping on the electronic properties of $LiFePO_4$: a first-principles investigation. Physica B 405, 803–807.

Yao, G.Y., Fan, G.H., Zhao, F., Ma, J.H., Chen, J., Zheng, S.W., Zeng, S.M., He, L.F., Zhang, T., 2012. In assisted realization of p-type C-doped ZnO: a first-principles study. Physica B 407, 3539–3542.

Yap, C.K., Tan, W.C., Alias, S.S., Mohamad, A.A., 2009. Synthesis of zinc oxide by zinc–air system. J. Alloy Compd. 484, 934–938.

Available online at www.sciencedirect.com

ScienceDirect

Procedia Chemistry 00 (2016) 000–000

Procedia Chemistry

www.elsevier.com/locate/procedia

5th International Conference on Recent Advances in Materials, Minerals and Environment (RAMM) & 2nd International Postgraduate Conference on Materials, Mineral and Polymer (MAMIP), 4-6 August 2015

Electronic Properties of ZnO Nanoparticles Synthesized by Sol-gel Method: A LDA+U Calculation and Experimental Study

Kausar Harun, Norsakinah Mansor, Zainal Arifin Ahmad, Ahmad Azmin Mohamad*

School of Materials and Mineral Recources Engineering, Universiti Sains Malaysia,14300 Nibong Tebal, Penang, Malaysia

Abstract

ZnO nanoparticles were prepared by sol-gel storage method to determine the optimum growth time. The precursor was zinc acetate dihydrate and methanol used as solvent. NaOH act as additive that changes the initial sol pH. The stabilize growth of ZnO nanoparticles was recorded after 12 hours aging time. Structural characterization revealed a single phase of ZnO with hexagonal wurtzite structure. Absorption spectra showed the synthesized ZnO nanoparticles exhibit an optical absorption in visible region. In addition, a systematic computational method within density functional theory frame work was used to elucidate the electronic properties of the synthesized ZnO nanoparticles. Calculations were performed using local-density approximation corrected by Hubbard U method. Hubbard U allowed the alteration of electronic state energy of Zn and O which improved the calculation. The calculated energy band gap demonstrates a value close to experimental data.

Peer-review under responsibility of School of Materials and Mineral Resources Engineering, Universiti Sains Malaysia.

Keywords: ZnO nanoparticles; density functional theory; sol-gel; electronic properties

* Corresponding author. Tel.: +604 599 6118; fax: +604 594 1011.
E-mail address: aam@usm.my

Peer-review under responsibility of School of Materials and Mineral Resources Engineering, Universiti Sains Malaysia.

Nomenclature

LDA Local density approximation
LDA+U Local density approximation with Hubbard U correction

1. Introduction

Over decades, rapid increase in number of research on ZnO has been marked. The great attention has risen due to its unique properties especially wide band gap energy (3.37 eV at ambient temperature) and large binding energy (60 meV). The wide band gap offers the electronic transition to occur down to visible light region. Also, the binding energy persist the event of excitonic absorption and recombination between electron and hole even at room temperature[1]. This process is enhanced with the nature of a direct type band structure that improved the efficiency of photo-generated electron transfer[2]. These properties serve as significant criteria in fabricating optoelectronic devices, such as lasers, photodiodes, and solar cell[3-5].

The formation of high purity ZnO nanoparticles is essential as it affect the resulting electronic properties. Various synthesis techniques have been applied to produce ZnO nanoparticles. Starting from high temperature synthesis protocol such as chemical vapor deposition and hydrothermal process, a wet chemical phase is also employed[6, 7]. Sol-gel method is a simple yet convenient technique that able to produce ZnO nanoparticles with preferred morphology and sizes. The ability to control hydrolysis and condensation rate has made sol-gel method relatively versatile[5].

Often, the first-principles calculation is used to elucidate the properties of ZnO. This technique facilitates the understanding of the ZnO behavior because they involved the calculation of the ground-state energy of the system by means of density functional theory (DFT). Several works has employed DFT with local density approximation (LDA) as the exchange-correlation functions [8, 9]. Due to drawbacks of LDA that underestimate the band gap of ZnO, the Hubbard U (or LDA+U) approach has been used[10]. However, the works involving the prediction of the electronic and optical properties from experimental input are still limited. The effort of correlating both experimental and physical models is essential in order to better explain the properties of synthesized ZnO nanoparticles.

In real situation, the ZnO nanoparticles are expected to be produced soonest possible. Thus, time has become the key factor. This work aims to study the stability of ZnO growth by means of shortest sol aging time. The quality of synthesized ZnO is then tested through structural and morphological characterization. The absorption spectra of ZnO nanoparticles are also examined. Also, the calculated results from first-principles method are compared and used to explain fundamental behavior and compliment experimental data.

2. Methodology

2.1 Synthesis of ZnO nanoparticles via sol-gel storage method

The ZnO sol was prepared by mixing 0.2 M zinc acetate dihydrate [$Zn(CH_3COO)_2.2H_2O$] and 200 mL of methanol (CH_3OH) at room temperature. The solution was stirred for 2 hours until a clear solution was obtained. A 1.0 M NaOH was later titrated into the solution until the pH reached pH 9. At this stage, the clear solution has transformed into milky white slurry. The resulted white slurry was stirred for another 1 hour to allow a homogeneous mixing. After that, the sample was left alone for 12 and 24 hours to allow the complete hydrolysis and gelation. The aged samples were then showing separation between a clear solution and white precipitate that sediment at the bottom of the storage bottle. Filtration process was the carried out to obtain the white precipitate and further dried in an oven at 120 °C for 2 hours. The dried samples were ground with mortar and pestle to yield ZnO powder. Finally, the powder was calcined at 600 °C in normal air to produce a well crystallize ZnO nanoparticles. Morphological characterization was done using field emission scanning electron microscope (FESEM) and structural behavior was analyzed by X-Ray diffraction (XRD) and Rietveld-refinement method. The UV-Visible (UV-VIS) spectroscopy was used to obtain the absorption spectra of synthesized ZnO. For comparison purpose,

sample with lesser storage time was also prepared. Sample after small sedimentation (approximately 4 hours) was chosen and subjected to similar procedure as mention above.

2.1 First-principle calculation of ZnO nanoparticles

The calculation of electronic and optical properties was performed using Material Studio 8.0 within Cambridge serial total energy package (CASTEP) computer code based on plane-wave ultrasoft pseudopotential approach. By using Rietveld-refinement data, the unit cell of ZnO was constructed. This structure was geometrically optimized by local-density approximation (LDA) exchange-correlation function corrected with Hubbard U method. The geometry optimization convergence thresholds were set with the maximum force of 0.01 eV/Å and the maximum atomic displacement of 0.0005 Å. The energy cutoff was fixed to 380 eV with k-point grid within Brillouin zone was 5 x 5 x 4.

3. Results and discussion

3.1 Structural and phase analysis

The diffracted patterns of ZnO nanoparticles at different aging time were indexed to the same ZnO wurtzite phase with ICSD no: 98-001-6787 (Fig. 1). The identical 2 theta position indicating no secondary phase present with the main peaks recorded at angle 2θ= 31.6°, 34.3°, 36.5°, 47.3°, 56.7°, 63.1°, and 67.8°. The most intense peaks were located at plane (010), (002) and (011). The sample with shortest aging time had the lowest intensity and increased upon prolonged aging. This phenomenon indicates that the crystallinity of ZnO powders were higher at longer aging time. An adequate time for complete hydrolysis, condensation and polymerization during aging have led to the formation of ZnO powders. However, as the time prolonged from 12 hours to 24 hours, it was apparent that the intensity does not change much. It thus deduced that 12 hour aging time was enough for a good quality of ZnO powders.

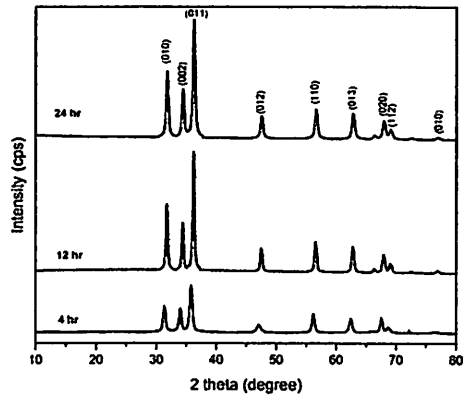

Fig. 1: The diffraction patterns of synthesized ZnO powders at different aging time

A quantitative Rietveld-refinement method was used to obtain the atomic parameter such as lattice dimension, atomic coordination and space group information. In this method, a new set of diffracted pattern was modelled as respect to the standard and observed patterns. These data were essential for first-principle calculation later on. Note that the adequacy of Rietveld analysis was dependent on residual (R) values and their reliability was governed by goodness of fit (GOF). The GOF was given by the ratio between weighted R value (R_{wp}) and expected residual value (R_{exp}). R_{wp} gave the affirmation between observed and calculated patterns, while R_{exp} was the least allowable R_{wp} value based on certain refinement parameters. For a reliable refinement result, the GOF value should be less than 2[11]. In this work, the GOF for all three samples were acceptable and lattice parameter a and c were also well matched to standard value (Table 1).

Table 1: The structural parameter and reliability factor from Rietveld analysis

Sample (hours)	a (Å)	c (Å)	V (Å^3)	Discrepancy factor		
				R_{wp}	R_{exp}	GOF
4	3.2424	5.1975	47.35	15.58677	10.99112	2.01108
12	3.4298	5.2068	47.622	15.56702	9.93207	2.45658
24	3.2501	5.2068	47.633	16.18223	10.65693	2.30575

3.2 Morphological analysis

The micrographs of synthesized ZnO are observed with aid of FESEM at 50,000 X magnification (Fig.2). An irregular shape was observed throughout all samples with some hexagonal-like form. Apparently, the sizes of ZnO were reduced upon prolonged aging. The longest aging time (24 hours) produced ZnO with 49 nm particle sizes in average while sample after 4 hours aging showed 200 nm particle sizes. The particle size for sample 12 hours was 80 nm. Based on morphology and structural characterization result, it was sufficient to precede the optical analysis with sample after 12 hours aging as it gave the optimum and good quality of ZnO nanoparticles.

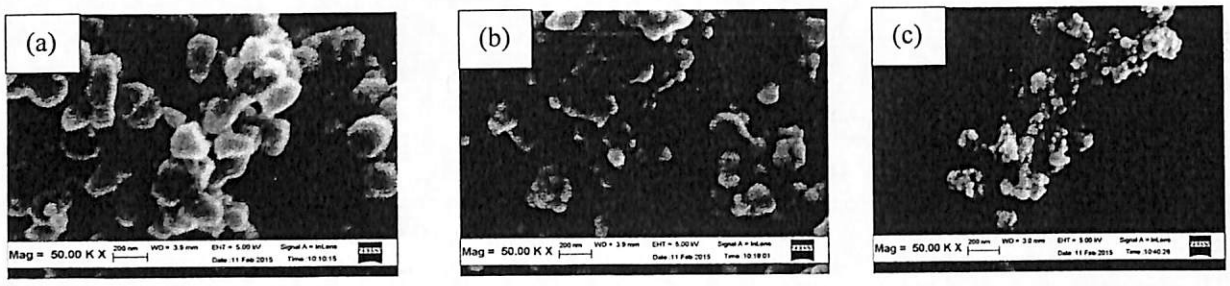

Fig. 2: FESEM micrograph of aged ZnO nanoparticles a) 4 hours, b) 12 hours and c) 24 hours

3.3 Optical analysis

The sample aged for 12 hours was tested for optical response to evaluate the quality of the synthesized ZnO nanoparticles. The absorption spectrum of ZnO nanoparticles was obtained after being examined using UV-Vis spectroscopy (Fig. 3). The plot of $\alpha h\nu^2$ versus photon energy was plotted and tangent line drawn until x-axis interception. The intercepted energy, E_g = 3.10 eV corresponded to the band gap energy of ZnO The result revealed synthesized ZnO exhibit an optical absorption in visible region. In order to enhance the fundamental understanding of electronic properties of ZnO nanoparticles, the first-principles method was use to simulate the band gap.

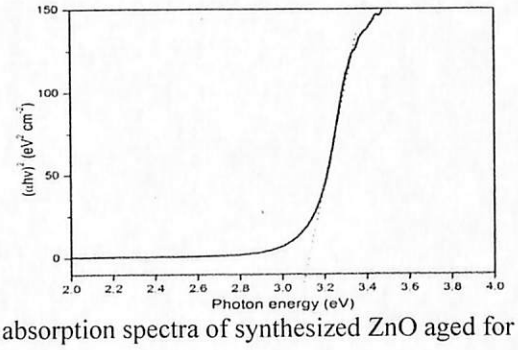

Fig. 3: The absorption spectra of synthesized ZnO aged for 12 hours

3.4 First-principles calculation of ZnO nanoparticles: modelling, optimization and band gap determination

The calculations began with constructing the hexagonal ZnO crystal structure by inserting the lattice parameter, atomic coordination and space group $P6_3mc$ obtained from Rietveld analysis. The built unit cell of ZnO consists of two Zn atoms attached to 3 O atoms (Fig. 4). The calculations throughout this work were based on this structure. Geometrical optimization onto the ZnO structure was done to obtain the unit cell with the lowest energy.

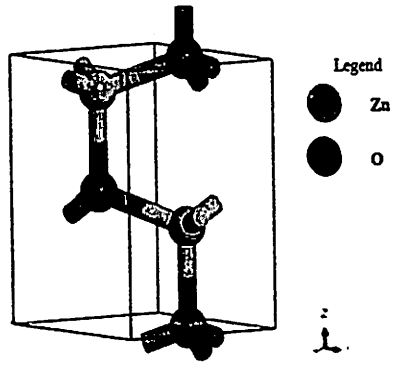

Fig. 4: The unit cell of ZnO generated by Material Studio 8.0-CASTEP computer code

By applying exchange-correlation functional LDA+U, the effective energy (U) of valence electron from each atom were adjusted during optimization process. This method improved the calculation as it defines the strongly correlated materials of *d* and *f* electron localization. The *3d*-state of Zn (U_d) was treated as valence state. Also, for transition metal oxide system, the *2p*-state of oxygen (U_p) was corrected as well to overcome the under-binding of Zn *3d* during calculation. In literatures, a variety of U values for both U_d and U_p been suggested[10, 12]. The preliminary study had shown that by adjusting the U_d value only starting from 7 eV would give a small effect on band gap energy. As there is no consensus regarding the procedure to choose the U value, several attempts have been made and the resulting energy band gaps are compiled (Table 2). It was fairly stated that by increasing the U_d value alone still lead the underestimation in energy band gap value even when the U_d was set as 10 eV. However, a good agreement with experimental data (3.10 eV) was achieved when U_d= 5 eV and U_p = 7 eV. An overestimation in energy band gap found when the U values were increased after this point.

Table 2: The value of effective energy (U) of zinc and oxygen and resulting energy band gap calculated using LDA+U functional

U_d values for Zn *3d* (eV)	U_p values for O *2p* (eV)	Functional	Band gap (eV)
7	**0**	LDA+U	1.19
8	**0**	LDA+U	1.23
9	**0**	LDA+U	1.26
10	**0**	LDA+U	1.29
4	**7**	LDA+U	2.98
5	**7**	LDA+U	3.08
6	**7**	LDA+U	3.17
7	**7**	LDA+U	3.24
8	**7**	LDA+U	3.31
8	**8**	LDA+U	3.59

An integration of first-principles LDA+U calculation with physical characterization on ZnO nanoparticles properties

Kausar Harun[1], Norsakinah Mansor[1], Muhamad Kamil Yaakob[2], Mohamad Fariz Mohamad Taib[2], Zainal Arifin Ahmad[1], Ahmad Azmin Mohamad[1*]

[1]School of Materials and Mineral Resources Engineering, Universiti Sains Malaysia, 14300, Nibong Tebal, Penang, Malaysia

[2]Faculty of Applied Sciences, Universiti Teknologi MARA, 40450 Shah Alam, Malaysia

*Corresponding e-mail address: aam@usm.my

Tel.: +604 599 6118, Fax: +604 594 1011

Abstract

The first-principles calculation was used to elucidate the electronic and optical properties of synthesized ZnO nanoparticles. Prior to calculation, ZnO nanoparticles were synthesized through a sol-gel reaction involving zinc acetate dihydrate, methanol and sodium hydroxide. The nanoparticles were calcined at 600 °C in normal air for 2 h followed by thermal, structural, microstructural and optical characterization. A single phase of pure ZnO was obtained in as-synthesized samples, and the crystallinity improved following a heat treatment process. Rietveld analysis shows that the synthesized ZnO belonged to the space group $P6_3mc$ and the refined structural data fit well with a goodness of fit value 2.46. To provide a bridge to experimental results, the ZnO unit cell was built based on the lattice parameters and atomic coordination obtained from Rietveld data. The calculated electronic band structure using the LDA+U functional agreed well with the absorption band edge obtained within the experimental approach

(3.06 eV). The corresponding optical properties were calculated with predictive accuracy and the results were elaborated fundamentally.

Keywords: ZnO; Characterization; Optical properties; LDA+U

1. Introduction

Zinc oxide (ZnO) has attracted a significant research interest, especially within the optoelectronic industry including light emitting diodes [1, 2], gas sensors [3-5], laser diodes [6], and solar cells [7-9]. Its wide band gap and direct type gap has made it robust toward large electric field and permitted the operation at high temperature and voltages. The sol-gel method has been favored during ZnO synthesis because it can take place at a lower temperature (< 100 °C), involves simple starting materials and produces ZnO with excellent chemical homogeneity [10]. In our group, two kinds of sol-gel routes commonly employed [11-13]; (1) sol-gel centrifuge (SGC) and (2) sol-gel storage (SGS) methods. The SGS method offer feasible processing condition without the need of extra equipment and allows for the monitoring of ZnO growth over time.

A significant ZnO growth mechanism has been proposed, to produce a thermodynamically-stable ZnO, through which an adequate aging time is needed. Previous literature has noted that stabilized ZnO can be obtained after short-time aging lasting 0 – 36 hours [14], 48 hours [12, 13] and even after a month [15]. The range of aging time is somewhat very wide and may lead to difficulty when the optimum aging time is to be chosen for practical consideration. If synthesis parameters such as reaction times can be optimized, then the production time can perhaps be efficiently reduced.

The quality of synthesized ZnO is manifested using various characterization techniques. Yet, details of the electronic and optical behavior of ZnO could be simulated using theoretical calculations based on density functional theory (DFT). Significant attention has been devoted to incorporating theoretical calculations with experimental result [16-18]. However, most of them have used lattice inputs from other literature during the structure modeling stage. In this work, the ZnO unit cell is built using a lattice input from the Rietveld refinement to intimately bridge experimental work to DFT calculation. The main motivation is to aid in the fundamental interpretation of experimental data. Prior to the calculation, the ZnO nanoparticles were synthesized via a sol-gel storage method with minimum aging time and characterized in terms of their structural and phases purity, morphology and response to ultra violet (UV) radiation. Later, first principles with corrective Hubbard model, LDA+U calculation was undertaken to explain the electronic and optical properties of the synthesized ZnO.

2. Experimental

2.1 Synthesis of ZnO powder

ZnO nanopowder was prepared through the sol-gel storage method using 0.8 g of zinc acetate dihydrate [$Zn(CH_3COO)_2.2H_2O$, Merck] as a precursor in 200 ml of methanol (CH_3OH, Merck). The molality of starting sol was set at 0.2 M. After 2 h of magnetic stirring, a clear solution was obtained. Titration with 1.0 M NaOH was conducted until the pH reached 9. At this point, the clear solution changed into milky-white slurry. Stirring continued for another 1 h to allow homogeneous mixing. The sample was then left alone at room temperature for 12 h for a complete the sol-gel process. Soon after aging, the white ZnO precipitate that settled to the bottom of the beaker was collected through filtration followed by several excess methanol

The quality of synthesized ZnO is manifested using various characterization techniques. Yet, details of the electronic and optical behavior of ZnO could be simulated using theoretical calculations based on density functional theory (DFT). Significant attention has been devoted to incorporating theoretical calculations with experimental result [16-18]. However, most of them have used lattice inputs from other literature during the structure modeling stage. In this work, the ZnO unit cell is built using a lattice input from the Rietveld refinement to intimately bridge experimental work to DFT calculation. The main motivation is to aid in the fundamental interpretation of experimental data. Prior to the calculation, the ZnO nanoparticles were synthesized via a sol-gel storage method with minimum aging time and characterized in terms of their structural and phases purity, morphology and response to ultra violet (UV) radiation. Later, first principles with corrective Hubbard model, LDA+U calculation was undertaken to explain the electronic and optical properties of the synthesized ZnO.

2. Experimental

2.1 Synthesis of ZnO powder

ZnO nanopowder was prepared through the sol-gel storage method using 0.8 g of zinc acetate dihydrate [$Zn(CH_3COO)_2.2H_2O$, Merck] as a precursor in 200 ml of methanol (CH_3OH, Merck). The molality of starting sol was set at 0.2 M. After 2 h of magnetic stirring, a clear solution was obtained. Titration with 1.0 M NaOH was conducted until the pH reached 9. At this point, the clear solution changed into milky-white slurry. Stirring continued for another 1 h to allow homogeneous mixing. The sample was then left alone at room temperature for 12 h for a complete the sol-gel process. Soon after aging, the white ZnO precipitate that settled to the bottom of the beaker was collected through filtration followed by several excess methanol

washes. Drying was carried out at 120 °C for 2 h and further ground to yield white powder. Finally, the ZnO nanopowder was calcined at 600 °C in normal air for a well crystallization. Throughout this work, the sample with no calcination effect was termed as as-synthesized ZnO.

2.2 Characterization of ZnO powder

The as-synthesized sample was subjected to the thermoanalytical technique before the calcination process took place using thermal gravimetric analysis (TGA, *Mettler Toledo*). A 10 mg sample was heated in normal air from room temperature until 800 °C. Within the same mode, the differential scanning calorimetry (DSC) testing was also conducted. The results were used to ascertain stability, weight loss and phase changes throughout the heat treatment process.

The phase purity and crystallinity of the synthesized ZnO powder was inspected from X-ray powder diffraction (XRD, *Bruker Advanced X-Ray Solution D8*) pattern, which were recorded at scanning angle 2θ range from 10° to 90°. The data was analyzed using the X'pert High Score Plus software. A quantitative measurement was also carried out using Rietveld-refinement method embedded in the software. The refined atomic parameters, including lattice dimensions, space group, and atomic coordination of respective elements were recorded.

The morphology and elemental composition were investigated by field emission scanning electron microscopy (FESEM, *Zeiss SUPRA 35*) and an energy dispersive X-ray (EDX) to further confirm the quality of synthesized ZnO. The optical properties were then tested using UV-Visible (UV-Vis, *Varian-Cary Win UV 100*) spectroscopy. The response of synthesized ZnO towards electromagnetic radiation was recoded at room temperature with a wavelength range from 350 – 900 nm.

2.3 Calculation models and methods

To ascertain a more comprehensive fundamental understanding, the first-principles calculation was performed using Material Studio 8.0 within the CASTEP computer code based on DFT framework. Electron-ion interactions were modelled using ultrasoft pseudopotential method. In this work, Zn-$4s^2 3d^{10}$ and O-$2s^2 2p^4$ were treated as valence electronic state. The ZnO wurtzite structure belonging to space group $P6_3mc$ was constructed using lattice parameter and atomic coordination data obtained from Rietveld refinement. Geometrical optimization was undertaken before the calculations with the exchange and correlation functional taken from local-density approximation (LDA). The self-consistent convergence accuracy was set at 5 x 10^{-6} eV/atom with allowable stress less than 0.02 GPa. The maximum force was set as 0.01 eV/Å and maximum atomic displacement was 5 x 10^{-4} Å. K-point grid sampling in the unit cell was taken as 5 x 5 x 4 and energy cut off 380 eV under plane wave basis set. To provide a precise explanation of the electronic structure, a semi-empirical LDA+U approach was adopted. The Hubbard U value was varied on both U_d and U_p according to the formalism in Eq. 1[19];

$$E_{LDA+U}[n(r)] = E_{LDA}[n(r)] + E_{HF}[n(r)] - E_{dc} \qquad Eq.1$$

where E_{LDA} represents the approximate DFT total energy and $n(r)$ is the electronic density. The Hartree-Fock-like energy functional, E_{HF} defined in CASTEP computer code consists of Coulomb energy U, which is combined with the exchange energy J to produce only single on-site Coulomb repulsion of U. The E_{dc} is subtracted in the last part to avoid double counting of interaction contained in another parameter. As the motivation of this work moved towards the electrical structure of synthesized ZnO, the associate optical properties were calculated based on

LDA+U functional and compared with experimental result. Details on the algorithm used for the optical calculation are well described by time-dependent perturbations of the ground electronic state [19].

3. Results and discussions

3.1 Thermal stability analysis of as-synthesized ZnO

The thermal event recorded by TGA and DSC revealed three distinguishable zones when the sample heated from room temperature up to 800 °C (**Fig. 1**). The process started with steep weight loss beginning from 30 °C to offset 100 °C associated by a small endothermic curve (T_{max} = 60 °C). Larger weight loss later occurred in zone B (100 – 410 °C) accompanied by the asymmetric exothermic effect observed at this temperature range (T_{max} = 370 °C). The sample continued to lose weight at a slow rate up to offset 410 °C and ended with a stagnant line upon reaching zone C. At this point, the TGA line stabilized yielding a residue of ZnO, with an overall experimental weight loss of 6%.

The thermal behavior of as-synthesized ZnO may be explained through chemical interaction. As the precursor dissolved in methanol, the zinc acetate dihydrate will be solvated, resulting in more stabilized zinc and acetate ions. Upon titration with NaOH, the zinc species later form zinc hydroxide [$Zn(OH)_2$], sodium acetate (CH_3COONa) and water molecules as summarized in Eq. 2 and 3 [12];

$$Zn(CH3COO)_2.2H_2O + 2NaOH = Zn(OH)_2 + 2CH_3COONa + 2H_2O \qquad Eq.2$$

$$Zn(OH)_2 \rightarrow ZnO + H_2O \qquad Eq.3$$

LDA+U functional and compared with experimental result. Details on the algorithm used for the optical calculation are well described by time-dependent perturbations of the ground electronic state [19].

3. Results and discussions

3.1 Thermal stability analysis of as-synthesized ZnO

The thermal event recorded by TGA and DSC revealed three distinguishable zones when the sample heated from room temperature up to 800 °C (**Fig. 1**). The process started with steep weight loss beginning from 30 °C to offset 100 °C associated by a small endothermic curve (T_{max} = 60 °C). Larger weight loss later occurred in zone B (100 – 410 °C) accompanied by the asymmetric exothermic effect observed at this temperature range (T_{max} = 370 °C). The sample continued to lose weight at a slow rate up to offset 410 °C and ended with a stagnant line upon reaching zone C. At this point, the TGA line stabilized yielding a residue of ZnO, with an overall experimental weight loss of 6%.

The thermal behavior of as-synthesized ZnO may be explained through chemical interaction. As the precursor dissolved in methanol, the zinc acetate dihydrate will be solvated, resulting in more stabilized zinc and acetate ions. Upon titration with NaOH, the zinc species later form zinc hydroxide [$Zn(OH)_2$], sodium acetate (CH_3COONa) and water molecules as summarized in Eq. 2 and 3 [12];

$$Zn(CH3COO)_2.2H_2O + 2NaOH = Zn(OH)_2 + 2CH_3COONa + 2H_2O \qquad Eq.2$$

$$Zn(OH)_2 \rightarrow ZnO + H_2O \qquad Eq.3$$

The conversion from $Zn(OH)_2$ to ZnO was seemingly spontaneous reaction at room temperature, supported by a small free energy difference of the reaction, ΔG_{298} = -1.13 kJ mol^{-1} [20]. An adequate OH^- supplied from NaOH enhanced the dissolution of $Zn(OH)_2$ to ZnO, leaving water as by product. Therefore, the weight loss at zone A was presumably thermal dehydration of precursor and mainly attributed by water elimination. At this point, the bond breakage required less heat due to the well-known low temperature decomposition behavior of zinc acetate dihydrate, yielding small endothermic curve.

The resulting $Zn(OH)_2$ compound was deduced to have mainly decomposed in zone B. An acetate group produced in Eq. 2 also decompose in this zone. The stable TGA curve after 410 °C indicated the complete removal and elimination of all complexes and the crystallization of ZnO took place. An exothermic peak observed proved that heat was released as the zinc molecule rearranged into a uniform and dense structure. From this analysis, it was shown that synthesized ZnO could be calcined at temperature above 410 °C. In this work, 600 °C was selected as calcinations temperature for better crystalline growth of ZnO nanoparticles.

3.2 Phase and structural analysis of synthesized ZnO

The diffraction patterns of ZnO nanoparticles both with and without calcination effect were indexed to hexagonal wurtzite structure, ICSD file no: 98-010-6787 (**Fig. 2**). Three most intense peaks were recorded at (010), (002) and (011) planes in both cases, and diffraction peaks from Zn or other impurities were absent indicating a phase pure ZnO. This finding further support the spontaneous conversion of $Zn(OH)_2$ to ZnO as proposed in Section 3.1. The drying stage at 120 °C also facilitated decomposition of $Zn(OH)_2$. Apparently, the peak

The conversion from $Zn(OH)_2$ to ZnO was seemingly spontaneous reaction at room temperature, supported by a small free energy difference of the reaction, ΔG_{298} = -1.13 kJ mol^{-1} [20]. An adequate OH^- supplied from NaOH enhanced the dissolution of $Zn(OH)_2$ to ZnO, leaving water as by product. Therefore, the weight loss at zone A was presumably thermal dehydration of precursor and mainly attributed by water elimination. At this point, the bond breakage required less heat due to the well-known low temperature decomposition behavior of zinc acetate dihydrate, yielding small endothermic curve.

The resulting $Zn(OH)_2$ compound was deduced to have mainly decomposed in zone B. An acetate group produced in Eq. 2 also decompose in this zone. The stable TGA curve after 410 °C indicated the complete removal and elimination of all complexes and the crystallization of ZnO took place. An exothermic peak observed proved that heat was released as the zinc molecule rearranged into a uniform and dense structure. From this analysis, it was shown that synthesized ZnO could be calcined at temperature above 410 °C. In this work, 600 °C was selected as calcinations temperature for better crystalline growth of ZnO nanoparticles.

3.2 Phase and structural analysis of synthesized ZnO

The diffraction patterns of ZnO nanoparticles both with and without calcination effect were indexed to hexagonal wurtzite structure, ICSD file no: 98-010-6787 (**Fig. 2**). Three most intense peaks were recorded at (010), (002) and (011) planes in both cases, and diffraction peaks from Zn or other impurities were absent indicating a phase pure ZnO. This finding further support the spontaneous conversion of $Zn(OH)_2$ to ZnO as proposed in Section 3.1. The drying stage at 120 °C also facilitated decomposition of $Zn(OH)_2$. Apparently, the peak

The conversion from $Zn(OH)_2$ to ZnO was seemingly spontaneous reaction at room temperature, supported by a small free energy difference of the reaction, ΔG_{298} = -1.13 kJ mol^{-1} [20]. An adequate OH^- supplied from NaOH enhanced the dissolution of $Zn(OH)_2$ to ZnO, leaving water as by product. Therefore, the weight loss at zone A was presumably thermal dehydration of precursor and mainly attributed by water elimination. At this point, the bond breakage required less heat due to the well-known low temperature decomposition behavior of zinc acetate dihydrate, yielding small endothermic curve.

The resulting $Zn(OH)_2$ compound was deduced to have mainly decomposed in zone B. An acetate group produced in Eq. 2 also decompose in this zone. The stable TGA curve after 410 °C indicated the complete removal and elimination of all complexes and the crystallization of ZnO took place. An exothermic peak observed proved that heat was released as the zinc molecule rearranged into a uniform and dense structure. From this analysis, it was shown that synthesized ZnO could be calcined at temperature above 410 °C. In this work, 600 °C was selected as calcinations temperature for better crystalline growth of ZnO nanoparticles.

3.2 Phase and structural analysis of synthesized ZnO

The diffraction patterns of ZnO nanoparticles both with and without calcination effect were indexed to hexagonal wurtzite structure, ICSD file no: 98-010-6787 (**Fig. 2**). Three most intense peaks were recorded at (010), (002) and (011) planes in both cases, and diffraction peaks from Zn or other impurities were absent indicating a phase pure ZnO. This finding further support the spontaneous conversion of $Zn(OH)_2$ to ZnO as proposed in Section 3.1. The drying stage at 120 °C also facilitated decomposition of $Zn(OH)_2$. Apparently, the peak

intensity increased after undergone a heat treatment process while the integral width of the diffraction patterns showed a significant reduction.

The increment in intensity after calcination was evident that the ZnO crystallinity had improved. As the Zn and O atoms rearranged into a more dense structure, more electrons were brought to sit at their respective sites and resulted in an efficient electron scattering with the incident X-ray radiations. Poor electron scattering occurred in amorphous or irregular orientation of ZnO molecules. By considering the broadening of the XRD peaks along (011) planes, the crystallite size of both samples were calculated using Scherrer formula provided in Eq. 4;

$$Crystallite\ size = \frac{180}{\pi} . \frac{\kappa \lambda}{\cos\theta . \sqrt{(FWHM)^2 - s^2}} \qquad Eq.4$$

where κ represents the Scherrer constant (0.89), λ was the wavelength of CuK_α radiation (1.5406 Å), and s referring to instrumental broadening (0). The θ used corresponded to (011) plane. It is noted that the width broadening was linked to the apparent crystal size, which was measured from the coherently diffracting domains and differ from the particle size due to powder aggregations. The reduction of full-width-half-maximum (FWHM) value after calcination gave a bigger crystallite size, governing by higher diffusion rate at higher temperature. This phenomenon can be explained by the collision and coalescence of particles with one another upon heating and thus enhanced the growth rate [21]. A crystallite size of 26.63 nm was observed for the as-synthesized sample and increased to 40.29 nm after calcination.

A quantitative structural analysis using Rietveld refinement method gave well fitted curves for both samples (**Fig. 3**). A small variation in lattice parameters, a and c were observed after

heat treatment, which manifested the rearrangement of atoms into close-pack structure (**Table 1**). However, these values were still closed with standard ZnO parameters as obtained from other refinement works [22, 23] and manual calculations [24, 25]. The crystallite size also deviated from that calculated via Eq. 4, mainly due to whole pattern consideration made in Rietveld refinement. The agreement indices, denotes as residual, *R*-factor were used to determine the quality of fitting process (**Table 2**), and further judged by goodness of fit (GOF) given from Eq. 5;

$$GOF = \frac{R_{wp}}{R_{exp}} \qquad Eq.5$$

The R_{wp} gives the affirmation between the observed and calculated patterns, while R_{exp} is the least allowable R_{wp} value based on certain refinement parameters. In present work, the GOF for as-synthesized ZnO was 2.28 and increased to 2.46 after heat treatment, which considered good and acceptable. Hence, the structural data (lattice parameter a & b and atomic coordination) could be used as basis input in first-principle calculation.

3.3 Morphology of ZnO nanopowder

The characterization continued with morphological investigation to confirm the quality of synthesized ZnO. A uniform morphology with a nearly spherical shape was found on both samples (**Fig. 4**). However, due to particles agglomeration in as-synthesized ZnO, the microstructure was observed to be unclear (**Fig. 4a**). Apparently, the particles size was larger and clearer after calcination process (**Fig. 4b**). The corresponding atomic percentage from the EDX results proved a correct stoichiometry of ZnO. Even though crystallite and particle size did not referring to the same entity, this observation could be used to offer an initial perspective on the calcination effect which were parallel to the crystallite size obtained from

heat treatment, which manifested the rearrangement of atoms into close-pack structure (**Table 1**). However, these values were still closed with standard ZnO parameters as obtained from other refinement works [22, 23] and manual calculations [24, 25]. The crystallite size also deviated from that calculated via Eq. 4, mainly due to whole pattern consideration made in Rietveld refinement. The agreement indices, denotes as residual, *R*-factor were used to determine the quality of fitting process (**Table 2**), and further judged by goodness of fit (GOF) given from Eq. 5;

$$GOF = \frac{R_{wp}}{R_{exp}} \qquad Eq.5$$

The R_{wp} gives the affirmation between the observed and calculated patterns, while R_{exp} is the least allowable R_{wp} value based on certain refinement parameters. In present work, the GOF for as-synthesized ZnO was 2.28 and increased to 2.46 after heat treatment, which considered good and acceptable. Hence, the structural data (lattice parameter a & b and atomic coordination) could be used as basis input in first-principle calculation.

3.3 Morphology of ZnO nanopowder

The characterization continued with morphological investigation to confirm the quality of synthesized ZnO. A uniform morphology with a nearly spherical shape was found on both samples (**Fig. 4**). However, due to particles agglomeration in as-synthesized ZnO, the microstructure was observed to be unclear (**Fig. 4a**). Apparently, the particles size was larger and clearer after calcination process (**Fig. 4b**). The corresponding atomic percentage from the EDX results proved a correct stoichiometry of ZnO. Even though crystallite and particle size did not referring to the same entity, this observation could be used to offer an initial perspective on the calcination effect which were parallel to the crystallite size obtained from

XRD. Initially, the OH^- in the starting sol had been adsorbed on the polar surfaces of Zn-growing particles and induced the increment of particle size. The alkaline condition (pH 9) served excess OH^-, leading to non-preferential growth of ZnO particles [21]. Hence, a more spherical particle shape observed. Considering practical application, high crystalline and uniform morphology were characteristic for a good ZnO. Taking the promising structural and good control of morphology of synthesized ZnO, it was then important to continue the optical observation on heat-treated ZnO only.

3.4 Band gap determination

After aging for 12 hours, the synthesized ZnO showed a characteristic excitonic absorption peak at about 380 nm (**Fig. 5**). Further validation was conducted by extrapolating the tangent line along the absorption edge curve. The corresponding intercepted wavelength was taken to calculate the energy band gap using Planck-Einstein relation as depicted in Eq. 6;

$$E_g = \frac{hc}{\lambda} \qquad Eq.6$$

with h is the Planck constant (4.13 x 10^{-15} eV-s), c is the speed of light (3.0 x 10^8 m/s) and λ is the wavelength of light radiation (nm). The calculated energy band gap was 3.06 eV which deviated from bulk ZnO (3.37 eV)[13]. The nanocrystalline nature had confined the electron in a smaller space yielded to smaller E_g.

3.5 First-principles calculation of synthesized ZnO: Geometrical optimization and electronic properties determination

To further simulate the optical properties of synthesized ZnO, a preliminary works including structure modeling, geometrical optimization and band gap calculation using several

XRD. Initially, the OH^- in the starting sol had been adsorbed on the polar surfaces of Zn-growing particles and induced the increment of particle size. The alkaline condition (pH 9) served excess OH^-, leading to non-preferential growth of ZnO particles [21]. Hence, a more spherical particle shape observed. Considering practical application, high crystalline and uniform morphology were characteristic for a good ZnO. Taking the promising structural and good control of morphology of synthesized ZnO, it was then important to continue the optical observation on heat-treated ZnO only.

3.4 Band gap determination

After aging for 12 hours, the synthesized ZnO showed a characteristic excitonic absorption peak at about 380 nm (**Fig. 5**). Further validation was conducted by extrapolating the tangent line along the absorption edge curve. The corresponding intercepted wavelength was taken to calculate the energy band gap using Planck-Einstein relation as depicted in Eq. 6;

$$E_g = \frac{hc}{\lambda} \qquad Eq.6$$

with h is the Planck constant (4.13 x 10^{-15} eV-s), c is the speed of light (3.0 x 10^8 m/s) and λ is the wavelength of light radiation (nm). The calculated energy band gap was 3.06 eV which deviated from bulk ZnO (3.37 eV)[13]. The nanocrystalline nature had confined the electron in a smaller space yielded to smaller E_g.

3.5 First-principles calculation of synthesized ZnO: Geometrical optimization and electronic properties determination

To further simulate the optical properties of synthesized ZnO, a preliminary works including structure modeling, geometrical optimization and band gap calculation using several

DFT functionals were required. The calculations were based on ZnO model built using an initial lattice parameter and atomic coordination presented in **Table 1**. Three O atoms were attached to two Zn atoms to construct a unit cell (**Fig. 6**). The conventional LDA and LDA+U functionals were adopted in optimization process to obtain a stable structure. Apparently, the E_g obtained using LDA functional was 0.795 eV, about 70% relative error from experimental result (**Fig. 7a**). This underestimation was due to a well-known LDA limitation faced with strongly-correlated system involving transition metal. The binding energy of *d*-state was not accurately determined, leading to overestimation on the hybridization with *p*-state. This situation enhances the *p-d* coupling effect and pushes the valence band upward, resulting in band gap reduction [26].

The implementation of LDA+U involved the adjustment of U values (**Table 3**). Initially, only $U_{d,Zn}$ was varied. In continuation from previous work, $U_{d,Zn}$ = 7 eV was selected [27]. However, increasing U_d alone still caused underestimation result even at high U_d value. A systematic study on the effect of U parameter towards calculated E_g proved a gradual increment of E_g from 1.19 to 1.29 eV when only $U_{d,Zn}$ varied from 7 to 10 eV (**Fig. 8a**). The underestimation in E_g still prevails which indicates the LDA+$U_{d,Zn}$ may not be adequate to describe the electronic structure of ZnO. Hence, the $U_{d,O}$ was adjusted as there was no consensus for determining the best U parameter (**Fig. 8b**). The resulted E_g close to experimental result then yielded at $U_{d,Zn}$ = 5 eV and $U_{d,O}$ = 7 eV. The calculated E_g was 3.08 eV and showed the characteristic of direct band gap (**Fig. 7b**).

Obtaining the correct E_g was an essential task as it governs the corresponding optical properties. Combined with density of state (DOS) spectra, a clear differentiation between LDA and LDA+$U_{d,Zn}$+$U_{p,O}$ could be observed. As the Fermi level was set at 0 eV, the lower

DFT functionals were required. The calculations were based on ZnO model built using an initial lattice parameter and atomic coordination presented in **Table 1**. Three O atoms were attached to two Zn atoms to construct a unit cell (**Fig. 6**). The conventional LDA and LDA+U functionals were adopted in optimization process to obtain a stable structure. Apparently, the E_g obtained using LDA functional was 0.795 eV, about 70% relative error from experimental result (**Fig. 7a**). This underestimation was due to a well-known LDA limitation faced with strongly-correlated system involving transition metal. The binding energy of *d*-state was not accurately determined, leading to overestimation on the hybridization with *p*-state. This situation enhances the *p-d* coupling effect and pushes the valence band upward, resulting in band gap reduction [26].

The implementation of LDA+U involved the adjustment of U values (**Table 3**). Initially, only $U_{d,Zn}$ was varied. In continuation from previous work, $U_{d,Zn}$ = 7 eV was selected [27]. However, increasing U_d alone still caused underestimation result even at high U_d value. A systematic study on the effect of U parameter towards calculated E_g proved a gradual increment of E_g from 1.19 to 1.29 eV when only $U_{d,Zn}$ varied from 7 to 10 eV (**Fig. 8a**). The underestimation in E_g still prevails which indicates the LDA+$U_{d,Zn}$ may not be adequate to describe the electronic structure of ZnO. Hence, the $U_{d,O}$ was adjusted as there was no consensus for determining the best U parameter (**Fig. 8b**). The resulted E_g close to experimental result then yielded at $U_{d,Zn}$ = 5 eV and $U_{d,O}$ = 7 eV. The calculated E_g was 3.08 eV and showed the characteristic of direct band gap (**Fig. 7b**).

Obtaining the correct E_g was an essential task as it governs the corresponding optical properties. Combined with density of state (DOS) spectra, a clear differentiation between LDA and LDA+$U_{d,Zn}$+$U_{p,O}$ could be observed. As the Fermi level was set at 0 eV, the lower

energy part in DOS spectra represents the valence band (VB) while upper part represents the conduction band (CB) (**Fig. 9 - 10**). In both cases, the VB was dominated by Zn-*3d* states and small tabulation of hybridized O-*2p* states. The CB was mainly from O-*2p* and Zn-*4s* states. Observing along *x*-axis, the LDA+ $U_{d,Zn}$+$U_{p,O}$ tend to shift the minima of CB upward, resulting in a wider gap between VB and CB (**Fig. 10c**). Only small effects were observed in CB shifting when both functionals employed. Indeed, the highest Zn-*3d* peaks in VB were found to down shifted from -6 eV in LDA (**Fig. 9c**) to -8 eV when LDA+ $U_{d,Zn}$+$U_{p,O}$ was adopted (**Fig. 10c**). This occurrence was due to the weaker effect of *p-d* coupling and stronger localization of Zn-*3d* states in Hubbard *U* approximation. The determination of Zn-*3d* localization from X-ray emission spectroscopy gave an average value at 8.27 eV below the VB, which was comparable with current result [26]. With the aforementioned explanation, the LDA+*U* functional with $U_{d,Zn}$ = 5 eV and $U_{d,O}$ = 7 eV was the optimum selection for a close E_g value with experimental result (3.06 eV).

3.6 First-principles calculation: Optical properties determination

The successful prediction in E_g (3.08 eV) closed to experimental result (3.06 eV) had a significant effect on the optical properties of synthesized ZnO. These properties could be quickly generated to study the suitability of ZnO for real application. For example, a good transparent conductive oxide was required to have low absorption in large wavelength region [28]. The simplest and yet informative result from first-principles calculation was the absorbance spectra (**Fig. 11**). The absorption edge as indicated in inset gave a direct comparison with E_g value obtained from UV-Vis absorption spectra. The synthesized ZnO was believed to absorb only ~ 1% of visible light. Indeed, the main absorption part was found

energy part in DOS spectra represents the valence band (VB) while upper part represents the conduction band (CB) (**Fig. 9 - 10**). In both cases, the VB was dominated by Zn-*3d* states and small tabulation of hybridized O-*2p* states. The CB was mainly from O-*2p* and Zn-*4s* states. Observing along *x*-axis, the LDA+ $U_{d,Zn}+U_{p,O}$ tend to shift the minima of CB upward, resulting in a wider gap between VB and CB (**Fig. 10c**). Only small effects were observed in CB shifting when both functionals employed. Indeed, the highest Zn-*3d* peaks in VB were found to down shifted from -6 eV in LDA (**Fig. 9c**) to -8 eV when LDA+ $U_{d,Zn}+U_{p,O}$ was adopted (**Fig. 10c**). This occurrence was due to the weaker effect of *p-d* coupling and stronger localization of Zn-*3d* states in Hubbard *U* approximation. The determination of Zn-*3d* localization from X-ray emission spectroscopy gave an average value at 8.27 eV below the VB, which was comparable with current result [26]. With the aforementioned explanation, the LDA+*U* functional with $U_{d,Zn}$ = 5 eV and $U_{d,O}$ = 7 eV was the optimum selection for a close E_g value with experimental result (3.06 eV).

3.6 First-principles calculation: Optical properties determination

The successful prediction in E_g (3.08 eV) closed to experimental result (3.06 eV) had a significant effect on the optical properties of synthesized ZnO. These properties could be quickly generated to study the suitability of ZnO for real application. For example, a good transparent conductive oxide was required to have low absorption in large wavelength region [28]. The simplest and yet informative result from first-principles calculation was the absorbance spectra (**Fig. 11**). The absorption edge as indicated in inset gave a direct comparison with E_g value obtained from UV-Vis absorption spectra. The synthesized ZnO was believed to absorb only ~ 1% of visible light. Indeed, the main absorption part was found

to lies in ultra-violet region with main peak located at 17 eV (peak A) corresponded to charge transfer from Zn-*4s* to O-*2p* states.

To this end, the information on electron transition from occupied to unoccupied states would also explained by the plot of dielectric function, ε (**Fig. 12**). The three most intense peaks A, B, and C in the imaginary part represent different electron transition phenomena. Combining with DOS of ZnO, peak A located at 3.1 eV could be attributed by optical transition between the maximum of VB toward minimum of CB. The O-*2p* states were dominated the electron transition to unoccupied Zn-*4s* and Zn-*4p* states. Meanwhile, peak B and C were resulted from transition between various occupied states to unoccupied states. These dielectric properties of ZnO were important especially in piezoelectric industry. By knowing the contribution of electronic transition, future work on tailoring the band gap using doping process could be easily understood.

4. Conclusion

A good quality of ZnO nanoparticles were successfully synthesized with short aging time (12 hours) through sol-gel process. The LDA+U calculation based on synthesized ZnO structure improved the LDA underestimation in E_g by adjusting both $U_{d,Zn} = 5$ eV and $U_{p,O} = 7$ eV. A good agreement in E_g value on both experimental (3.06 eV) and first-principles calculation (3.08 eV) facilitated the detailed explanation on electronic transition upon exposure to light. The occupied states in valence band maxima was dominated by O-*2p* states while the unoccupied states at conduction band minima was mainly from mixed Zn-*4s* and Zn-*4p* states.

Acknowledgements

The authors would like to thanks MOSTI (FRGS-203/PBAHAN/6071262 and FRGS/2/2013/TK04/USM/02/1), USM Fellowship and MyBrain15 for financial support throughout this project.

References

[1] A. Tsukazaki, A. Ohtomo, T. Onuma, M. Ohtani, T. Makino, M. Sumiya, K. Ohtani, S.F. Chichibu, S. Fuke, Y. Segawa, H. Ohno, H. Koinuma, M. Kawasaki, Repeated temperature modulation epitaxy for p-type doping and light-emitting diode based on ZnO, Nat Mater., 4 (2005) 42-46.

[2] P.-H. Lei, M.-J. Ding, Y.-C. Lee, M.-J. Chung, Textured zinc oxide prepared by liquid phase deposition (LPD) method and its application in improvement of extraction efficiency for 650nm resonant-cavity light-emitting diode (RCLED), J. Alloys Compd., 509 (2011) 6152-6157.

[3] B. Baruwati, D.K. Kumar, S.V. Manorama, Hydrothermal synthesis of highly crystalline ZnO nanoparticles: A competitive sensor for LPG and EtOH, Sens. Actuator B-Chem., 119 (2006) 676-682.

[4] M. Cittadini, M. Sturaro, M. Guglielmi, A. Resmini, I. Tredici, U. Anselmi-Tamburini, P. Koshy, C. Sorrell, A. Martucci, ZnO nanorods grown on ZnO sol–gel seed films: Characteristics and optical gas-sensing properties, Sens. Actuator B-Chem., 213 (2015) 493-500.

[5] G.F. Fine, L.M. Cavanagh, A. Afonja, R. Binions, Metal oxide semi-conductor gas sensors in environmental monitoring, Sensors, 10 (2010) 5469-5502.

[6] P. Kumar, J. Singh, V. Parashar, K. Singh, R. Tiwari, O. Srivastava, K. Ramam, A.C. Pandey, Investigations on structural, optical and second harmonic generation in solvothermally synthesized pure and Cr-doped ZnO nanoparticles, CrystEngComm, 14 (2012) 1653-1658.

[7] J. El Ghoul, M. Kraini, O. Lemine, L. El Mir, Sol–gel synthesis, structural, optical and magnetic properties of Co-doped ZnO nanoparticles, J. Mater. Sci. Mater. Electron., 26 (2015) 2614-2621.

[8] Y.-M. Sung, F.-C. Hsu, Y.-F. Chen, Improved charge transport in inverted polymer solar cells using surface engineered ZnO-nanorod array as an electron transport layer, Sol. Energy Mater. Sol. Cells, 125 (2014) 239-247.

[9] S. Rani, P. Suri, P. Shishodia, R. Mehra, Synthesis of nanocrystalline ZnO powder via sol–gel route for dye-sensitized solar cells, Sol. Energy Mater. Sol. Cells, 92 (2008) 1639-1645.

[10] L. Znaidi, Sol–gel-deposited ZnO thin films: a review, Mater. Sci. Eng., B, 174 (2010) 18-30.

[11] M.Z. Yahaya, M.Z. Abdullah, A.A. Mohamad, Centrifuge and storage precipitation of TiO2 nanoparticles by the sol–gel method, J. Alloys Compd., 651 (2015) 557-564.

[12] S. Alias, A. Ismail, A. Mohamad, Effect of pH on ZnO nanoparticle properties synthesized by sol–gel centrifugation, J. Alloys Compd., 499 (2010) 231-237.

[13] A.L. Tan, L.J. Khoo, S.S. Alias, A.A. Mohamad, ZnO nanoparticles and poly (acrylic) acid-based polymer gel electrolyte for photo electrochemical cell, J. Sol-Gel Sci. Technol., 64 (2012) 184-192.

[6] P. Kumar, J. Singh, V. Parashar, K. Singh, R. Tiwari, O. Srivastava, K. Ramam, A.C. Pandey, Investigations on structural, optical and second harmonic generation in solvothermally synthesized pure and Cr-doped ZnO nanoparticles, CrystEngComm, 14 (2012) 1653-1658.

[7] J. El Ghoul, M. Kraini, O. Lemine, L. El Mir, Sol–gel synthesis, structural, optical and magnetic properties of Co-doped ZnO nanoparticles, J. Mater. Sci. Mater. Electron., 26 (2015) 2614-2621.

[8] Y.-M. Sung, F.-C. Hsu, Y.-F. Chen, Improved charge transport in inverted polymer solar cells using surface engineered ZnO-nanorod array as an electron transport layer, Sol. Energy Mater. Sol. Cells, 125 (2014) 239-247.

[9] S. Rani, P. Suri, P. Shishodia, R. Mehra, Synthesis of nanocrystalline ZnO powder via sol–gel route for dye-sensitized solar cells, Sol. Energy Mater. Sol. Cells, 92 (2008) 1639-1645.

[10] L. Znaidi, Sol–gel-deposited ZnO thin films: a review, Mater. Sci. Eng., B, 174 (2010) 18-30.

[11] M.Z. Yahaya, M.Z. Abdullah, A.A. Mohamad, Centrifuge and storage precipitation of TiO2 nanoparticles by the sol–gel method, J. Alloys Compd., 651 (2015) 557-564.

[12] S. Alias, A. Ismail, A. Mohamad, Effect of pH on ZnO nanoparticle properties synthesized by sol–gel centrifugation, J. Alloys Compd., 499 (2010) 231-237.

[13] A.L. Tan, L.J. Khoo, S.S. Alias, A.A. Mohamad, ZnO nanoparticles and poly (acrylic) acid-based polymer gel electrolyte for photo electrochemical cell, J. Sol-Gel Sci. Technol., 64 (2012) 184-192.

[6] P. Kumar, J. Singh, V. Parashar, K. Singh, R. Tiwari, O. Srivastava, K. Ramam, A.C. Pandey, Investigations on structural, optical and second harmonic generation in solvothermally synthesized pure and Cr-doped ZnO nanoparticles, CrystEngComm, 14 (2012) 1653-1658.

[7] J. El Ghoul, M. Kraini, O. Lemine, L. El Mir, Sol–gel synthesis, structural, optical and magnetic properties of Co-doped ZnO nanoparticles, J. Mater. Sci. Mater. Electron., 26 (2015) 2614-2621.

[8] Y.-M. Sung, F.-C. Hsu, Y.-F. Chen, Improved charge transport in inverted polymer solar cells using surface engineered ZnO-nanorod array as an electron transport layer, Sol. Energy Mater. Sol. Cells, 125 (2014) 239-247.

[9] S. Rani, P. Suri, P. Shishodia, R. Mehra, Synthesis of nanocrystalline ZnO powder via sol–gel route for dye-sensitized solar cells, Sol. Energy Mater. Sol. Cells, 92 (2008) 1639-1645.

[10] L. Znaidi, Sol–gel-deposited ZnO thin films: a review, Mater. Sci. Eng., B, 174 (2010) 18-30.

[11] M.Z. Yahaya, M.Z. Abdullah, A.A. Mohamad, Centrifuge and storage precipitation of TiO2 nanoparticles by the sol–gel method, J. Alloys Compd., 651 (2015) 557-564.

[12] S. Alias, A. Ismail, A. Mohamad, Effect of pH on ZnO nanoparticle properties synthesized by sol–gel centrifugation, J. Alloys Compd., 499 (2010) 231-237.

[13] A.L. Tan, L.J. Khoo, S.S. Alias, A.A. Mohamad, ZnO nanoparticles and poly (acrylic) acid-based polymer gel electrolyte for photo electrochemical cell, J. Sol-Gel Sci. Technol., 64 (2012) 184-192.

[14] Y. Li, L. Xu, X. Li, X. Shen, A. Wang, Effect of aging time of ZnO sol on the structural and optical properties of ZnO thin films prepared by sol–gel method, Appl. Surf. Sci., 256 (2010) 4543-4547.

[15] K.P. Misra, R. Shukla, A. Srivastava, A. Srivastava, Blueshift in optical band gap in nanocrystalline Zn1-xCaxO films deposited by sol-gel method, Appl. Phys. Lett., 95 (2009) 31901.

[16] R. Liu, Y. Li, B. Yao, Z. Ding, R. Deng, L. Zhang, H. Zhao, L. Liu, Experimental and first-principles study of photoluminescent and optical properties of Na-doped CuAlO2: the role of the NaAl-2Na i complex, J. Phys. D: Appl. Phys., 48 (2015) 335102.

[17] Y. Wang, W. Tang, J. Liu, L. Zhang, Stress-induced anomalous shift of optical band gap in Ga-doped ZnO thin films: Experimental and first-principles study, Appl. Phys. Lett., 106 (2015) 162101.

[18] J. Arul Mary, J. Judith Vijaya, J.H. Dai, M. Bououdina, L. John Kennedy, Y. Song, Experimental and first-principles DFT studies of electronic, optical and magnetic properties of cerium–manganese codoped zinc oxide nanostructures, Mater. Sci. Semicond. Process., 34 (2015) 27-38.

[19] M. Yaakob, M. Taib, L. Lu, O. Hassan, M. Yahya, Self-interaction corrected LDA+ U investigations of BiFeO3 properties: plane-wave pseudopotential method, Mater. Res. Express, 2 (2015) 116101.

[20] N.J. Nicholas, G.V. Franks, W.A. Ducker, The mechanism for hydrothermal growth of zinc oxide, CrystEngComm, 14 (2012) 1232-1240.

[21] D. Dutta, Optimization of process parameters and its effect on particle size and morphology of ZnO nanoparticle synthesized by sol–gel method, J. Sol-Gel Sci. Technol., (2015) 1-9.

[14] Y. Li, L. Xu, X. Li, X. Shen, A. Wang, Effect of aging time of ZnO sol on the structural and optical properties of ZnO thin films prepared by sol–gel method, Appl. Surf. Sci., 256 (2010) 4543-4547.

[15] K.P. Misra, R. Shukla, A. Srivastava, A. Srivastava, Blueshift in optical band gap in nanocrystalline Zn1-xCaxO films deposited by sol-gel method, Appl. Phys. Lett., 95 (2009) 31901.

[16] R. Liu, Y. Li, B. Yao, Z. Ding, R. Deng, L. Zhang, H. Zhao, L. Liu, Experimental and first-principles study of photoluminescent and optical properties of Na-doped CuAlO2: the role of the NaAl-2Na i complex, J. Phys. D: Appl. Phys., 48 (2015) 335102.

[17] Y. Wang, W. Tang, J. Liu, L. Zhang, Stress-induced anomalous shift of optical band gap in Ga-doped ZnO thin films: Experimental and first-principles study, Appl. Phys. Lett., 106 (2015) 162101.

[18] J. Arul Mary, J. Judith Vijaya, J.H. Dai, M. Bououdina, L. John Kennedy, Y. Song, Experimental and first-principles DFT studies of electronic, optical and magnetic properties of cerium–manganese codoped zinc oxide nanostructures, Mater. Sci. Semicond. Process., 34 (2015) 27-38.

[19] M. Yaakob, M. Taib, L. Lu, O. Hassan, M. Yahya, Self-interaction corrected LDA+ U investigations of BiFeO3 properties: plane-wave pseudopotential method, Mater. Res. Express, 2 (2015) 116101.

[20] N.J. Nicholas, G.V. Franks, W.A. Ducker, The mechanism for hydrothermal growth of zinc oxide, CrystEngComm, 14 (2012) 1232-1240.

[21] D. Dutta, Optimization of process parameters and its effect on particle size and morphology of ZnO nanoparticle synthesized by sol–gel method, J. Sol-Gel Sci. Technol., (2015) 1-9.

[22] A. Kaushik, B. Dalela, R. Rathore, V. Vats, B. Choudhary, P. Alvi, S. Kumar, S. Dalela, Influence of Co doping on the structural, optical and magnetic properties of ZnO nanocrystals, J. Alloys Compd., 578 (2013) 328-335.

[23] A.A. Mohamad, M.S. Hassan, M.K. Yaakob, M.F.M. Taib, F.W. Badrudin, O.H. Hassan, M.Z.A. Yahya, First-principles calculation on electronic properties of zinc oxide by zinc–air system, J King Saud Uni Sci, (2015) in press, DOI: 10.1016/j.jksues.2015.08.002.

[24] R. Elilarassi, G. Chandrasekaran, Structural, optical and magnetic properties of nanoparticles of ZnO:Ni—DMS prepared by sol–gel method, Mater. Chem. Phys., 123 (2010) 450-455.

[25] A. Khorsand Zak, W.H. Abd. Majid, M.E. Abrishami, R. Yousefi, X-ray analysis of ZnO nanoparticles by Williamson–Hall and size–strain plot methods, Solid State Sci, 13 (2011) 251-256.

[26] X. Ma, Y. Wu, Y. Lv, Y. Zhu, Correlation Effects on Lattice Relaxation and Electronic Structure of ZnO within the GGA+ U Formalism, J. Phys. Chem. C, 117 (2013) 26029-26039.

[27] M. Yaakob, N. Hussin, M. Taib, T. Kudin, O. Hassan, A. Ali, M. Yahya, First Principles LDA+ U Calculations for ZnO Materials, Integr Ferroelectr., 155 (2014) 15-22.

[28] A. Slassi, S. Naji, A. Benyoussef, M. Hamedoun, A. El Kenz, On the transparent conducting oxide Al doped ZnO: First Principles and Boltzmann equations study, J. Alloys Compd., 605 (2014) 118-123.

Figure Captions

Figure 1: The TGA and DSC curves of sol-gel synthesized ZnO aged for 12 hours

Figure 2: Diffraction patterns of synthesized ZnO nanoparticles stored for 12 hours (a) before calcination and (b) after calcinations at 600 °C

Figure 3: Observed, calculated and difference of diffracted intensities obtained after Rietveld-refinement

Figure 4: FESEM images of ZnO nanoparticles (a) before calcine and (b) after calcined at a magnification of 50,000 X with their corresponding EDX elemental analysis

Figure 5: UV–Vis absorption spectrum of ZnO nanoparticles stored for 12 hours

Figure 6: The unit cell of ZnO nanoparticles generated from the CASTEP computer code

Figure 7: Calculated energy band gap of ZnO using different functionals (a) LDA and (b) LDA+U

Figure 8: The band gap energies of ZnO nanoparticles (a) U_p was fixed at 0 eV and (b) U_p was fixed at 7 eV. The dashed arrows in (b) specify the U parameters that correspond to the experimental band gap

Figure 9: The density of state for (a) Zn (b) O (c) ZnO and (d) total density of state (TDOS) of ZnO using LDA functional

Figure 10: The density of state for (a) Zn (b) O (c) ZnO and (d) total density of state (TDOS) of ZnO using LDA+U functional

Figure 11: The absorption spectra of pure ZnO nanoparticles using LDA + U functional

Figure 12: The calculated dielectric function of pure ZnO nanoparticles using LDA + U functional

Table Captions

Table 1: Lattice parameter, crystallite size and unit cell volume determined from XRD Rietveld-analysis for ZnO nanoparticles before and after calcination

Table 2: Rietveld-analysis of ZnO nanoparticles before and after calcinations

Table 3: The calculated band gap of ZnO nanoparticles using LDA + U functional

Figure 1:

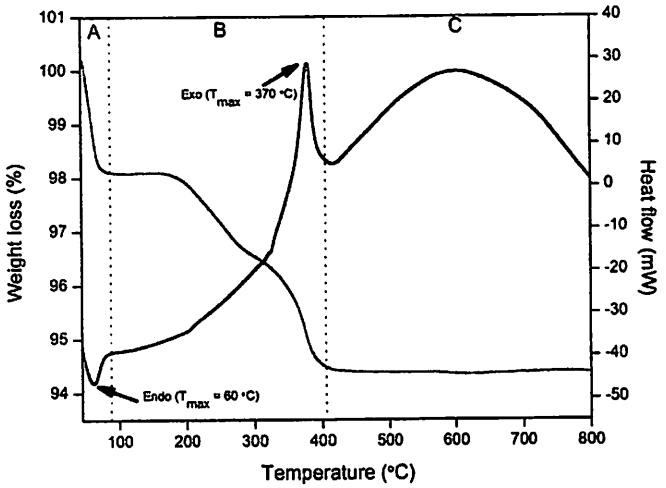

Figure 2:

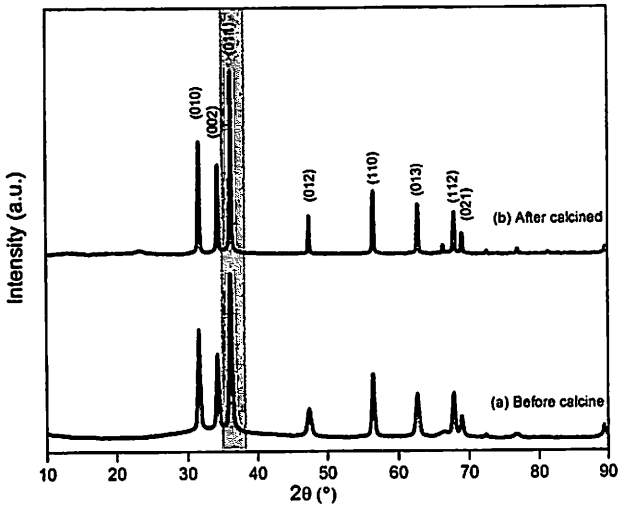

Figure 1:

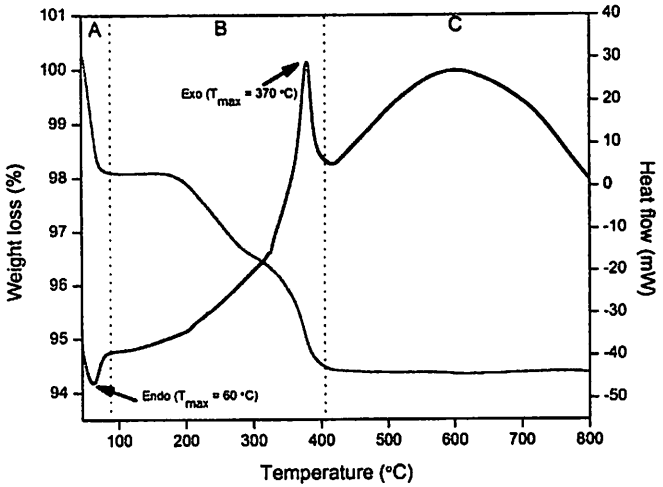

Figure 2:

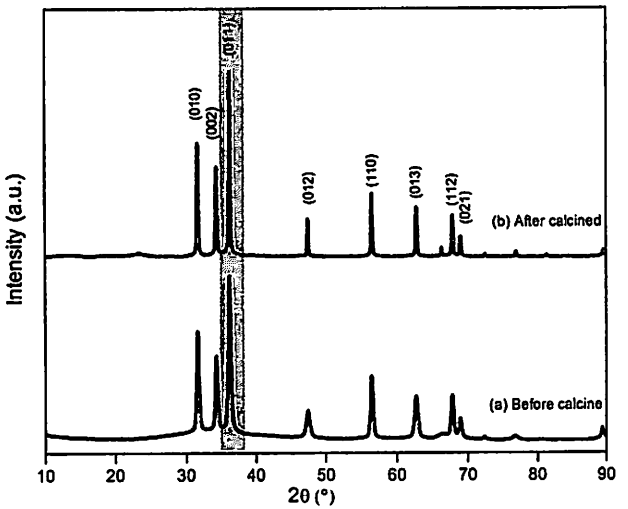

Figure 3:

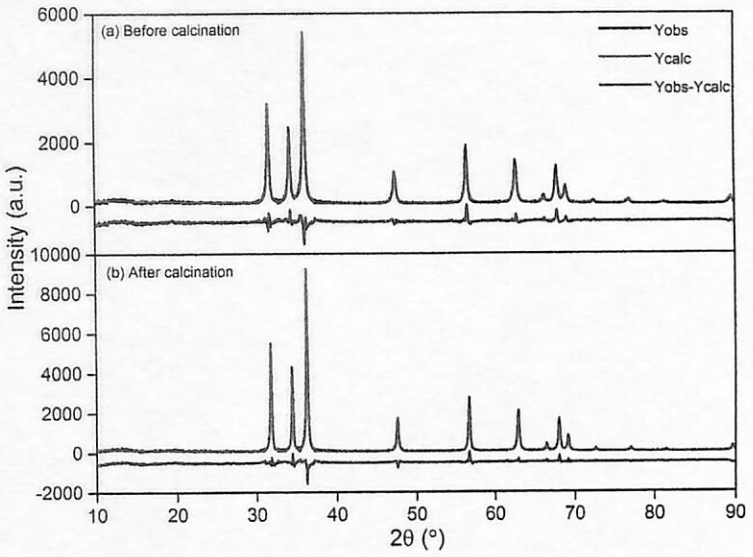

Figure 4:

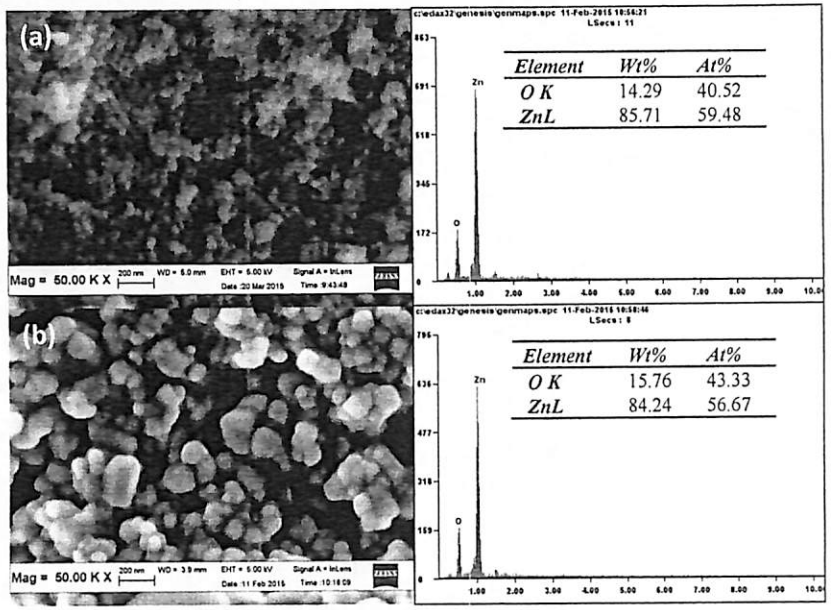

Figure 5:

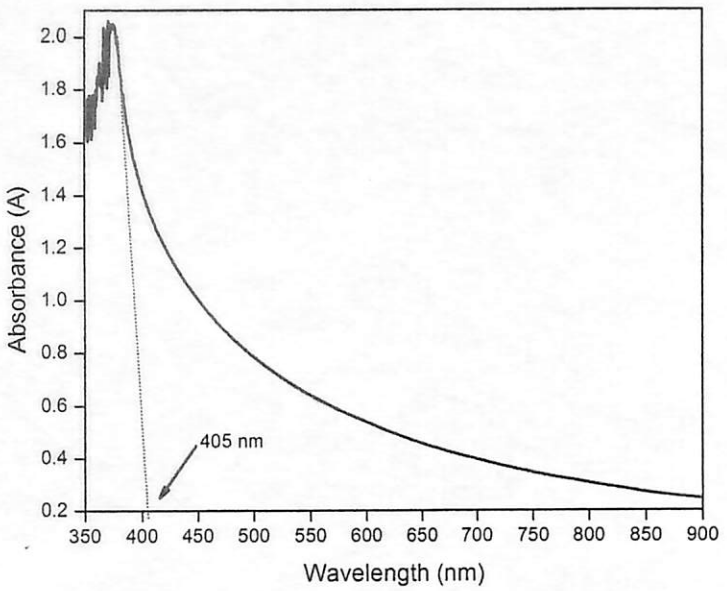

Figure 6:

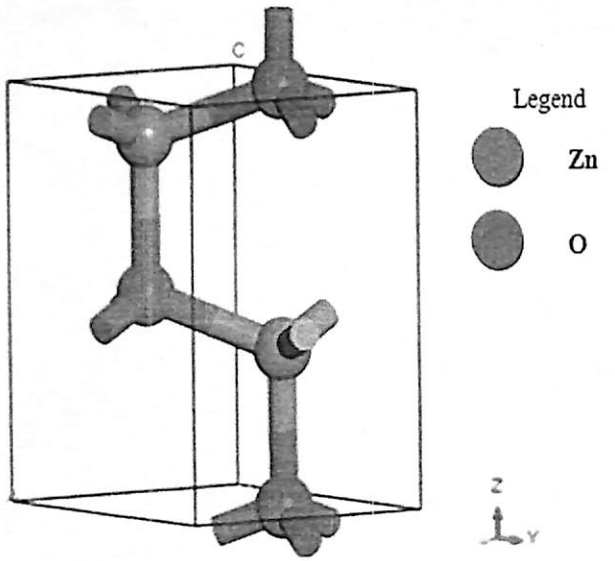

Figure 7:

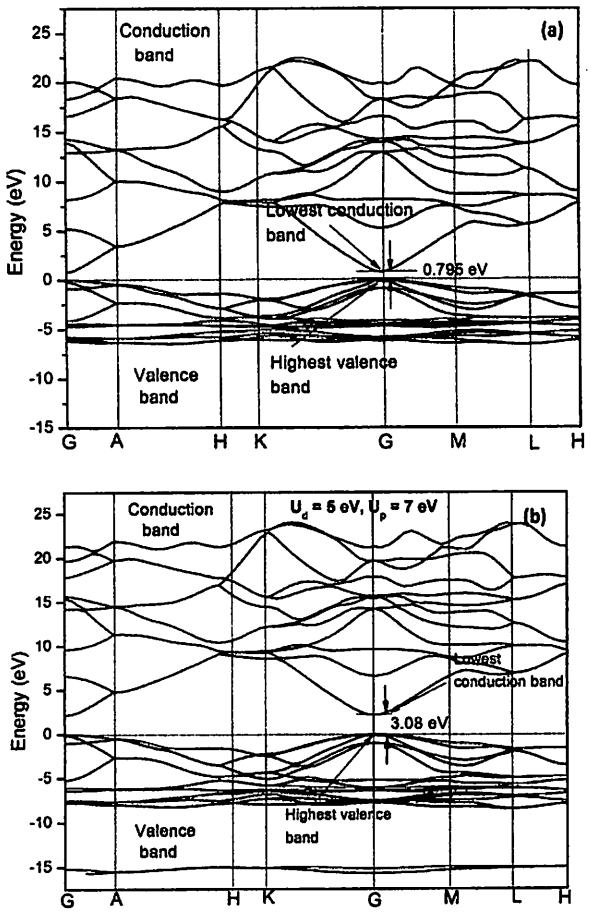

Figure 8:

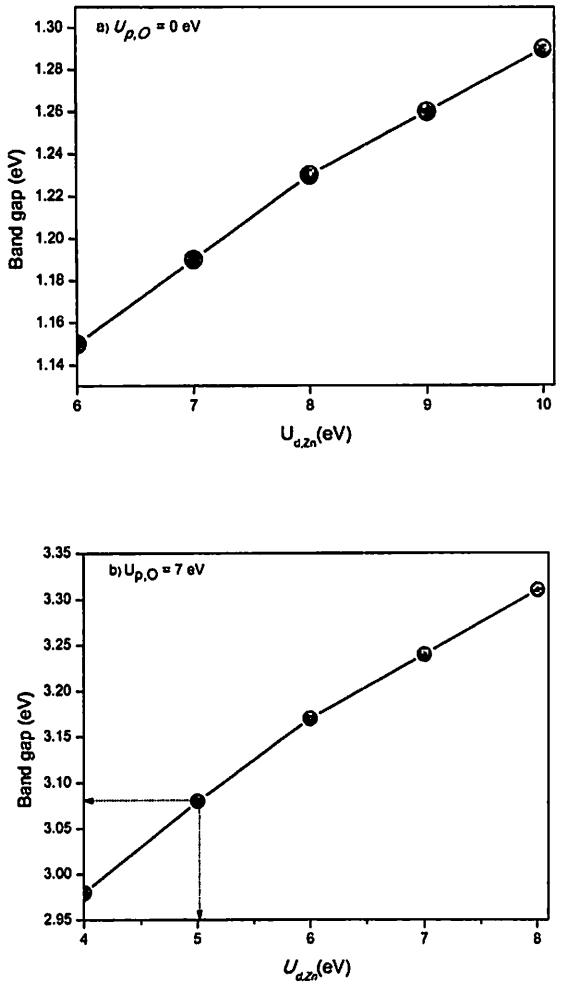

Figure 9:

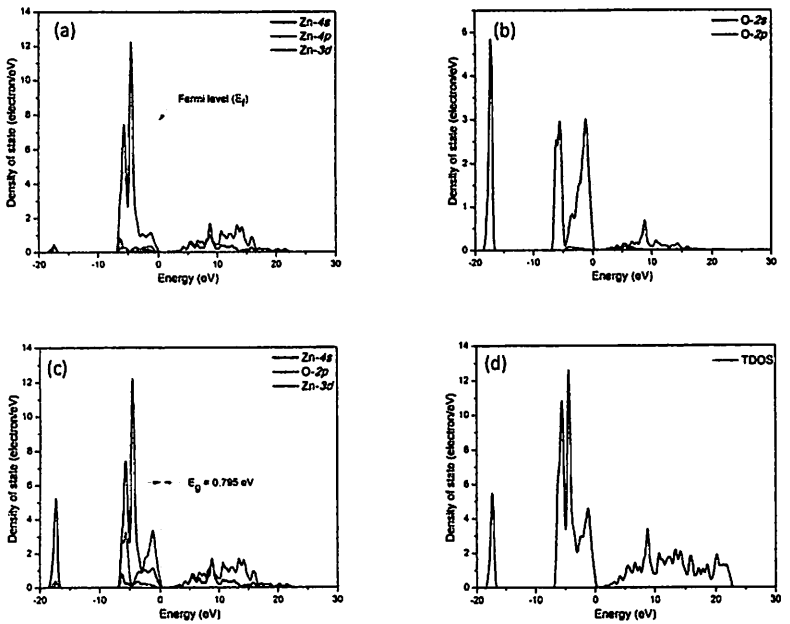

Figure 10:

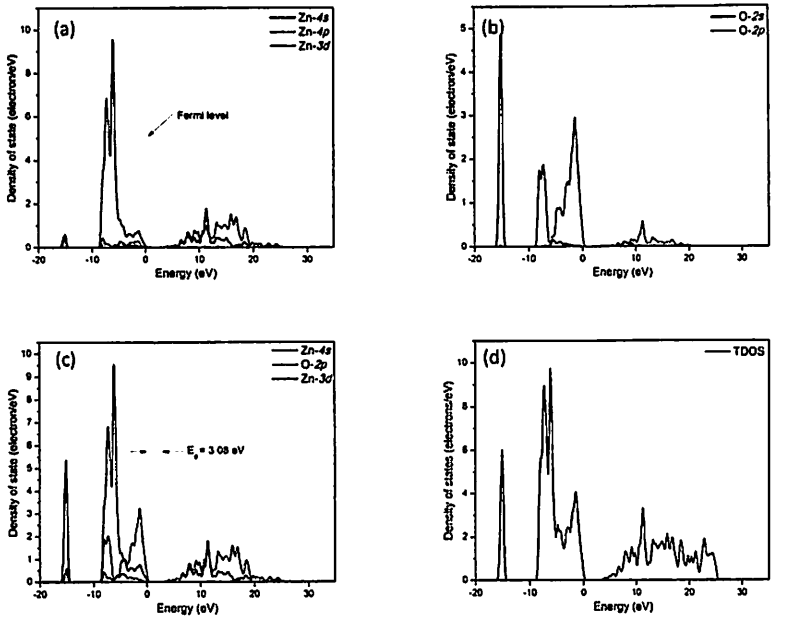

Figure 11:

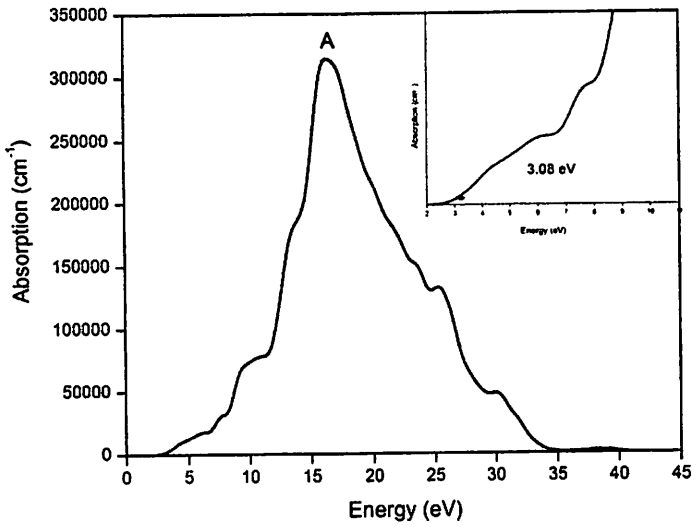

Figure 12:

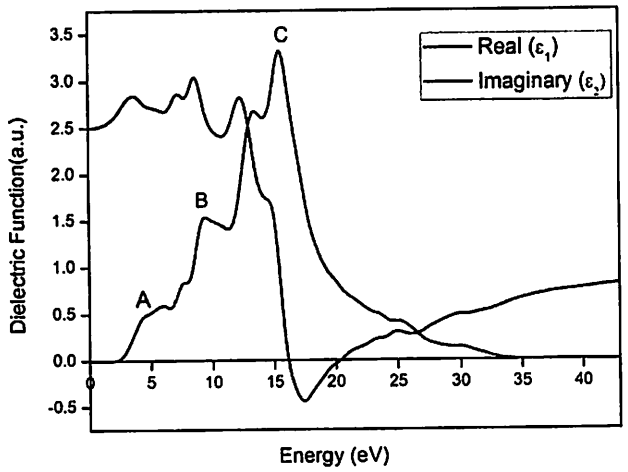

Table 1:

Parameter	ICSD (98-010-6787)			Rietveld-refinement (This work) Before calcination		After calcination
Crystal system	Hexagonal			Hexagonal		
Space group	*P6₃mc* (186)			*P6₃mc* (186)		
a (Å)	3.253			3.253		3.249
b (Å)	3.523			3.253		3.249
c (Å)	5.211			5.209		5.207
Alpha (°)	90			90		90
Beta (°)	90			90		90
Gamma (°)	120			120		120
Volume ($V/10^6 pm^3$)	47.76			47.690		47.622
Crystallite sizes (Å)	-			50.26		84.84
Atomic position	x	y	z	x	y	z
Zn	0.3333	0.6667	0	0.3333	0.6667	0
O	0.3333	0.6667	0.375	0.3333	0.6667	0.375

Table 2:

Parameter	Before calcinations	After calcinations
R_{wp}	15.68	15.57
R_{exp}	10.39	9.93
GoF	2.28	2.46

Table 3:

U_d values for Zn 3*d*	U_p values for O 2*p*	Functional	Band gap (eV)
7	0	LDA + U	1.19
8	0	LDA + U	1.23
9	0	LDA + U	1.26
10	0	LDA + U	1.29
4	7	LDA + U	2.98
5	7	LDA + U	3.08
6	7	LDA + U	3.17
7	7	LDA + U	3.24
8	7	LDA + U	3.31
8	8	LDA + U	3.59

FIRST-PRINCIPLES DENSITY FUNCTIONAL THEORY CALCULATIONS ON ZINC OXIDE GROWTH MECHANISM

NORSAKINAH BINTI MANSOR

KAUSAR BINTI HARUN

AHMAD AZMIN MOHAMAD

ACKNOWLEDGEMENTS

Ministry of Science Technology and Innovation for financial support under Fundamental Research Grant Scheme (203/PBAHAN/6071262 and FRGS/2/2013/TK04/USM/02/1).

TABLE OF CONTENTS

LIST OF TABLES

LIST OF FIGURES

LIST OF ABBREVIATIONS

CASTEP	Cambridge Serial Total Energy Package
VASP	Vienna Ab-initio Simulation Package
ABINIT	Ab-initio Package
DOS	Density of States
PDOS	Partial Density of States
TGA	Thermogravimetry Analysis
XRD	X-ray Diffraction
FESEM	Field Emission Scanning Electron Microscopy
UV-Visible	UV-Visible Spectroscopy
UV	Ultraviolet
LDA	Local Density Approximation
U	Hubbard-U
DFT	Density Functional Theory
EDX	Energy Dispersive X-Ray
DSSC	Dye-sensitize solar cell
ICSD	Inorganic Centre of Structural Data

LIST OF SYMBOLS

^{o}	Degree
λ	Wave length
>	More than
%	Percentage
Wt. %	Weight percent
^{o}C	Degree Celsius
$^{o}C\ min^{-1}$	Degree Celsius per minute
nm	Nanometer
hr	Hour
R	Reflectivity
n	Refractivity index
L	Energy-loss function
α	Absorption coefficient
$\hat{H}$	Hamiltonion operator
φ	wavefunction
E	Energy
E_g	Band gap energy
P_1	Momentum of the ions
P_2	Momentum of the electrons
m	Mass
Z	Charge of the ion

LIST OF CHEMICAL FORMULA

$Zn(CH_3COO)_2.2H_2O$	Zinc acetate dihydrate
CH_3OH	Methanol
$NaOH$	Sodium hydroxide
H_2O	Deionized water
$Zn(OH)_2$	Zinc hydroxide
$Zn(OH)_4^{2-}$	Zincate ion

FIRST-PRINCIPLES CALCULATIONS OF ZINC OXIDE NANOPARTICLES PROPERTIES USING LOCAL DENSITY APPROXIMATION CORRECTED BY HUBBARD-U

ABSTRAK

ZnO nanopartikel telah disediakan melalui kaedah penyimpanan sol-gel menggunakan zink asetat dihidrat sebagai bahan pemula dan metanol sebagai pelarut utama. Masa yang optimum dalam pembentukan nanopartikel ZnO yang berkualiti telah dikaji. Pembentukan nanopartikel ZnO yang berkualiti tinggi telah diperoleh apabila masa penyimpanan dipanjangkan selama 12 jam. Analisis jurang jalur diperolehi melalui eksperimen bagi partikel nano ZnO adalah 3.06 eV dan digunakan sebagai perbandingan dengan jurang jalur yang diperolehi melalui kedah prinsip pertama. Suhu pembakaran 600 °C telah dipilih untuk pertumbuhan kristal yang lebih baik bagi ZnO nanopartikel. Pembentukan ZnO nanopartikel dengan penghabluran tinggi selepas pembakaran telah dibuktikan dengan analisis fasa dan struktur kuantitatif dengan menunjukkan parameter kekisi a = b = 3.249 Å, c = 5.207 Å. Morfologi nanopartikel ZnO menunjukkan pembentukan yang hampir seragam dengan saiz purata 67 nm. Pengiraan prinsip pertama telah digunakan untuk mengkaji jurang jalur dan sifat optik nanopartikel ZnO. Pengiraan ini menggunakan anggaran ketumpatan tempatan dan diperbetulkan oleh Hubbard-U. Jurang jalur yang diperolehi (0.795 eV) melalui fungsi LDA rendah dan dengan menggunakan LDA + U, jurang jalur yang diperolehi (3.08 eV) menunjukkan keputusan yang selari dengan jurang jalur eksperimen (3.06 eV). Ciri optik ZnO nanopartikel seperti penyerapan, indeks biasan, pantulan dan fungsi kehilangan tenaga juga telah dikira. Ia menunjukkan bahawa ZnO nanopartikel berada di fasa ultraungu (UV).

FIRST-PRINCIPLES CALCULATIONS OF ZINC OXIDE NANOPARTICLES PROPERTIES USING LOCAL DENSITY APPROXIMATION CORRECTED BY HUBBARD-U

ABSTRACT

ZnO nanoparticles were prepared by sol–gel storage method using zinc acetate dihydrate as precursor and methanol as a main solvent. The optimum aging time for the formation of good quality and pure ZnO nanoparticles was studied. High purity of ZnO nanoparticles were obtained upon prolonged the storage time to 12 hours. The obtained experimental band gap for ZnO nanoparticles was 3.06 eV which was used as comparison with the band gap obtained from first-principles calculation. The calcination temperature 600 °C was selected for optimum crystalline growth of ZnO nanopaticles. The high crystallinity of ZnO nanoparticles formation after calcination was proved by phases and structural quantitative analysis with lattice parameter a = b = 3.249 Å, c = 5.207 Å. The morphology of ZnO nanoparticles showed nearly uniform shape with average particles size at 67 nm. Then, first principles calculation was used to study the structural, electronic band structure, density of states and optical properties of ZnO nanoparticles. This calculation was implemented using local density approximation and corrected by the Hubbard-U. The band gap (0.795 eV) obtained using LDA functional was underestimate and by adopted LDA + U functional, the calculated band gap (3.08 eV) was comparable with the experimental band gap (3.06 eV). The optical properties of ZnO nanoparticles such as absorption, refractive index, reflectivity and energy loss function were calculated. It showed that ZnO nanoparticle was in ultraviolet (UV) range.

CHAPTER 1

INTRODUCTION

1.0 Background

Zinc Oxide (ZnO) is a multifunctional material pertaining to its unique physical and chemical properties, such as high chemical stability, high electrochemical coupling coefficient, broad range of radiation absorption and high photostability. The variety structures of ZnO make it classified among new materials with potential applications in many fields of nanotechnology. ZnO can occur in one, two, and three-dimensional structures. In recent years, one-dimensional (1D) nanostructures such as rods, wires, tubes and particles attracted much attention due to its unique properties make it potential to be use in electronics, optoelectronics, and dye-sensitize solar cell (DSCC) [1].

ZnO is used as a photoanode material in DSSC. They serve as a medium for electrons transportation to conducting substrate upon sunlight exposure. The efficiency of ZnO to utilize the lights is one of the main important issues and it is highly rely on the band gap energy [2]. The formation of ZnO nanoparticles with desired band gap energy can be carried out experimentally which later involve certain synthesis route and controlling several parameters. ZnO are commonly synthesized by sol-gel method as the morphology of the nanoparticles could be easily controlled.

ZnO nanoparticles characterization is of utmost significance to establish understanding and control of ZnO nanoparticles during the synthesis. The quality of phases form, morphology, structural information and properties of ZnO nanoparticles are determined from several characterization testing. The ZnO nanoparticles can be characterized by several machine and probes such as X-ray diffraction, thermogravimetric analysis, scanning electron microscope, and UV-visible spectroscopy.

Normally, experimental required several testing equipment which are high in cost, longer time and many test is needed to determine the electronic and optical properties. By performing first-principles calculation, these properties could be easily determined with less equipment and time required to obtain the result of those properties. The accuracy is also high as it can predict the ground state properties of ZnO nanoparticles. First-principles calculations are based on the quantum mechanics by means it described the electron and nuclei interaction.

Various computer codes were used for first-principles calculations such as Vienna Ab-initio Simulation Package (VASP), Ab-initio Package (ABINIT) and Cambridge Serial Total Energy Package (CASTEP). Among this code, CASTEP computer code was the most popular used. CASTEP uses a plane wave basis set and a pseudopotential within the frame-work of Kohn–Sham density functional theory (DFT) [3]. This computational study allowed the calculation of electronic and optical properties of ZnO nanoparticles using several approximations.

1.1 Problem statement

The formations of high purity ZnO nanoparticles are essential as it will affect the resulting properties, especially the electronic and optical properties. Being the most commonly used technique, the sol-gel method is best to be employed in view of their simplicity, repeatability, relatively mild synthesis condition and low production cost. As compared with sol-gel centrifuge method, storage is preferred as it efficiently separate species of different sizes, masses, or densities. By using storage method, all the desirable properties can be obtained closed to the experimental. In fact, storage method can improve the structural, morphological, and optical properties of ZnO compared with centrifuge method.

During aging, the ZnO sol will stabilize and slowly form nanoparticles. Time then become a key factor to be considered in sol-gel synthesis. An appropriate aging will allow a fine formation of ZnO structure with good optical properties. By considering practical application, the ZnO nanoparticles are expected to be prepared as soon as possible with a promising quality. Therefore, it is important to reduce the storage time during synthesis of ZnO nanoparticles. Previous study shown that ZnO nanoparticles are produced after 48 hours of storage at ambient temperature without being disturbed by other system [4]. Thus, there is need to the investigation of producing ZnO nanoparticles with lesser storage time.

As the synthesized ZnO nanoparticles produced, the electronic and optical properties could be experimentally examined via physical testing or computationally calculated. By knowing the advantages of using computational method, the selection of best yet simple approximations that underlay beneath DFT is crucial. Several attempts that

employed local density approximation (LDA) functional had shown an underestimation value of electronic properties [5]. However, this conventional LDA approach is collapsible for strongly correlated transition element cases that cannot efficiently describe the localization of strongly correlated *d* and *f* electrons. Thus, the method based on LDA with semi-empirical Hubbard-U (LDA + U) was applied to correct the performance and accuracy of the Kohn–Sham plane-wave DFT method.

1.2 Objectives

In this work, there are two main objectives which are:

i. To synthesize and characterize ZnO nanoparticles prepared via sol-gel storage method

ii. To determine the electronic and optical properties of synthesized ZnO via first-principles calculation.

1.3 Scope of thesis

Chapter 1 presents an overview to the thesis with a brief explanation on the problems and the objectives of the study. Chapter 2 reviews the nature of ZnO properties as promising materials for DSCC application as well as some basic concepts regarding the mechanism of ZnO with significant existing literature studies. Besides, the fundamental knowledge behind the synthesis route and characterization technique of ZnO nanoparticles are discussed. At the end of Chapter 2, the underlying concept behind first-principles calculation is elaborated. Also, the used of computational method to determine electronic and optical properties of ZnO by other researchers are discussed.

CHAPTER 2

LITERATURE REVIEW

2.0 Introduction

This chapter presents a review from other literatures that are related to this research. Generally, it is divided into two major parts which are:

i. The structure, properties and synthesis route of ZnO nanoparticles by sol-gel method

ii. The first-principles method and the underlying typical calculation procedures

2.1 General properties of ZnO

Over the years, ZnO has been astonishingly investigated due to their diverse applications. ZnO is one of the earliest materials studied in gas sensor devices due to high electron mobility and good thermal stability under operating conditions [6]. To date, ZnO nanoparticles are widely incorporated as building blocks in electronic and optoelectronic devices, actuator and solar cell [7]. ZnO crystallized in three distinct crystal structure namely stable wurtzite crystal structure under ambient conditions, rock salt structure which is obtained at relatively high pressure and zinc blend structure upon growing from the cubic substrate [8]. Among these three, wurtzite structure with space group $P6_3mc$ is widely synthesized and studied [9, 10].

ZnO is a wide band gap oxide semiconductor with band gap energy 3.44 eV at low temperature and 3.37 eV at ambient temperature [11]. The wide band offers the electronic transition to occur down to visible light region. This process is enhanced with the nature of

a direct type band structure. It is commonly define as an occurrence of lowest conduction band and highest valence band located at the same k-point along Brillouin zone. This behavior results in more effective electron excitation and photon emission process. ZnO also owned a large binding energy (60 meV) which persist the event of excitonic absorption and recombination between electron and hole even at room temperature [12]. Larger excitons binding energy are desirable as greater stability against thermal dissociation could be achieved.

2.2 Brief on sol-gel route

In literature, the selections of practical and effective technique to produce ZnO nanoparticles are carefully studied. It does include the feasibility to obtain a good quality of nanoparticles, ease control of the starting materials and design parameters, reasonable cost and short production time. All these advantages are greatly owned by sol-gel method [7]. As a wet chemical route, sol-gel allows the production of solid materials from a solution initiated by sol or gel at much lower temperature than other possible method such as laser ablation, hydrothermal, electrochemical depositions, chemical vapor deposition, thermal decomposition [13].

Basically, sol-gel process involves the use of precursor, solvent, additive and in certain case, a stabilizer. In recent years, the commonly used zinc precursor in sol-gel process is metal salt. Nitrate, chloride, perchlorate and acetate are among the ligands that attached to zinc atom forming a metal salt. Metal alkoxide such as ethoxide and propoxide is also used during synthesis as they react readily with water. Since alkoxides and water

are immiscible, a common solvent, such as an alcohol (ethanol, methanol, isopropanol) were used [14].

In the synthesis work, it is crucial to highlight the mechanism and reaction behind every stage. Generally, sol-gel occurs in four stages of transformations which are hydrolysis, condensation and polymerization, growth of particles, and aging. The growth mechanism of ZnO nanoparticles are influenced by the pH, precursor concentration, aging time, and annealing temperature [15-17]. In most cases where acetate dihydrate were used as precursor, they will first being solvated in preferred solvent to produce a zero charged precursor [15].

In the first stage, the intercalated acetate ions are removed followed by the production of metal hydroxide colloidal. Both Alias et al. [15] and Dutta and Ganguly [18] agreed zinc precipitated as zinc hydroxide [$Zn(OH)_2$] during hydrolysis stage (Eq. 2.1). Further reaction between $Zn(OH)_2$ and water (H_2O) thus form the growth unit of zincate ion [$Zn(OH)^{2-}_4$] (Eq. 2.2). At this stage, high chemical potential of OH^- are necessary to ensure the conversion of zincate ion to ZnO that changed initial pH from 5 to 12 (Eq. 2.3). Eq. 2.1 to 2.3 summarized the reaction between zinc acetate dihydrate, methanol, and sodium hydroxide.

$$Zn(CH_3COO)_2.2H_2O + 2NaOH \rightarrow Zn(OH)_2 + 2CH_3COONa + 2H_2O \quad \text{Eq. 2.1}$$

$$Zn(OH)_2 + 2H_2O \rightarrow Zn(OH)_4^{2-} + 2H^+ \quad \text{Eq. 2.2}$$

$$Zn(OH)_4^{2-} \rightarrow ZnO + H_2O + 2OH^- \quad \text{Eq. 2.3}$$

From the structural point of view, the zinc acetate dihydrate [$Zn(CH_3COO)_3$] which in octahedral form later changed to tetrahedral $Zn(OH)_2$ coordination upon titration with methanol (CH_3OH). Soon after filtration, excess washing and drying, a partially ordered ZnO produced. At this stage, the ZnO can be describing as a tetrahedral coordinated structure that stacks among each others. If sufficient heat is applied, the tetrahedral structures rearrange and form alternating plane at each corner [7]. Besides, the starting materials used also will affect the chemical reaction that occurred. The selection of starting materials toward the production of ZnO nanoparticles are tabulated in Table 2.1.

Table 2.1: Production of ZnO nanoparticles via sol-gel method

Method	Materials	Synthesis conditions	Particles size and shape	References
Sol-gel	Zinc acetate dihydrate, oxalic acid, ethanol	Reactions: 50 °C, 60 min; Dried of gel: 80 °C,20 hr; Calcined: under flowing air for 4 hour at 650 °C	Hexagonal wurtzite structure, uniform, spherically shaped of particles	[19]
	Zinc acetate dihydrate, methanol	Reaction: room temperature; Centrifuge: 3000 rpm, 30 min; Aging:48 hr; Drying;120 °C, 2 hr	Hexagonal wurtzite structure, uniform and spherically shaped of particles	[4]
	Zinc 2-ethylhexanoate, ethanol, 2-propanol	Reaction: room temperature; Drying: 60 °C	Cylinder-shaped crystallites, D: 25–30 nm, L: 35–45 nm	[20]

2.3 Properties of ZnO synthesized by sol-gel method

The phase identification, morphological study, elemental analysis and optical properties are studied by various technique and method to characterize ZnO nanoparticles. This can be achieved using several spectroscopy which are thermogravimetry analysis (TGA), X-ray diffraction (XRD), scanning electron microscopy (SEM) coupled with auxiliary energy dispersive X-ray (EDX) and UV-Visible spectroscopy (UV-Vis).

2.3.1 Thermal properties of ZnO

The thermal properties of synthesized ZnO nanoparticles are analyzed by TGA. The TGA is used to measure the mass change of a pure ZnO material as a function of temperature and time, in a controlled atmosphere. It is ideally avail to access volatile content, thermal stability, degradation characteristics, and reaction kinetics of the ZnO nanoparticles [21]. The TGA curve is plotted by percentage of mass loss (wt %) versus temperature (^{o}C). From the typical TGA curve, zero mass loss steps will be analyzed as it indicated the eliminations of all impurities for ZnO nanoparticles which are important for the calcinations process.

Bagheri et al. [22] performed thermal analysis of pure ZnO synthesized by sol-gel method in the temperature range of 30 °C to 800 °C. The TGA curve shows two mass loss steps in temperature ranges 30-150 °C and 160-450 °C (Figure 2.1). A gradual weight loss (18.9 %) is observed at the first region. This is mainly attributed to the evaporation of surface adsorbed water. The second mass loss step occurred at 160-450 °C result in weight loss about 32.6 %. It is believed that volatilization and combustion of organic species

occurred in this region. After 400 °C, no more weight loss recorded, indicating a full decomposition of all complexes.

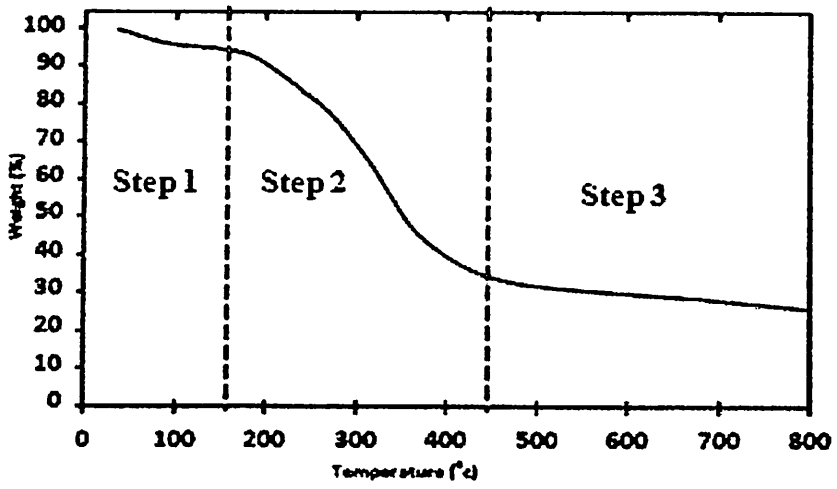

Figure 2.1: TGA curve of pure ZnO samples in normal air at 5 °C/min [22]

By using the similar method, Adly et al. [23] also described the TGA curve for pure ZnO. However, their TGA curve shows only a small weight loss which is due to the evaporation of the moisture and volatile materials. The thermal stability of ZnO nanoparticles which indicated the elimination of impurities observed from this curve is identified at temperature above 400 °C. Based on this literature, it can be deduced that ZnO stabilized at T > 400 °C depending on the starting materials used. Thus, the calcinations of as-synthesized ZnO can be deduced at temperature more than 400 °C.

2.3.2 Phases properties of ZnO

The XRD is a powerful technique for structural determination of ZnO nanoparticles as it provides information on the phases that present in synthesized ZnO samples [13]. From the XRD graph of intensity (cps) against 2θ (°) that is plotted, the intensity which indicated the degree of crystallinity and peak broadening which indicated the crystallite size of ZnO are observed [21].

An instance, Ghosh et al. [24] described the diffraction pattern of ZnO nanoparticles that successfully synthesized by sol-gel method with zinc acetate dihydrate is used as precursors. Their work focused on the effect of different calcinations temperature on pure ZnO (Figure 2.2). By matching with the standard data JCPDS 76-0704, the phase present on the synthesized materials is confirmed as ZnO phase with hexagonal wurtzite structure. By comparing 3 different peaks, they concluded that ZnO sample calcined at 900 °C give the best calcinations temperature for pure ZnO as the crystallinity improved and the size of particles become bigger.

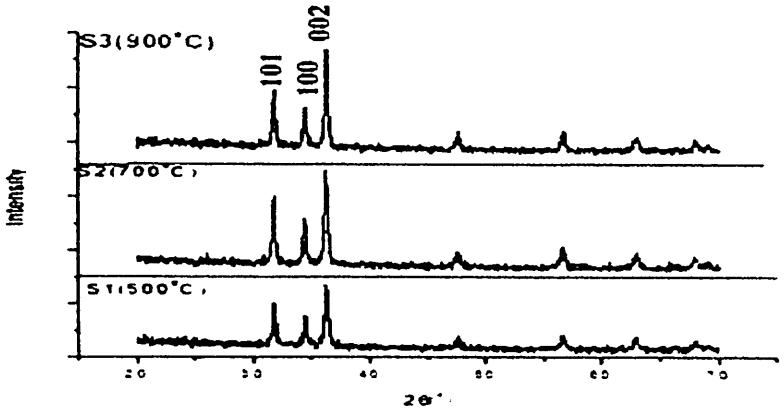

Figure 2.2: Comparison of XRD for three sample S1, S2 and S3 calcined at 500 °C , 700 °C and 900 °C, respectively [24]

As comparison with the previous literature, Dutta and Ganguly [18] also determined the phase of synthesized ZnO under the same synthesis method and precursor. They determined the effect of different concentration of folic acid on the formation of ZnO using XRD technique. The diffraction pattern shows a good agreement with the standard XRD peaks (JCPDS card No. 36–1451) and confirmed the phase present is hexagonal wurtzite ZnO structure. All the ZnO samples showed high crystallinity except for the sample with 4.8 % of folic acid which showed partial crytallinity which is due to the high concentration of ensconced folic acid molecules present in the sample.

2.3.3 Structural quantitative properties of ZnO

The quantitative analysis can be extended through Rietveld-refinement method. It is also known as secondary analysis of XRD patterns after the phase identification process. This technique create a virtual separation of the overlapping peaks, thereby provide an accurate determination of the crystalline structure and atomic parameters of ZnO materials [25]. From Rietveld-analysis, the structural parameter such as lattice dimension, profile shape, preferred orientation and atomic coordination are refined.

When a Rietveld calculation is performed, it is necessary to analyze the efficiency of the fittings based on the residual (R) values. The R weight profiles (R_{wp}), R expected profiles (R_{exp}) and goodness of fit (GOF) are used as a way of addressing the values obtained after the fitting calculations are performed [26]. For an acceptable refinement, the values of R_{wp} must be less than 10 % and GOF must be less than 2 % [27]. The ideal GOF value is found to be 1 which indicated the perfect fitting for ZnO sample. The values of R_{wp}, R_{exp} and GOF are derived from Eq. 2.4 to 2.6:

$$R_{wp} = [(\sum wi(y_i(obs) - y_i(calc))^2)/(\sum w_i(y_i(obs)^2))\ ]^{1/2} \quad \text{(Eq. 2.4)}$$

$$R_{exp} = [(N - P)/(\sum w_i(y_i(obs)^2))]^{1/2} \quad \text{(Eq. 2.5)}$$

$$GOF = [(S_y)/(N - P)]^{1/2} = R_{wp}/R_{exp} \quad \text{(Eq. 2.6)}$$

whereby y_i = intensity at the i-th step, w_i = weighting factor, N = number of observations, P = number of parameters, *obs* = observed and *calc* = calculated.

The R factors and GOF obtained from refinement of ZnO nanoparticles are summarized in Table 2.2. R_p and R_{wp} are found to be slightly large. This is due to the lower value of diffraction peak to background ratio was low which is due to its nanocrystalline nature. The GOF value observed is closed to 1 which indicated an acceptable structure of experimental data [28]. The Rietveld-refinement that yields an acceptable lattice parameter and unit cell volume of ZnO are obtained by Kumar et al. [28] and Brehm et al. [29].

Table 2.2: Reliability factors, lattice constant, and crystallite size of pure ZnO sample [28]

Parameters	Values
R_p (%)	10.1
R_{wp} (%)	13.1
R_{exp} (%)	8.33
R_B (%)	6.48
R_F (%)	4.17
GOF	1.81
a=b (Å)	3.25094(33)
c (Å)	5.20753(33)
Crystalline size (nm)	20

2.3.4 Morphological and elemental properties of ZnO

The morphology, chemical composition, and crystalline structure of the synthesized ZnO nanoparticles are determined using FESEM. The FESEM provides high-resolution and long-depth-of-field images of the ZnO sample surface. Various magnifications are used to demonstrate ZnO morphology. ZnO nanoparticles synthesized by sol-gel method are expected to produces hexagonal structure [30]. Coupled to FESEM, EDX is used for the elemental analysis or chemical characterization of a ZnO sample [1].

Bhatt et al. [31] described the morphology of synthesized ZnO particles by sol-gel method as they study the growth and characteristics of pure and doped ZnO (Figure 2.3). In general, pure ZnO particles have hexagonal rod like morphology and most of the particles have holes. The particles size also is found to be larger. This indicated that nanoparticles are not a single crystal but consist of smaller coherently diffracting domains. These may arise due to presence of various lattice defects. It is also possible that growth of particles may be taking place by development of small crystals which coalesce to give rise to larger particles.

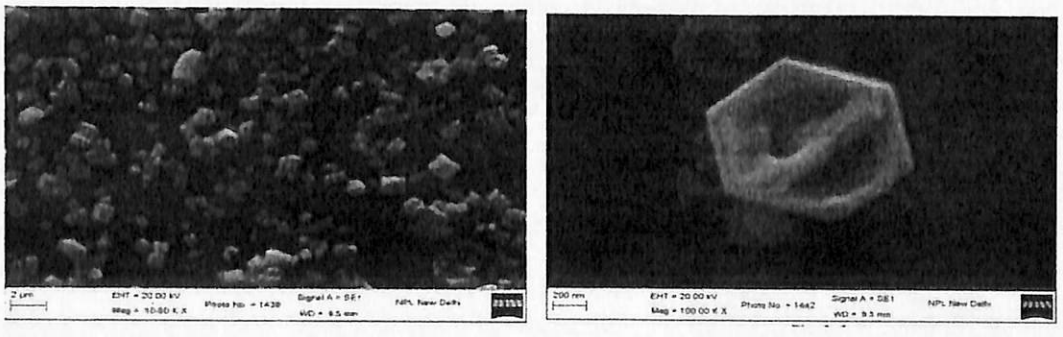

Figure 2.3: (a) SEM micrograph and (b) cross-sectional view of single hexagonal particle of pure ZnO sample [31]

On the other hand, Ghosh et al. [24] which study the effect of calcinations temperature on morphology synthesized by the same method showed the spherical hexagonal structure of ZnO nanoparticle (Figure 2.4). The ZnO sample calcined at 900 °C produced larger particle size compared to calcined at 700 °C. This indicated that the nucleation and growth rate increase with increase in calcination temperature. Thus, higher calcinations temperature increases the size of ZnO nanoparticles.

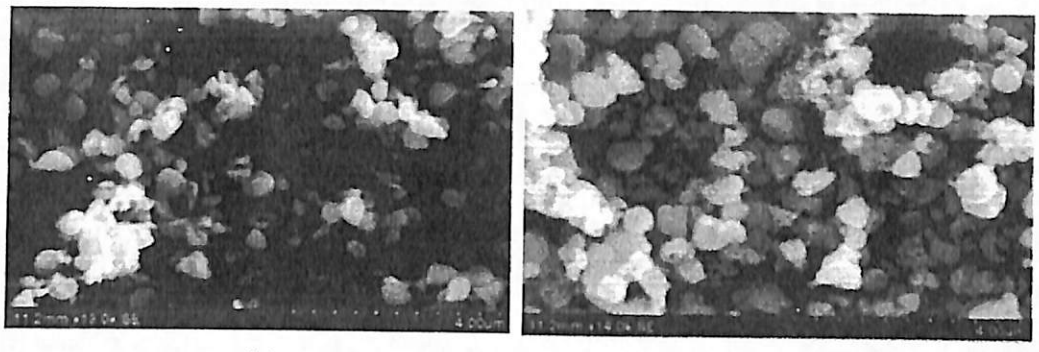

(a) (b)

Figure 2.4: SEM of sample calcined at (a) 700 °C and (b) 900 °C for 4 hours [24]

2.3.5 Band gap properties of ZnO

As ZnO nanoparticles are widely used in dye sensitize solar cell (DSCC), the optical properties become crucial. To examine the optical properties of ZnO nanoparticles, UV-visible absorption spectroscopy is commonly used. UV-visible analysis is important as it can measure the absorbance or transmittance of ZnO nanoparticles from the UV range to the visible wavelength range. From UV-Vis analysis, the absorption spectra of ZnO nanoparticles can be analyzed and usually recorded in the wavelength range of 200 nm to 800 nm [32]. The absorption behavior can be expressed from the graph of absorption coefficient, α versus wavelength (nm) and transmittance (%) versus wavelength (nm).

From the extrapolation plot, the absorption edge was analyzed which is important to identified the band gap (E_g) values.

Kumar et al. [33] showed the absorption spectrum of ZnO nanoparticle quantum dots synthesized via sol-gel method. The spectrum exhibits a strong absorption peak at 298 nm (Figure 2.5). The significant sharp absorption of ZnO structure indicated the monodispersed nature of the nanoparticles distribution. The E_g of ZnO nanoparticles obtained is found to be 3.27 eV using Tauc plot [$(\alpha h\nu)^2$ versus $h\nu$], corresponding to the bulk ZnO. The calculated E_g of ZnO nanoparticles are depended on different synthesis method. Table 2.3 listed the calculated E_g of ZnO nanoparticles obtained from different synthesis methods.

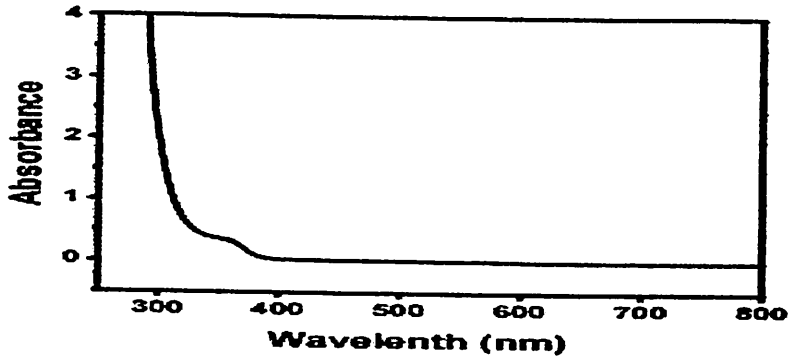

Figure 2.5: UV-vis absorption spectrum of ZnO nanoparticles [33]

Table 2.3: The experimental band gap of ZnO nanoparticles obtained from different synthesis methods

Synthesis method	Calculated band gap (eV)	References
Hydrothermal	3.08	[34]
Microemulsion	3.06	[35]
Sol-gel	3.02	[36]
	3.14	[15]

The transmittance spectra of the samples by UV-Vis spectroscopy can be used to study the effect of aging time on optical properties of ZnO films (Figure 2.6). It is found that all the samples exhibit transmittance above 65 % in the visible range. Increasing the storage time improve the strong absorption properties of ZnO films in visible range but do not influence in the ultraviolet range. The absorption edge for all the samples lied at ~370 nm. Basically, there are two major factors that affect the transmittance which is surface scattering and grain-boundary scattering. It is found that irregular shape of grain boundary inducing a low transmittance in the visible range [16].

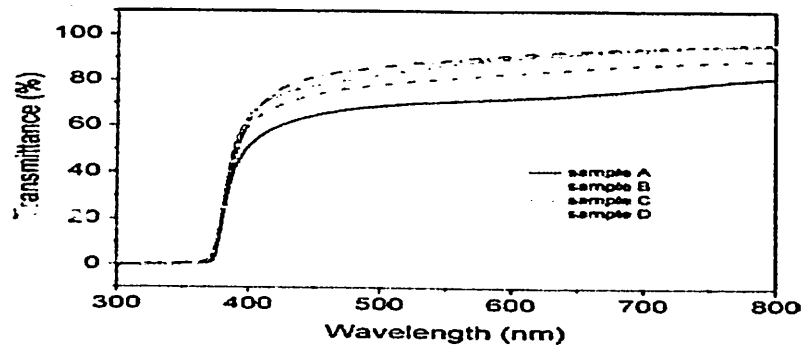

Figure 2.6: The transmission spectra of pure ZnO [16]

2.4 First-principles calculation

2.4.1 Density functional theory

An "Ab initio" or "First-principles" is computational methods that are useful for structural, electronic and optical properties identification of ZnO nanoparticles. Usually, the plane-wave soft-pseudopotential approached is applied to calculated this properties using Cambridge Serial Total Energy Package (CASTEP) computer code [37]. The pseudopotential approached is one of the fastest currently available methods. Efforts are

being made to develop faster techniques without sacrificing the accuracy of the calculation [38]. First-principles calculation is based on the quantum mechanics. Initially, the equation for first-principles calculation is extracted from the set of one electron Schrodinger (Kohn Sham) wave function equation which can be expressed in Eq. 2.7 as [39]:

$$\hat{H}\varphi = E\varphi \qquad \text{Eq. 2.7}$$

whereby, $\hat{H}$ is the Hamiltonion operator, φ is the wavefunction, and E is the energy of the system. This wavefunction depends on the coordinates of the electrons and nuclei.

The Hamiltonion equation, $\hat{H}$ in the Schrodinger equation composed of several parts which described the kinetic and potential energies due to coulomb interaction of a system of atomic nuclei and electrons. In Hamiltonian equation, many-atom system is treated as it composed of electrons and nuclei without considered the empirical parameter [40]. Eq. 2.8 described the Hamiltonian equation as:

$$\hat{H} = \sum_{I=1}^{N} \frac{P_I^2}{2M_I} + \sum_{i=1}^{n} \frac{P_i^2}{2m_i} + \sum_{i>j} \frac{e^2}{|r_i - r_j|} + \sum_{I>J} \frac{Z_I Z_J e^2}{|R_I - R_J|} - \sum_{i,I} \frac{Z_I e^2}{|R_I - r_i|} \qquad \text{Eq. 2.8}$$

Kinetic energy nuclei	Kinetic energy electron	Coulomb interaction electron	Coulomb interaction nuclei	Coulomb interaction electron + nuclei

whereby, P_1 and P_2 refer as momenta of the ions and electrons, r and R refers to the coordinates of electrons and ions, Z and e the charge of the ion and electron, m and M their masses. However, Eq. 2.8 is very complex differential equation. Thus, to make the equation computionally controllable especially in a system of many-particles, several approximations have been made.

There are many approaches that had been developed to accurately solve the complexity of Schrodinger equation. Among them, density functional theory (DFT) is one of the most successful methods. The basic concepts of DFT are introduced by Hohenberg and Kohn (1964) and Kohn and Sham (1965) in which they proved that the uniquely density of electrons determines the external potential which related to the nuclei-electron interactions up to a constant [41]. The minimum value of the total energy functional is the ground-state energy of the system. Thus from DFT theory, the potential determined all ground stated properties of the system by formulated the density of electron which is used as basic variable [42].

However, the kinetic energy and coulomb interaction energy from the Hamiltonian equation are unknown so that the accuracy method was essential to the approximation of the exchange-correlation energy. Thus, the accuracy of the DFT calculation depends on the quality of exchange-correlation (XC) energy approximation [39]. There are four types of XC energy approximation which are generalized gradient approximation (GGA), meta-GGA hybrid functional and local density approximation (LDA) but the most extensive approximation used for ZnO nanoparticles is LDA functional [37].

2.4.2 Local density approximation

The LDA functional states that, for regions of a material where the charge density is slowly varying, the XC at that point can be considered the same as that for a locally uniform electron gas of the same charge density. The use of the LDA considerably simplifies the solution of the Schrodinger equation by mapping it into a single-electron equation [38]. In LDA, the equation E_{XC}^{LDA} is described as Eq. 2.9:

$$E_{XC}^{LDA}[\rho] = \int \rho(r)\varepsilon_{XC}[\rho]dr \qquad \text{Eq. 2.9}$$

whereby, E_{XC}^{LDA} represents the exchange-correlation energy per electron of a uniform electron gas, $\rho(r)$ is ground state of electron density and ε_{XC} refers to exchange correlation set. However, this conventional LDA function approach tends to underpredict atomic ground state energies and ionisation energies, while overpredicting binding energies. It is also known to overly favour high spin state structures [43].

This underestimation of the band gap is the result of well-known limitations related to the standard used in DFT. The failure in DFT is due to the failure in coulomb interactions among orbital electrons. Thus, for these reasons the modification and improvement of this functional have been attempts to move beyond the LDA, by adopted LDA + Hubbard-U (LDA + U) functional [5]. The LDA + U functional are accurately determined the electronic and optical properties of ZnO nanoparticles.

2.4.3 Local density approximation with Hubbard-U

The Hubbard-U approximation or LDA + U is implemented in order to treat the strong on-site coulomb interaction of localized electrons, which is not correctly described by LDA functional [5]. The on-site coulomb interactions are particularly strong for localized $d + f$ electrons, but can be also important for p localized orbitals [44]. The strength of the on-site interactions was described by parameters U (on site Coulomb) and J (on site exchange). These parameters U and J can be extracted from ab-initio calculations, but usually are obtained semi-empirically [42].

Expressed in terms of the Hubbard model, the Hamiltonian made up of two components. The first component is typically represented by the letter J as it represents the kinetic energy of electrons hopping between atoms. The second term in the Hubbard model is then the on-site repulsion, typically represented by the letter U because it represents the potential energy arising from the charges on the electrons [40]. Written out in second quantization notation, the Hubbard-Hamiltonian then takes the form in Eq. 2.10 as:

$$H = -J\sum_{(i,j),\sigma}(c_i^t\, c_{j,\sigma} + c_{j,\sigma}^t c_{i,\sigma}) + U\sum_{i=1}^{N} n_{i\uparrow}\, n_{i\downarrow} \qquad \text{Eq. 2.10}$$

where i, j represents nearest-neighbor interaction on the lattice. By implemented Hubbard-U, the performance and accuracy of LDA functional has been improved [42] .

A single effective U_{eff} = U−J parameter accounts for the coulomb interaction, neglecting thereby any higher multi-polar terms. However, Hubbard-U correction is only related to the modification of potential energy (U) of electron based on the Hamiltonian equation. The insufficient description of strongly localized electrons such as those occupying the Zn 3*d* states in ZnO and the underestimation of their binding energies is a main problem in LDA function [45]. This can be corrected by LDA + U which successfully predicted the properties of ZnO with better described the localization of transition metal Zn 3*d* electron [40].

However, it has been found that the *p*-state of oxygen also have to be corrected in order to produced a result closed to the experimental E_g (3.37 eV) [44]. This is rise due to the underestimation of binding energy in *d*-state of zinc which leads to the overestimation

of the hybridization in the valence *p*-state of oxygen. This can be improve by enhanced the p-d coupling. This is the reason the correction of *p*-state of oxygen in Hubbard-U is required. By implemented Hubbard-U calculation, the performance and accuracy of conventional LDA functional has been improved [40].

2.4.4 Structure modeling

Structure modeling is a set of model made of compound or sample that resembles to ZnO sample. The structure modeling is very important as all the calculations are based on the model that has been designed. The input that can be obtained from this model is a bonding between the Zn and O atom, unit cell of hexagonal crystal structure and atomic position of Zn and O atom [46].

There are two types of interatomic bonding that can be considered for ZnO which are covalent bond and ionic bond. For ZnO, it is found that ionic bond is much stronger as compared to the covalent bond. A unifying of 3D molecular structures resulting from interatomic bonding and subject to holding the atomic positions in an outer region is referred as geometry optimizers [42].

An instance, Fu et al. [47] built the primitive cell of wurtzite-type structure of ZnO belong to $P6_3mc$ space group, a C6v−4 symmetry system (Figure 2.6). The unit cell contains two Zn cations and two O anions. The ZnO crystal thus can be viewed as a sequence of O-Zn double layers stacked along the c-axis or the (0001) direction. The lattice parameters are the second nearest neighbour distances a = b = 0.3253 nm, c = 0.521

nm with the angle $\alpha = \beta = 90°$, $\gamma = 120°$. The 2×2×2 supercell consisting of 32 atoms are built and displayed in Figure 2.7.

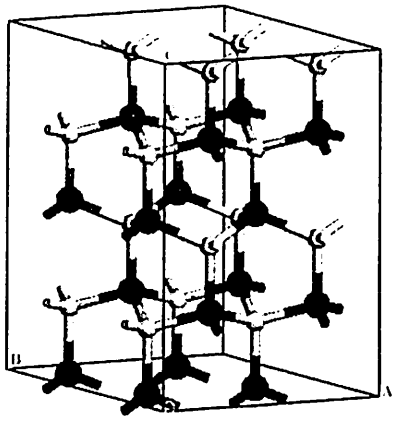

Figure 2.7: Supercell of ZnO. White atoms are oxygen and black atoms are zinc [47]

2.4.5 Geometrical optimization

Geometry optimization is a method to predict the three-dimensional arrangement of the atoms in a molecule by means of minimization of model energy. Geometry optimization is performed after the crystal structure of materials is completely built using Material Studio (MS) Visualizer. The phenomenon of binding, in which the tendency of atoms and molecules to conglomerate into stable larger structures, as well as the emergence of specific structures depending on the constituting elements which is a result of geometry optimization [46].

In geometry optimization, the convergence thresholds for energy change, maximum stress, and maximum displacement between optimization cycles need to be setup first before perform a calculation. The optimization process will stop when all these criteria are

satisfied. Four sets of convergence thresholds available in CASTEP computer code are coarse, medium, fine and ultrafine but mostly ZnO are treated with ultrafine threshold [46].

2.4.6 Electronic properties determination

The electronic properties of pure ZnO can be determined by LDA and the calculations are corrected by LDA + U approached. The Fermi energy (E_F), band structure and density of states (DOS) are important information that can be extracted from electronic structure calculation [48]. The calculation of E_g using conventional LDA method showed result far smaller than experimental E_g (3.37 eV) [44]. This underestimation of the E_g is the result of well-known limitations related to the standards used in DFT [49]. Thus, for these reasons the modification and improvement of this functional have been corrected by adopted LDA + U method.

The electronic E_g are calculated along the direction of high-symmetry Brillouin zone. Brillioun zone can be described as a primitive cell of the reciprocal lattice. Usually, ZnO was known as direct gap semiconductor with smallest energy gap at the center of the Brillouin zone (Γ/G) [45]. At the center of the Brillouin zone, the density of the electron will be highest. Thus, this will give the desired gap with smallest E_g between the lowest conduction band and the highest valence band.

Wu et al. [44] reported that the LDA has been underestimated the Eg of pure ZnO. To correct this calculation, LDA + U method was adopted. The calculated E_g using LDA functional (Figure 2.8a) showed the E_g of ZnO was 0.733 eV [50] which is consistent with Li et al. [51], but an underestimate comparison with the experimental value of 3.37 eV, due

to the limitation of DFT. However, the E_g is corrected to 3.363 eV which is closed to the experimental values when LDA + U is adopted (Figure 2.8b). The calculated E_g of ZnO nanoparticles using LDA functional is corrected by LDA + U functional is presented in Table 2.4.

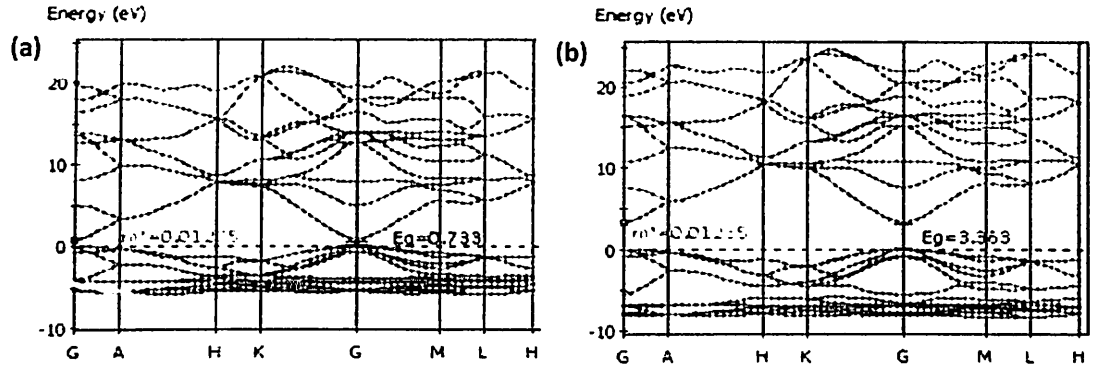

Figure 2.8: Band structure of ZnO primitive cell for (a) LDA ($U_d = 0, U_p = 0$) and (b) LDA + U ($U_d = 10, U_p = 7$) [50]

Table 2.4: Different band gap energy of ZnO calculated from LDA and LDA + U functional

Functional	Computer code	Calculated band gap energy (eV)	Energy state (eV)	Reference
LDA	CASTEP	0.79	$U_d = 0, U_p = 0$	[52]
LDA	CASTEP	1.12	$U_d = 0, U_p = 0$	[47]
LDA+U	CASTEP	1.154	$U_d = 6, U_p = 0$	[53]
LDA+U	CASTEP	3.37	$U_d = 10, U_p = 7$	[54]
LDA+U	CASTEP	3.40	$U_d = 10.5, U_p = 7$	[55]

Further insight into the electronic structure can be obtained from an analysis of density of states (DOS). The calculation of DOS shows a better description of the localization of transition metal of Zn 3*d* electron and O 2*p* electron of the ZnO nanoparticles [52]. Tsegaye et al. [48] described the DOS as quantity used to described the electronic states of a solid. Basically, DOS is the result of the electronic band formation of ZnO band structure.

Karazhanov et al. [40] reported the calculated total DOS (TDOS) and partial DOS (PDOS) for pure ZnO (Figure 2.9). From LDA calculation, Zn 3*d* band showed relatively wider and located closed to the upper valence band, which contradicts with experimental data. The discrepancy can be removed using LDA + U functional. The Zn 3*d* band becomes more localized and shifted toward lower energies in agreement with experimental data. The valence band, which lied between Fermi-level is composed of the O 2*p* orbital states with a small contribution from Zn 3*d* states. The lower valences are mainly formed by 2*p* state of O and 3*d* states of Zn.

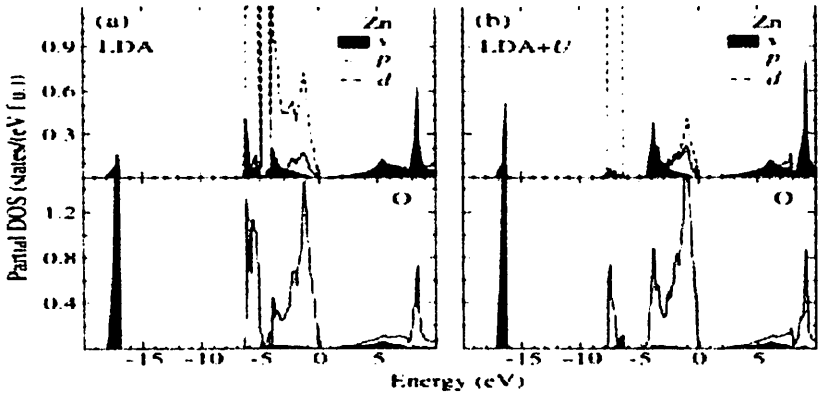

Figure 2.9: Total density of states for wurtzite-type ZnO calculated from the LDA and LDA + U approaches [40]

2.4.7 Optical properties determination

The optical properties are closely related the transitions between the occupied and unoccupied state that were caused by the absorption or emission of the photon [44]. The calculation of optical spectra also involved the character of the bands. The calculation of optical properties provided from first-principles calculation produced numerous outcome which were absorption coefficient (α), reflectivity (R), refractivity index (n), and energy-loss function (L) and dielectric function compared to the experimental analysis. [56]. From optical calculation, the complex dielectric function $\varepsilon(\omega) = \varepsilon_1(\omega) + i\varepsilon_2(\omega)$ in which the real part (ε_1) is obtained by imaginary part (ε_2) that were calculated theoretically based on the DFT [54].

The imaginary part of the dielectric function $\varepsilon_2(\omega)$ is calculated by the sum of all possible direct transitions from the occupied and unoccupied states over the Brilliouin zone. The imaginary part can be calculated based on electronic structure on DOS given as Eq. 2.11:

$$\varepsilon_2 = \frac{2\pi e^2}{\Omega \varepsilon_0} \sum_{k.v.c} K\varphi_k^c |u.r|^2 \delta(E_k^c - E_k^v - E) \qquad \text{Eq. 2.11}$$

where e refers to electron charge, and φ_k^c are the covalent band and valence band wave functions at k. Meanwhile, The α, R, n, and L can be described as [57]:

$$\alpha = \sqrt{2}\omega[\sqrt{\varepsilon_1^2(\omega) + \varepsilon_2^2(\omega) - \varepsilon_1(\omega)}]^{1/2} \qquad \text{Eq. 2.12}$$

$$R = \left|\frac{\sqrt{\varepsilon_1(\omega) + j\varepsilon_2} - 1}{\sqrt{\varepsilon_1(\omega) + j\varepsilon_2(\omega)} + 1}\right|^2 \qquad \text{Eq. 2.13}$$

$$n = [\sqrt{\varepsilon_1^2}(\omega) + \varepsilon_2^2(\omega)]^{1/2}/\sqrt{2} \quad \text{Eq. 2.14}$$

$$L = \varepsilon_2(\omega)/[\varepsilon_1^2(\omega) + \varepsilon_2^2(\omega)] \quad \text{Eq. 2.15}$$

where $\varepsilon_1(\omega)$ refers to real part and $\varepsilon_2(\omega)$ refers to imaginary part of dielectric function

To investigate the optical properties of the ZnO nanoparticles, it is necessary to calculate the imaginary part of the dielectric function $\varepsilon_2(\omega)$. The effect of pure and doped ZnO to the dielectric function, ε_2 spectra is investigated (Figure 2.10). For pure ZnO ε_2 spectrum, there are three main dielectric peaks observed. The first peak located at 2.7 eV corresponds to the optical transition between O 2*p* and Zn 4*s* states. The second peak appeared at 7.2 eV which related to the transition from O 2*p* to Zn 3*d* states. Meanwhile, the third peak of optical transition of pure ZnO is located about 11.3 eV which mainly caused from the intrinsic transition between Zn 3*d* at the conduction band and O 2*s* states at valence band [55].

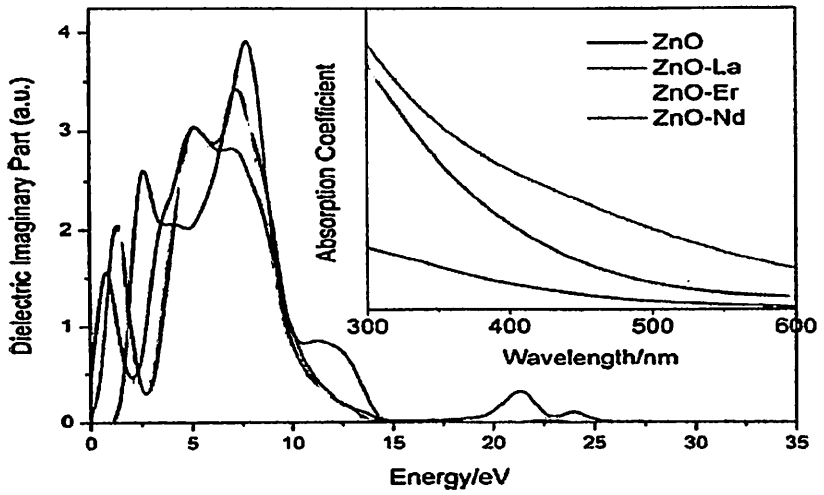

Figure 2.10: Imaginary part, ε_2 of dielectric function of the pure and doped ZnO [55]

Aside to dielectric constant, the absorption coefficient, α also is discussed. In practice, the energy gap can be easily determined from optical absorption under wide range of wavelength. From graph absorption versus wavelength, the absorption spectra of the pure and doped ZnO samples lied in the range between 200 nm and 1200 nm (Figure 2.11). Pure ZnO occupied states closed to the conduction band minimum which induced slight absorption in the red and infrared (IR) regions. The transmittance in these regions is slightly smaller. At wavelength 600 nm, pure ZnO can only utilized smaller UV energy. Larger band gap will results the absorption edge moving toward shorter wavelengths and significantly improved the transmittance in UV region [44].

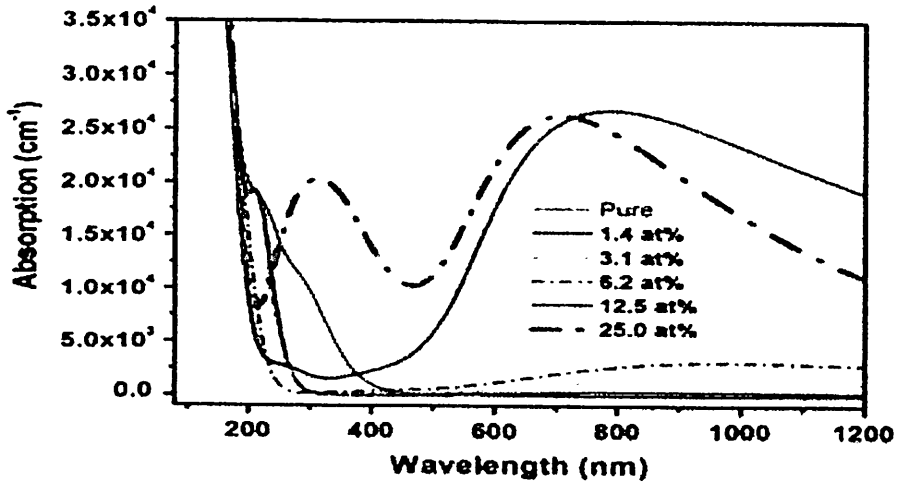

Figure 2.11: Absorption of pure and doped ZnO at various Ga concentrations [44]

Besides, the reflectivity (*R*), refractivity index (*n*), and energy-loss (*L*) spectrum of the pure ZnO also can be analyzed from optical calculation. The refractivity index is an important concept in optical properties as it determined the amount of light refracted or propagates when entering the ZnO nanoparticles. Meanwhile, reflectivity can be calculated

from the refractive index by described the amount of light reflected when passed through the ZnO nanoparticles. For the energy-loss function calculation, it described the energy loss of the electrons when traversing the material. The peaks of energy-loss spectra is corresponded to the trailing edges in the reflection spectrum [51].

Li et al. [51] described the reflectivity (R), refractivity index (n), and energy-loss (L) spectrum of the pure and doped ZnO nanoparticles (Figure 2.12). The main energy loss is 14.9 eV which described the energy loss of the electrons traversing the material. The peaks of energy-loss spectra also corresponded to the trailing edges in the reflection spectrum. The reflectivity reduced abruptly at 4.1 eV and 14.9 eV, which is due to the peaks of the energy-loss spectrum. Meanwhile, the reflectivity and refractivity index showed an opposite trend. Further increase in Cr doping concentration leads to increase in the refractive index value.

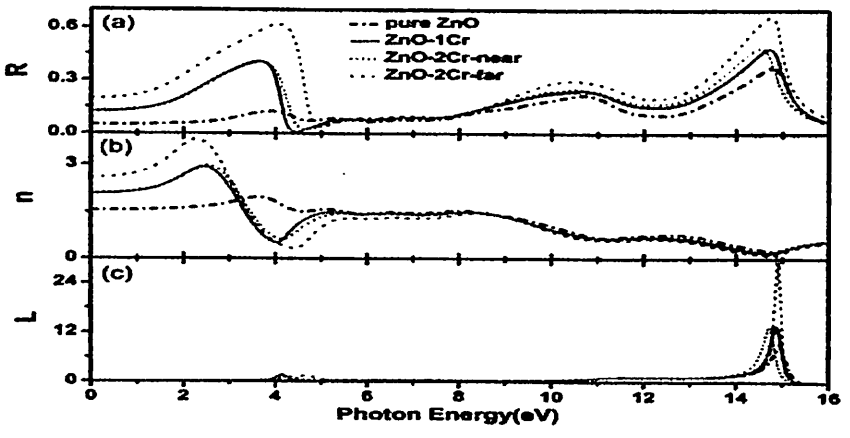

Figure 2.12: The reflectivity, refractivity index, and energy-loss functions of ZnO systems with four different structures [51]

CHAPTER 3

METHODOLOGY

3.0 Introduction

This chapter describes the materials, equipment, sample preparation, characterization techniques and computational method used in this study. Generally, this work consists of three main sections which are:

i. Synthesis of ZnO nanoparticles via sol-gel storage method

ii. Characterization of synthesized ZnO nanoparticles

iii. First-principles calculation of ZnO nanoparticles properties

3.1 Material and experimental apparatus

The materials used in this experiment involved are listed in Table 3.1. Both chemical formulae and their respective manufacturer are stated. All materials are used without any modification.

Table 3.1: The materials involved in the formation of ZnO nanoparticles by sol-gel method

No.	Materials	Manufacturer
i.	Zinc acetate dihydrate [$Zn(CH_3COO)_2.2H_2O$]	Sigma-Aldrich
ii.	Methanol (CH_3OH)	Emsure®Acs
iii.	Sodium hydroxide (NaOH)	Merck
iv.	Deinonized water (H_2O)	MILLIPORE, Synergy UV

Table 3.2 summarized the equipment and software involved during characterization of synthesized ZnO nanoparticles and simulation work.

Table 3.2: List of major equipments and software involved

No.	Equipment and software	Manufacturer
i.	Thermo gravimetric analysis (TGA)	TGA Mettler Toledo
ii.	Powder X-Ray diffraction (XRD)	Bruker Advanced X-Ray Solution D8
iii.	Field emission scanning electron microscope (FESEM)	Zeiss SUPRA 35
v.	UV-Visible spectroscopy (UV-Vis)	Varian-Cary Win UV 100
iv.	Oven	Memmert
vi.	Alumina tube furnace	CARBOLHF,STF
vii.	Ultrasonic machine	SONO SWISS SWI2H
viii.	Hot plate	IKA C-MAGHS7
ix.	Cambridge serial total energy package (CASTEP) computer code	Biovia Material Studio (MS) 8.0
x	X'pert Highscore plus	PANalytical X-ray diffractometers

3.2 Flow chart

Figure 3.1 summarized the synthesis route and first-principles calculation of ZnO nanoparticles.

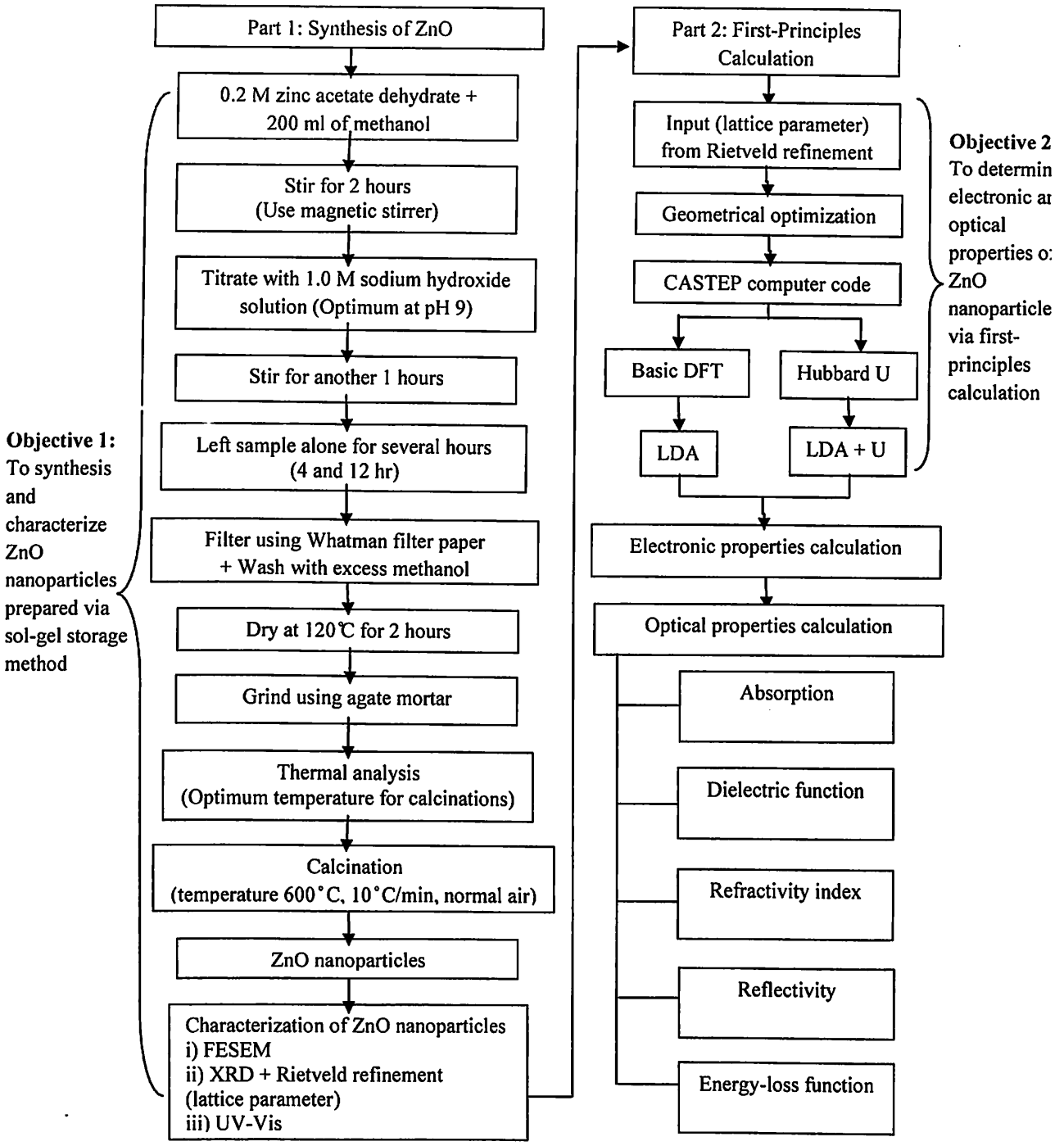

Figure 3.1: Flow chart of the preparation of ZnO nanoparticles via sol-gel storage method and first-principles calculation method

3.3 Synthesis of ZnO nanoparticles via sol-gel storage method

The ZnO sol was prepared by mixing 0.2 M zinc acetate dihydrate [$Zn(CH_3COO)_2.2H_2O$] and 200 mL of methanol (CH_3OH) at room temperature. Zinc acetate dihydrate was used as the precursor whereas methanol acts as solvent. The solution was stirred for 2 hours until a clear solution was obtained. Then, the clear solution was titrated with 1.0 M sodium hydroxide (NaOH) solution until it reached pH 9. The NaOH solution was prior prepared by dissolving 8.0 g NaOH pellet into 200 mL of dionize water.

As the solution was titrated, the clear solution was transformed into milky-white slurry. pH 9 was chosen for titration as it demonstrated highest crystallite sizes and desired particle morphology. The resulted milky-white slurry was then stirred for another 1 hour to ensure a homogeneous sol. After that, the sample was stored for 12 hours to allow the complete hydrolysis and gelation. Figure 3.2 illustrated the synthesis step in formation of ZnO nanoparticles.

(a) (b) (c)

Figure 3.2: Synthesis of zinc oxide (a) mixture of zinc acetate dihydrate and methanol, (b) a milky-white slurry obtained after titration, and (c) the sedimentation of ZnO sample after 12 hours storage

The aged sample was filtered using Whatman filter paper, followed by washed with an excess of methanol to remove remaining starting materials. Filtered sample was dried at 120 °C for 2 hours and then ground with mortar and pestle to yield ZnO powders. The ZnO powders obtained after dried was calcined at temperature 600 °C. The calcinations process of dried ZnO was done in tube furnace with atmospheric environment and soaked for 2 hours. The heating rate employed in calcinations process was 10 °C/min. Figure 3.3 illustrated the preparation of ZnO nanoparticles after the sample was stored for 12 hours.

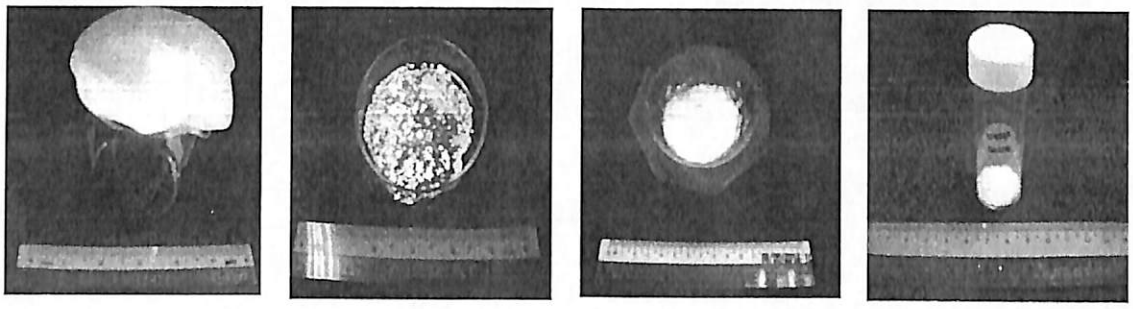

(a) (b) (c) (d)

Figure 3.3: Preparation of ZnO nanoparticles (a) filtering, (b) after drying, (c) grinding and (d) final ZnO nanoparticles after calcinations

After calcinations, the ZnO sample obtained was further characterized in term of their phases, morphology, particle size and optical properties. For comparison purpose, sample with lesser storage time was also prepared. Sample after small sedimentation (approximately 4 hours) was chosen and undergone the same procedure as mention above. The schematic diagram of ZnO nanoparticles synthesized by sol-gel method was illustrated in Figure 3.4.

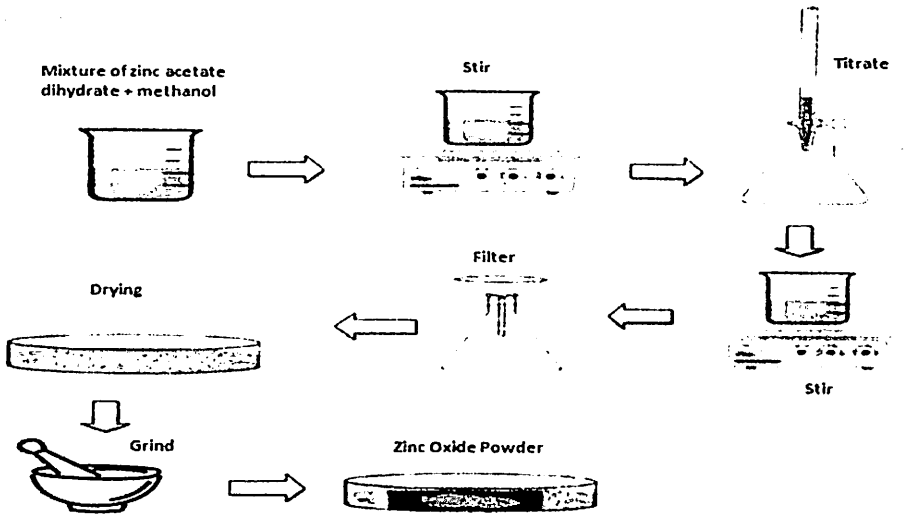

Figure 3.4: Scheme for ZnO nanoparticles synthesis by sol-gel method

3.4 Sample characterization

ZnO nanoparticles were characterized using several material characterisation techniques. The characterisation techniques used were TGA, XRD, FESEM, EDX, and UV-Vis.

3.4.1 Thermal identification

In order to determine the stable calcination temperature for ZnO nanoparticles, TGA analysis was performed. A 10 mg of as-synthesized ZnO nanoparticles were heated in flow of normal air. The temperature range for this analysis was from 25 °C to 800 °C and heating rate was maintained at 10 °C/min. The graph of weight loss (%) against temperature (°C) was plotted and analyzed.

3.4.2 Phase characterization

The phase present in synthesized ZnO nanoparticle was examined by XRD (Bruker Advanced X-Ray Solution D8) in the scanning angle of 2θ range from 10° to 90°. The data was collected and the XRD patterns were analyzed by using X'pert High Score Plus software. The pattern was then compared with the Inorganic Crystal Structure Database (ICSD) files in order to confirm the phase present. The graph of intensity (cps) against angle in degree (2θ) was plotted.

3.4.3 Structural quantitative refinement

The quantitative analysis which was extended from XRD pattern was carried out using Rietveld-refinement method. The further analysis of rietveld-refinement of ZnO sample can be fulfilled using X'pert High Score Plus software. This analysis was employed to identify the structural parameter of ZnO including the lattice dimension, space group, and atomic coordination of Zn and O. A new diffracted model was designed and compared with standard diffracted pattern. This information was then used as main input in the first-principle calculation.

3.4.4 Morphological and elemental characterization

For the microstructural and morphological study, the sample was examined by FESEM Before microstructure analyses were performed, 0.1 mg ZnO nanoparticles were mixed with 27 mL of methanol. Then, the sample was ultrasonically stirred for 10 minutes in order to obtain a homogeneous solution. The solution then was dropped on top of the

aluminium holder and sputtered at 1000 rpm for 30 seconds using spin coating machine to obtained well distribution of ZnO layer.

Once the ZnO layer was prepared, the sample was coated with a thin layer of gold (Au) to provide conductivity (charging of sample with electron beam in conventional SEM mode) and some protection from the beam damage. Data was collected over a selected area of the sample surface and 2-dimensional image of ZnO morphological was displayed on the screen. Meanwhile, the element present was examined by EDX in embedded FESEM machine.

3.4.5 Band gap determination

For the purpose of comparison with first-principle calculation, the optical properties of calcined ZnO nanoparticles were analyzed using UV-Visible spectroscopy (Varian-Cary Win UV 100). At first, the ZnO nanoparticles solution was prepared using the same route mentioned in Section 3.4.4. Then, a 3.5 mL of ZnO solution was poured into the cuvette and the UV radiation was scan through the solution from 200-900 nm wavelength range. After finish, the data was collected and graph of absorbance (A) against wavelength (nm) and transmittance (%) against wavelength (nm) was plotted.

3.5 First-principles calculation of ZnO nanoparticles

3.5.1 Computational software

In this computational modeling, the calculation of electronic and optical properties of ZnO nanoparticles was performed within MS 8.0 software. A CASTEP computer code was chosen throughout all calculation with different exchange-correlation approximations. The local density approximation (LDA) and effective Hubbard-U correction (LDA + U) was employed as the basis for all underlying analyses.

3.5.2 Structure modeling

The structural modeling was used to build a model that resembles the crystal structure of ZnO. This model was important as all the calculations are based on the model that has been designed. The input that was used to build this model was lattice parameter, space group and atomic position of Zn and O atom.

Firstly, space group for ZnO nanoparticles was selected to build the crystal (Figure 3.5). After that, lattice parameters of ZnO nanoparticles were set as indicated in Figure 3.6. On similar task, the atomic position of Zn and O atom was inserted (Figure 3.7). Then, the software was activated and ZnO wurtzite hexagonal structure was constructed. All the input was based on the Rietveld-analysis obtained from Section 3.4.3.

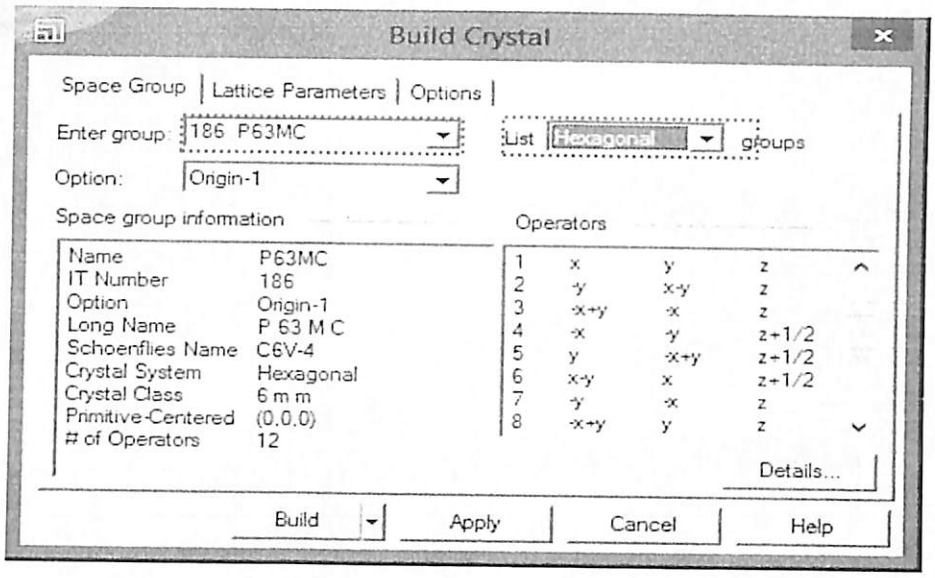

Figure 3.5: Build crystal by inserted space group of ZnO nanoparticles (Enter group: 186 *P6₃mc*, List: Hexagonal, Option: Origin-1)

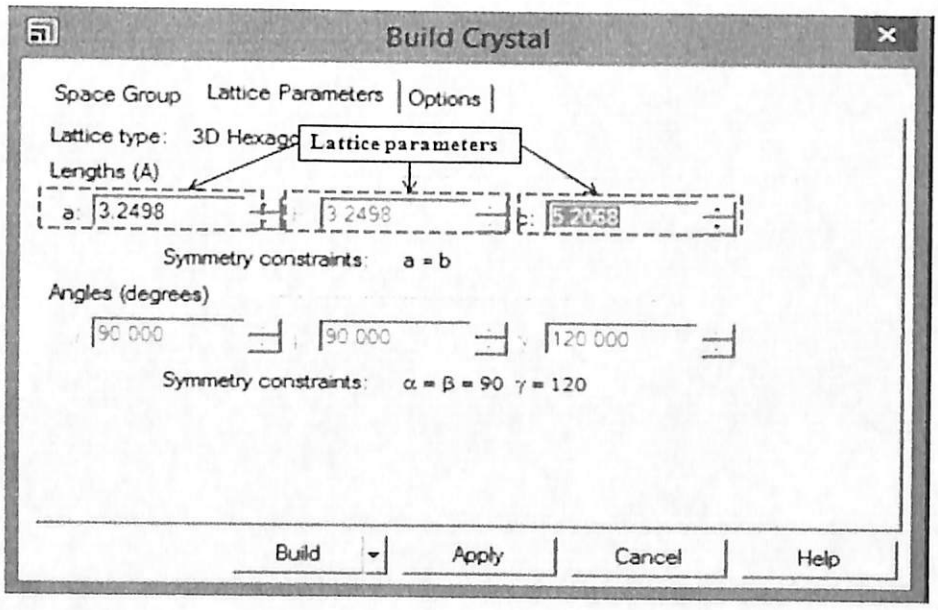

Figure 3.6: Lattice parameter of a, b and c insertion (a = b = 3.2498, c = 5.2068)

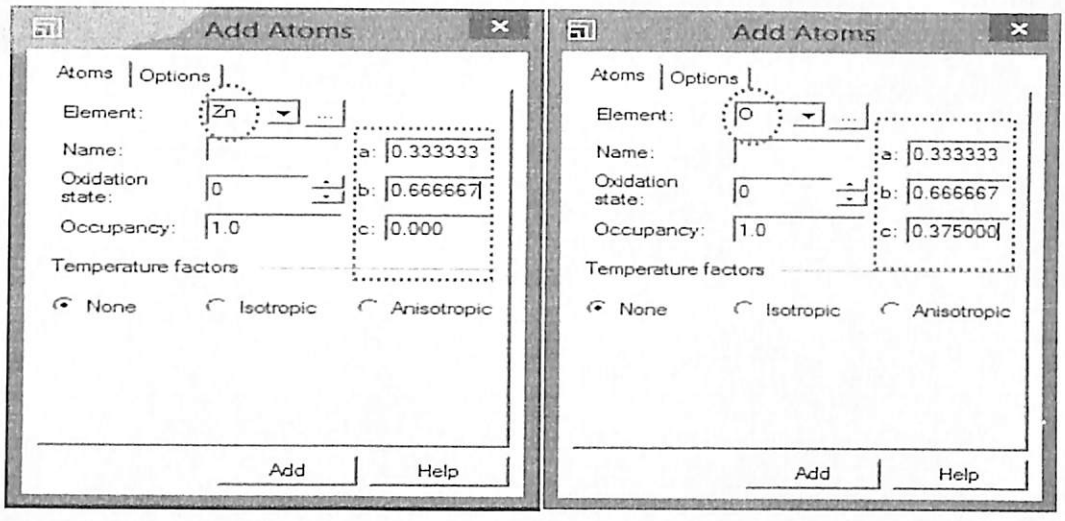

(a) (b)

Figure 3.7: Adding the atom coordinated (x, y, z) for (a) zinc and (b) oxygen

3.6 Geometrical optimization

Geometry optimization is a method to obtain the lowest energy structure of ZnO before the calculation was performed. The geometric of 3D periodic system was refined as well. This step was performed once the crystal structure of ZnO nanoparticles was completely built. In geometrical optimization, several approximation was used which is LDA functional and corrected by LDA + U functional in order to modify the energy of *d*-state of zinc and *p*-state of oxygen.

First, the internal coordinates and lattice parameters of pure ZnO was optimized to obtain stable and accurate results. Then, geometric optimization calculation was performed with less than 5×10^{-6} eV per atom convergence threshold of energy change, 0.01 eV per Å, and 0.02 GPa maximum force and stress, respectively, and not more than 5.0×10^{-4} Å

atomic displacement. The optimization process will stop when all these criteria are satisfied.

For result improvement, Hubbard-U correction was employed to obtain the result closed to the experimental. The semiempirical LDA + U approach was employed by adjusting the energy of *d*-state of zinc and *p*-state of oxygen as shown in Figure 3.8.

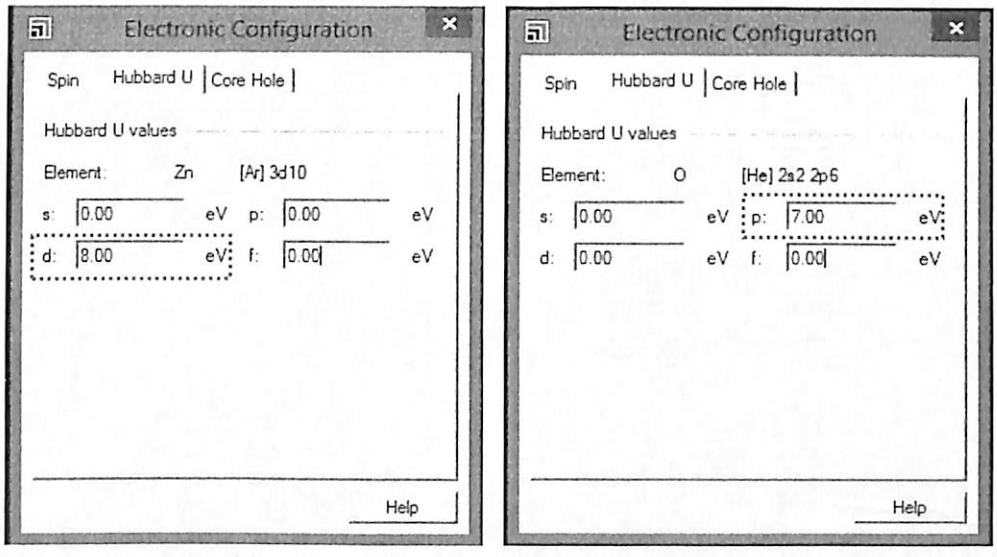

(a) (b)

Figure 3.8: Change in electronic configuration of (a) *d*-state of zinc (b) *p*-state of oxygen

3.7 Calculation and analysis

3.7.1 Electronic structures

The first-principles calculation area was based on ultrasoft pseudopotential method which only considered the valence electron in calculation. Ultrasoft pseudopotentials allowed the calculation to be performed at lower cut-off energy. This pseudopotential was used for the calculation of electronic and optical properties. After the stable structure was

obtained, the energy calculation was computed to calculate the electronic and optical properties. From the energy calculation, the band gap, density of state (DOS) and optical properties were calculated with respect to the structure that has been optimized.

For the electronic calculation, the 5 × 5 × 4 k-point grid with 0.07 $Å^{-1}$ k-point separations was used. The Monkhorst–Pack k-point sampling scheme was employed to perform the k-space integrations over the first Brillouin zone to the same level of convergence. For the isolated molecule, only one k point (the Brillouin zone centre) was required. In this study, the BZ was set in hexagonal ($P6_3mc$) for pure ZnO. Finer sampling was not necessary, since the electronic bands was effectively dispersed less for a single molecule.

Meanwhile, the electronic DOS of ZnO nanoparticles was investigated to understand the electronic band structure based on the occupied in valence bands (VB) and unoccupied of the conduction bands (CB). From DOS calculation, the total DOS (TDOS) and partial DOS (PDOS) of ZnO was analyzed. The TDOS was obtained by summations over all bands while PDOS was contributed by the energy states of the respective element.

3.7.2 Optical properties

The optical properties of ZnO sample were calculated based on the optimized cell. The calculation of the optical properties for ZnO nanoparticles closely related to the electronic band structure and phonon dispersion. Generally, the optical properties can be explained based on the complex dielectric function in Eq. 3.1:

$$\varepsilon(\omega) = \varepsilon_1(\omega) + i \qquad \text{Eq. 3.1}$$

whereby, $\varepsilon(\omega)$ was contributed by the both direct and indirect band gap transitions. The optical properties calculation provided information about the absorption coefficient (α), dielectric function, refractivity index (n), reflectivity (R) and energy-loss function (L) of pure ZnO.

CHAPTER 4

RESULTS AND DISCUSSIONS

4.0 Introduction

This chapter present the experimental and characterization result of ZnO nanoparticles. Also, it described the finding on calculation of ZnO nanoparticles properties. The discussion was divided into two main parts:

i. Properties of ZnO nanoparticles synthesized by sol-gel storage method

ii. First-principles calculation on electronic and optical properties of ZnO nanoparticles

4.1 Characterization of ZnO nanoparticles

In this work, the synthesized ZnO nanoparticles were characterized by thermogravimetry analysis (TGA), powder X-ray diffraction (XRD), field-emission scanning electron microscopy (FESEM) and UV-Visible (UV-vis) spectroscopy. Extensive quantitative measurement from XRD data was used as a main input first-principles calculation.

4.1.1 Thermal analysis

Figure 4.1 showed the thermal properties of synthesized ZnO nanoparticles analysed by TGA. Two samples with different parameter for example after separation (4 hours) and stored for 12 hours were prepared. The TGA results for both ZnO samples showed two pronounced mass loss steps in the temperature ranges 30–100 °C and 100–400

°C. Based on this temperature range, three main zones were identified along the curve. Zone A started from 30 °C to offset of 100 °C. The weight loss occurred in this zone was mainly attributed by the water elimination.

Zone B showed large weight loss percentage started from 100 °C and ended at 400 °C due to the decomposition of alcoholic compound which was zinc hydroxide [$Zn(OH)_2$] that have melting temperature at 125 °C. At Zone C, the stable temperature for ZnO was found at more than 400 °C indicated by a stagnant line. At this zone, the percentage of weight loss was almost zero. This occurrence proved the removal and elimination of all complexes and impurities were completed. Therefore, it can be deduced that crystallization of ZnO start to occur [22].

The weight loss for sample stored for 4 hours showed higher percentage (16 %) as compared to the sample stored for 12 hours. Low weight loss in sample stored for 12 hours indicated that after some aging, polycondensation reaction continues completing the formation of the gel [15]. Therefore, the obtained sediment was mostly ZnO precipitate and some intermediate compounds which were physically separated from water. Shorter storage time (4 hours) caused an incomplete hydrolysis and condensation process. Thus, from the analysis, it showed that the sample could be calcined at temperature above 400 °C to obtain well-crystallite ZnO nanoparticles. In this work, 600 °C was selected as calcinations temperature for better crystalline growth of ZnO nanopaticles.

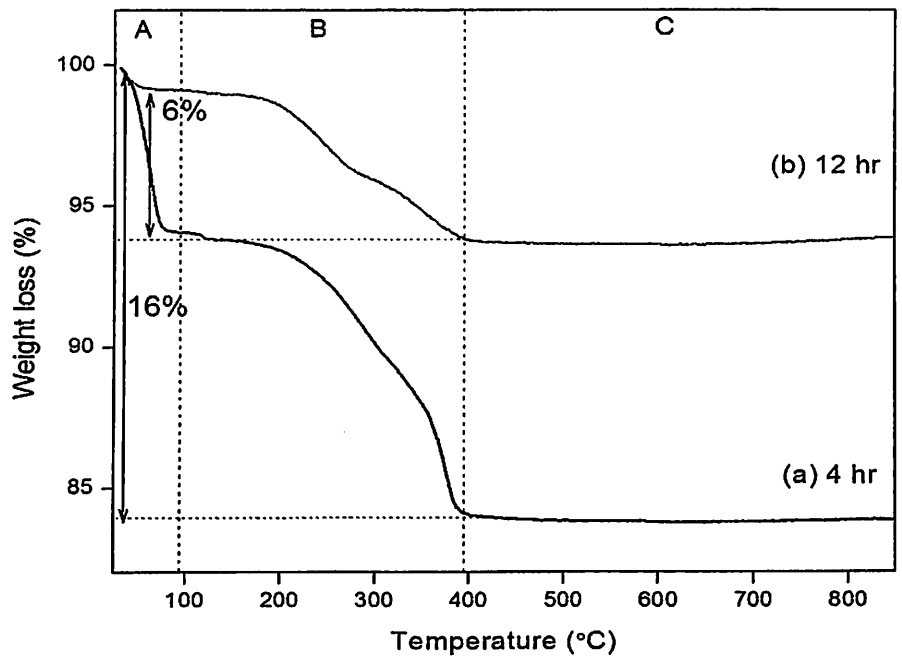

Figure 4.1: TGA curve of synthesized ZnO nanoparticles (a) stored for 4 hours (b) stored for 12 hours by heating the ZnO sample in air at 10 °C/min

4.1.2 Phase identification

Figure 4.2 and 4.3 showed the diffraction pattern of the ZnO nanoparticles before and after calcinations analyzed by the XRD. The result showed that all the diffracted peaks were indexed to ZnO phase (Inorganic Centre of Structural Data (ICSD): 98-010-6787, space group $P6_3mc$) with hexagonal crystal structure. All the peaks diffracted on the plane (010), (022), (011), (012), (110), (013), (020) and (112) suggested that ZnO samples were close to typical hexagonal structure.

The existence of well-defined Bragg peaks demonstrates the formation of a highly crystallized ZnO phase even before the calcinations (Figure 4.2). Before calcination, sample stored for 12 hours showed narrow peak as compared to sample stored for 4 hours. Narrow peak indicated larger crystallite size. It can be seen that the diffraction line become narrower with increasing the storage time. Thus, it showed that sample stored for 12 hours had larger crystallite size. Besides, higher intensity was observed for sample stored for 12 hours. High intensity indicated that the sample had high degree of crystallinity. This showed that samples stored for 12 hours had highest crystallinity recorded at orientation (011) plane and $2\Theta = 36.3\ ^{\circ}$. Highest intensity at (011) plane indicated that the number or concentration of atoms on that crystalline plane was high [21].

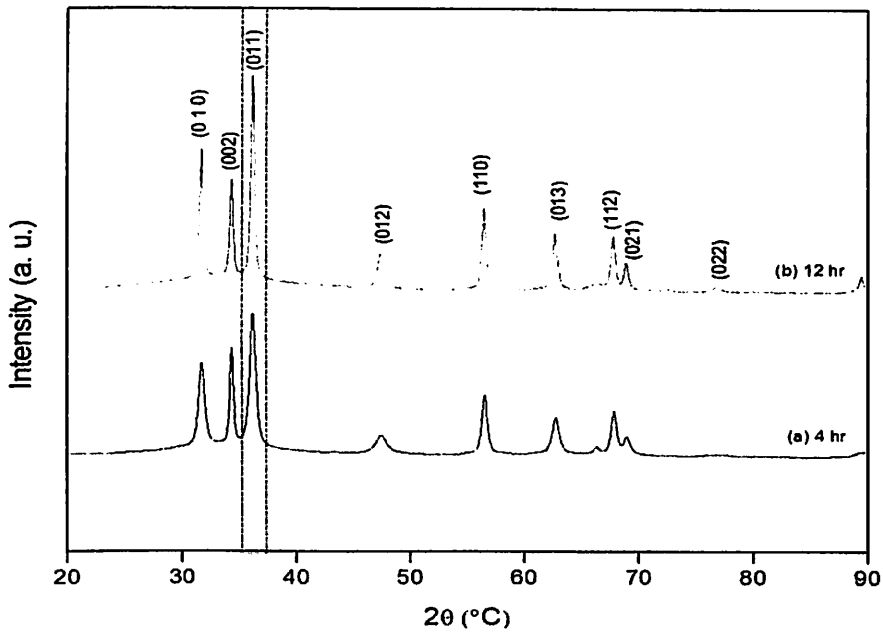

Figure 4.2: Diffraction pattern of pure ZnO nanoparticles before calcinations (a) stored for 4 hours (b) stored for 12 hours

For the calcined samples at 600 °C (Figure 4.3), sharper and narrower diffraction peaks was observed, implying that the high crystallinity of ZnO nanoparticles formation had been established. Sample stored for 12 hours still showed highest intensity and narrower peak as compared to sample stored for 4 hours. Thus, it showed that after calcinations, sample stored for 12 hours established higher degree of crystallinity and larger crystallite size. After calcinations, all the undesired anions were completely removed from the sample and gradually increase the purity of ZnO nanoparticles [2]. Thus, from this analysis, sample stored at 12 hours provided the optimum storage (formation) time for ZnO nanoparticles as it presented the highest crystallinity and larger crystallite size.

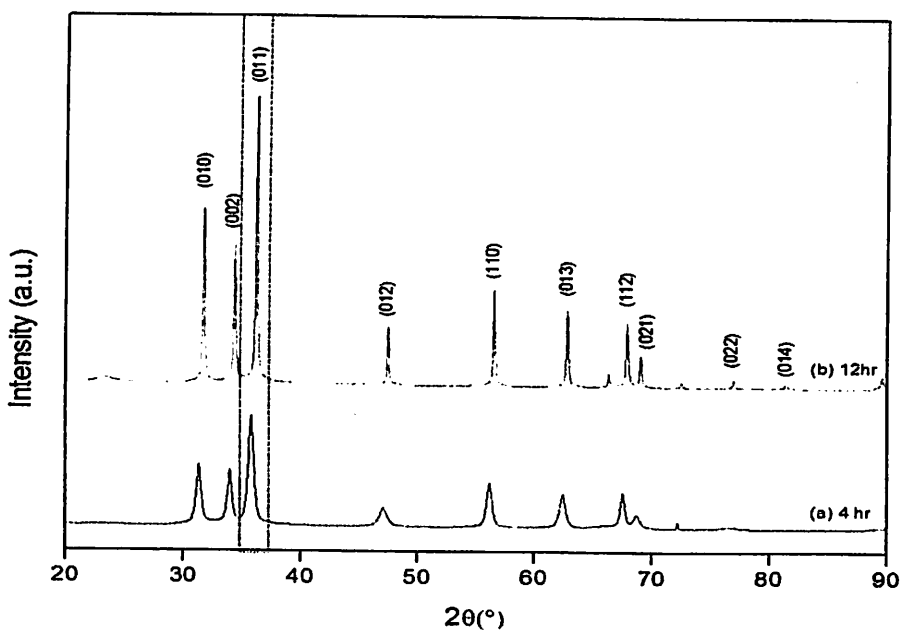

Figure 4.3: Diffraction pattern of pure ZnO nanoparticles calcined at 600 °C (a) stored for 4 hours (b) stored for 12 hours

4.1.3 Structural quantitative by Rietveld-analysis

Table 4.1 and 4.2 presented the quantitative Rietveld-analysis performed to obtain the atomic parameter of synthesized ZnO with the aid of the X'pert Highscore Plus software. The structural parameter such as lattice dimension, profile shape, preferred orientation and atomic coordination were refined. Table 4.1 showed the reliability of the calculated pattern during refinement verified by residual (R) values and the goodness of fit (GOF) values. In refinement process, two types of R-values had been observed which were R expected profiles (R_{exp}) and R weight profile (R_{wp}). It showed that R_{wp} value was high which due to the nature of nanocrystalline material having low background in diffracted patterns. This indicated that a significant part of the intensity was not accounted by the background function which leads to low diffraction peak to the background ratio [28].

On the other hand, the R_{exp} value observed was small which was due to over collected data during profile fitting process, leading to GOF value larger than 2. The GOF value before calcinations also showed the decreasing trend as the storage time was increased. The diffraction patterns fit well with the standard pattern due to more ZnO precipitate disaggregated when the ZnO stored for 12 hours. Thus, more ZnO particles were formed. In contrast, GOF value for sample after calcination fluctuates and does not follow any trend. However, the GOF value after calcinations for ZnO nanoparticles sample still reliable, acceptable and comparable with results obtained by Kumar et al. [28].

Table 4.1: Rietveld-analysis of ZnO nanoparticles before and after calcinations

Parameter	Criteria	Before calcinations		After calcinations	
		4 hours	12 hours	4 hours	12 hours
R_{wp}	N/A	15.449	15.68	15.587	15.57
R_{exp}	< 10	7.301	10.39	10.99	9.93
GoF	< 2	4.478	2.28	2.011	2.46

Table 4.2 showed the lattice parameter (length and angle), crystal structure, space group, crystallite size, volume and atomic position of ZnO nanoparticles before and after calcinations. These parameters proved that ZnO nanoparticles had hexagonal structure with a space group $P6_3mc$. The mean crystallite size of ZnO nanoparticles were measured and estimated using the calculation from the X'pert highscore plus software. The range of crystallite size lied between 16.66-84.44 nm. The crystallite size of ZnO nanoparticles showed a variation in size for all sample before and after calcined. From this analysis, it showed that crystallite size increased upon prolong the storage time. This indicated that the particles were allowable to growth as increasing the storage time.

The 'a' and 'c' values were consistent and does not change abruptly. The unit cell volume (V) also presented a consistent result for all samples before and after calcinations. Upon prolong the storage time, just small significance change in lattice parameter (1-2 % deviation) occurred. Thus, it showed that the structural parameter of the sample stored for 12 hours after calcined was the best sample by taking into account the optimum degree of crystallinity as presented in Section 4.1.2. From this analysis, the lattice parameter and

atomic position for Zn and O atom (x, y, z) for sample stored 12 hours after calcined as stated in Table 4.2 were used in first-principles calculation.

Table 4.2: Lattice parameter, crystallite size and unit cell volume determined from XRD Rietveld-analysis for ZnO nanoparticles before and after calcinations

Parameter	Before calcination		After calcination	
	4 hours	12 hours	4 hours	12 hours
Crystal system	hexagonal		hexagonal	
Space Group Number	*P6₃mc* (186)		*P6₃mc* (186)	
a (Å)	3.251	3.253	3.243	3.249
b (Å)	3.251	3.253	3.243	3.249
c (Å)	5.212	5.209	5.198	5.207
alpha (°)	90	90	90	90
beta (°)	90	90	90	90
gamma (°)	120	120	120	120
Volume ($V/10^6 pm^3$)	47.705	47.690	47.350	47.622
Crystallite sizes (Å)	16.66	50.26	21.18	84.84

Atomic position Atom	x	y	z
Zn	0.33333	0.66667	0
O	0.33333	0.66667	0.37500

4.1.4 Morphological and elemental analysis

Figure 4.4 showed the morphology of ZnO nanoparticles before and after calcinations for sample stored for 4 hours and 12 hours. Most of the ZnO nanoparticles showed uniform morphology with nearly spherical shape and homogeneous distribution. The SEM images of ZnO nanoparticles before calcination process (Figure 4.4a and 4.4b) showed irregularly and spherical shaped overlapped nanoparticles and high agglomeration. This was due to inhomogenous nucleation which leads to spherical-shaped particles. High agglomeration also was due to ZnO reacts with too much OH^- which leads to the dissolution of ZnO [58]. The dissolution made the crystallites and particles became smaller and agglomerated.

On the other hand, the SEM image of ZnO nanoparticles after calcinations for all samples showed homogeneous and uniform shape with some of the particles showed hexagonal structure (Figure 4.4c and 4.4d). The more uniform ZnO nanoparticles after calcined could be attributed to the lower polarity of methanol leading to slower ionization and deposition rate [59]. Removal of lattice water and all complexes upon calcination process enhanced the nanoparticles features.

Majority of the particles had uniform shape and size in the range of ~ 44.7- 89.3 nm with average size at 67 nm. In order to study deeply size and crystallinity of ZnO nanoparticles, further confirmation was performed by comparing with the XRD patterns. From SEM analysis, the average particle size for ZnO nanoparticles was analyzed. The entire sample showed the increased in particles size which also indicated in increasing of the crystallite size as the particle was made up of several crystallites. Thus, the particle size

obtained from the SEM analysis can be compared with the crystallite size obtained from the XRD analysis.

For ZnO sample after calcined, the average particle size provided from SEM analysis increased which comparable to the increasing in crystallite size from the XRD analysis. The higher crystallite size after calcinations indicated that migration of grain boundaries occurred, causing the coalescence of small grains and formation of larger grains [59]. From this analysis, it can be seen that all the samples after calcinations synthesized by sol-gel method produced nearly uniform and shape with average size at 67 nm.

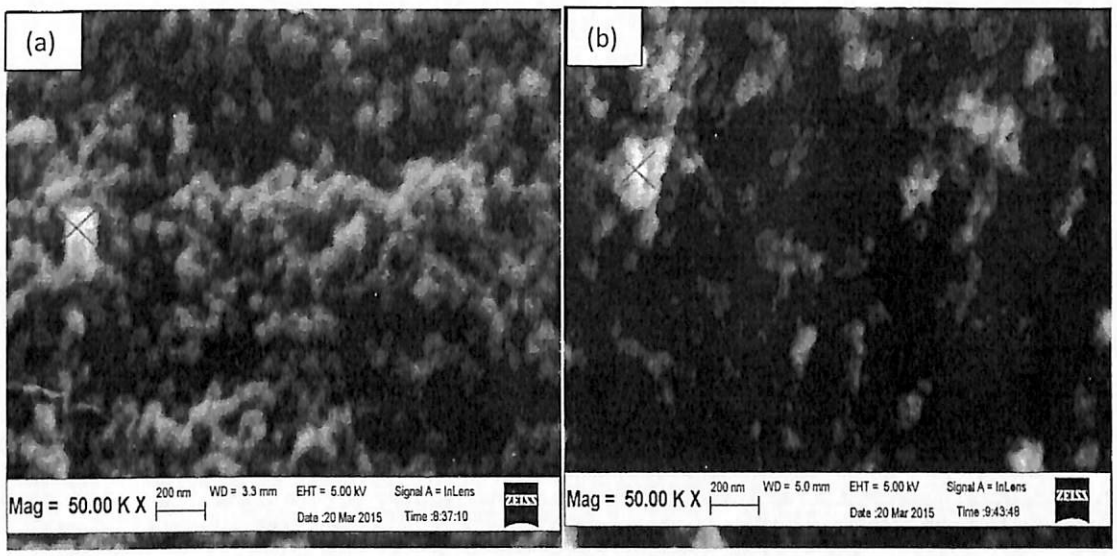

Figure 4.4: FESEM image of ZnO nanoparticles (a) sample stored for 4 hours before calcine (b) sample stored for 12 hours before calcine (c) sample stored for 4 hours after calcined (d) sample stored for 12 hours after calcined with magnification 50.00KX (continue)

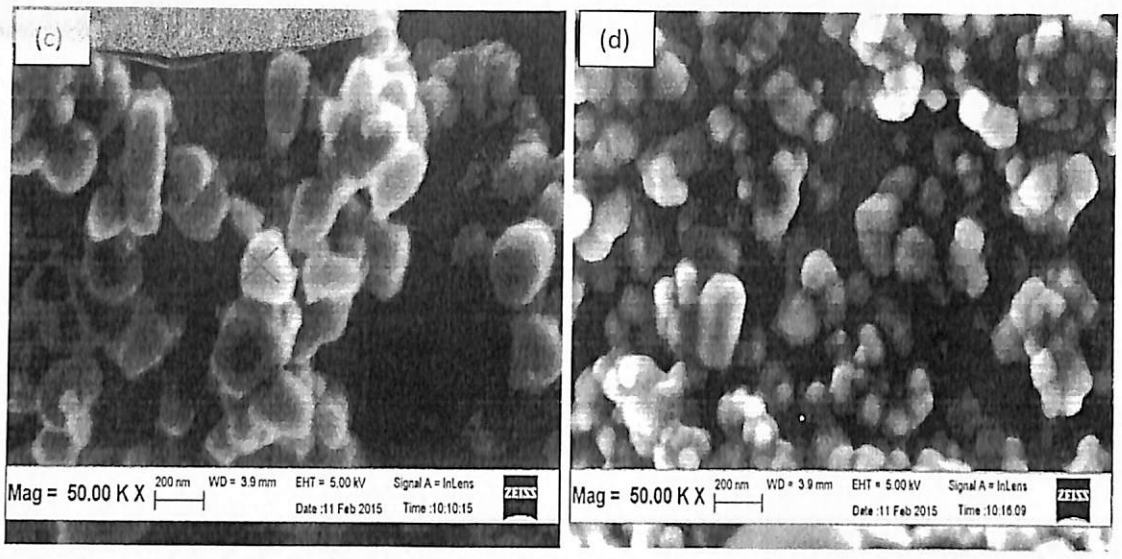

Figure 4.4: FESEM image of ZnO nanoparticles (a) sample stored for 4 hours before calcine (b) sample stored for 12 hours before calcine (c) sample stored for 4 hours after calcined (d) sample stored for 12 hours after calcined with magnification 50.00KX

Figure 4.5 present the chemical compositions of the ZnO nanoparticles sample before and after calcinations predicted using EDX analysis in 'X' region as marked in Figure 4.4. The EDX analyses for uncalcined and calcined samples indicated the purity of all the synthesized samples with no peaks other than Zn and O. All the samples revealed a high peak of intensity and free of impurities. Besides, EDX analysis also showed the atomic percentage of ZnO nanoparticles. From the atomic percentage, the chemical stoichiometric of the ZnO nanoparticles was calculated. By resulting ratio 1:1 for Zn and O, respectively from the calculation, this implying that the synthesized sample was pure ZnO.

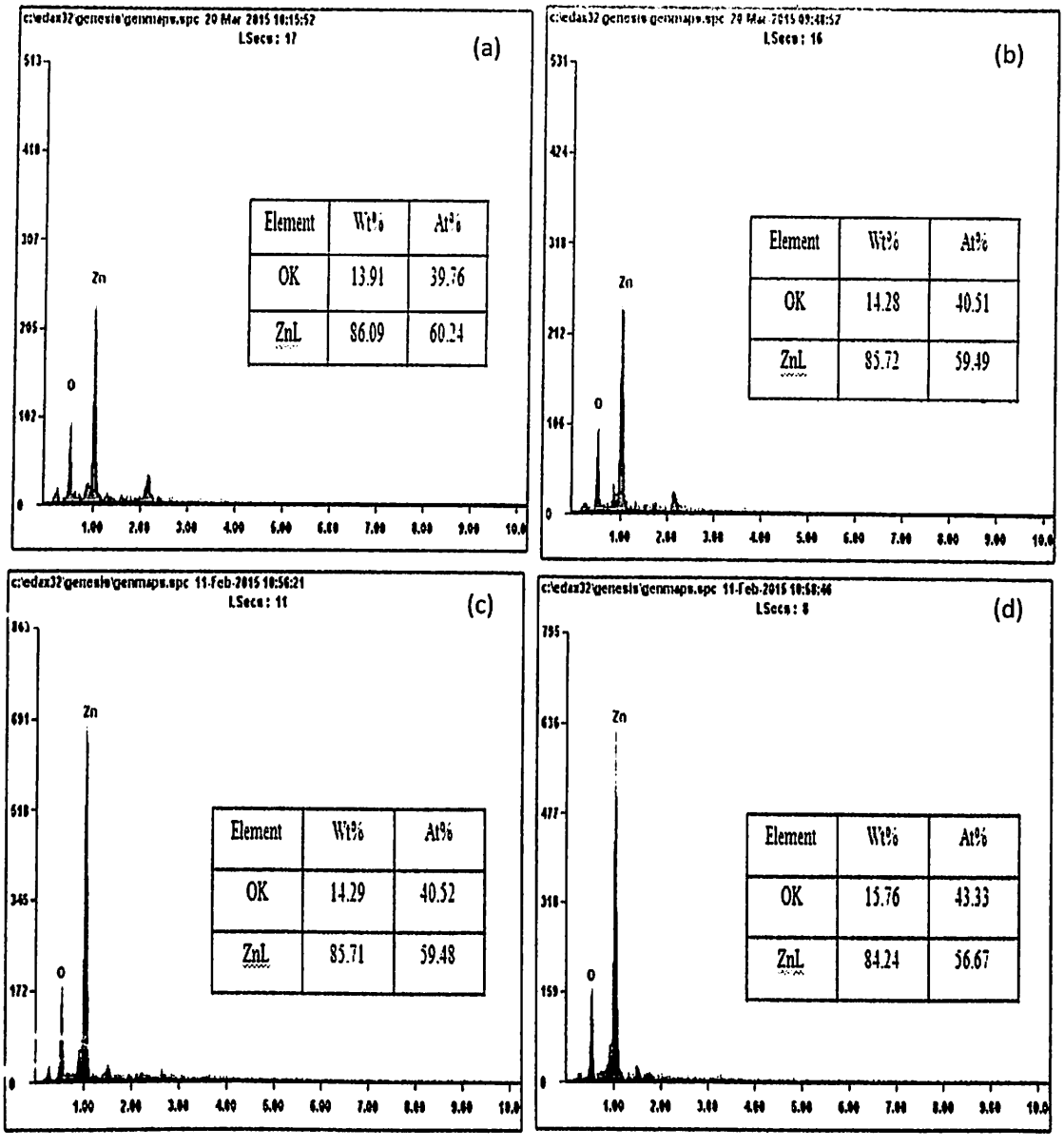

Figure 4.5: EDX of (a) uncalcined ZnO sample stored for 4 hours (b) uncalcined ZnO sample stored for 12 hours (c) calcined ZnO sample stored for 4 hours (d) calcined ZnO sample stored for 12 hours

4.1.5 Band gap analysis

Figure 4.6 showed the calculated band gap of ZnO nanoparticles by UV-Visible spectroscopy analysis. From the extrapolation plot, the absorption edge was analyzed which important to identified the energy band gap (E_g). This E_g was later used in comparison with the E_g obtained from the first-principles calculation. The UV–Vis absorbance spectrum of ZnO nanoparticles for both sample stored for 4 hours and 12 hours showed strong absorption peak at 395 nm. This finding indicated that the synthesized ZnO nanoparticles absorbed ultraviolet (UV) radiation from the sunlight. ZnO was transparent to visible light but strongly absorbs UV light below 400 nm.

Further validation of optical properties ZnO nanoparticles was determined directly from UV–vis spectra analysis with the Eq. 4.1:

$$E = \frac{hc}{\lambda} \qquad \text{Eq. 4.1}$$

whereby E is energy of photon (J), λ is the wavelength of light (nm), c is the speed of light (3.0×10^8 m/s) and h is the Planck's constant (6.634×10^{-34} J-s). The E_g was determined at the intersection point of the absorption edge. The absorption edges for samples stored for 4 hours lied at 410 nm while samples stored for 12 hours lied at 405 nm. Specifically, the E_g calculation showed ZnO sample stored for 4 and 12 hours have absorbance curve in the UV region with E_g 3.02 eV and 3.06 eV, respectively. The obtained E_g of ZnO nanoparticles was consistent with the E_g obtained by Li et al. [35].

The level of optical absorption strongly depends on particles size. The experimental E_g obtained for ZnO nanoparticles was found to be slightly lower than E_g of reported bulk ZnO (3.37 eV) due to the effects of nanosize particles to the electron band gap [18]. The E_g values increased with increasing the particle size [16]. As stated in morphological analysis, the particles size increased as the storage time increased. Consequently, the size of the particles influenced the ability of ZnO nanoparticles to absorb UV light. It was mainly because the density of free exciton was increased due to the improvement of crystalline quality of ZnO nanoparticles upon prolong the storage time [16]. Thus, it proved that sample stored for 12 hours showed better absorption and produced experimental E_g (3.06 eV) comparable with the reported E_g (3.08 eV) [34] for ZnO nanoparticles. This result was used in comparison with the result obtained from the first-principles calculation.

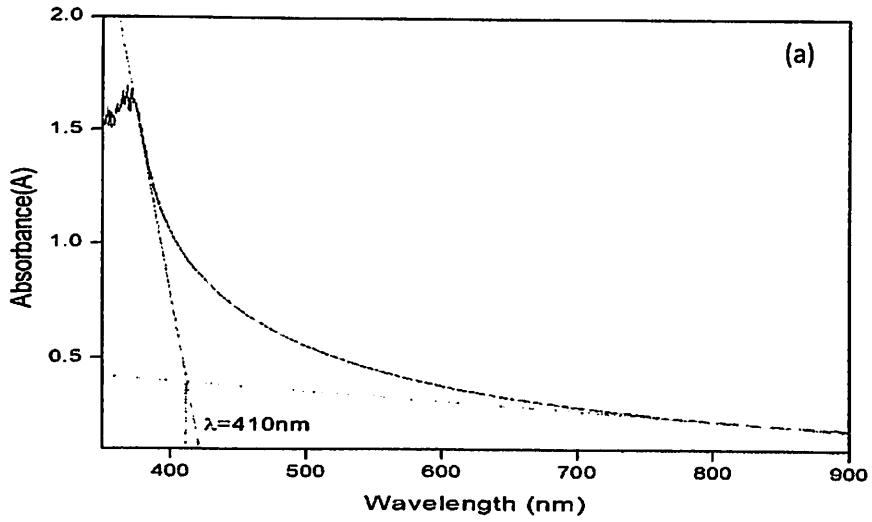

Figure 4.6: UV–vis absorption spectrum of ZnO nanoparticles (a) sample stored for 4 hours (b) sample stored for 12 hours (continue)

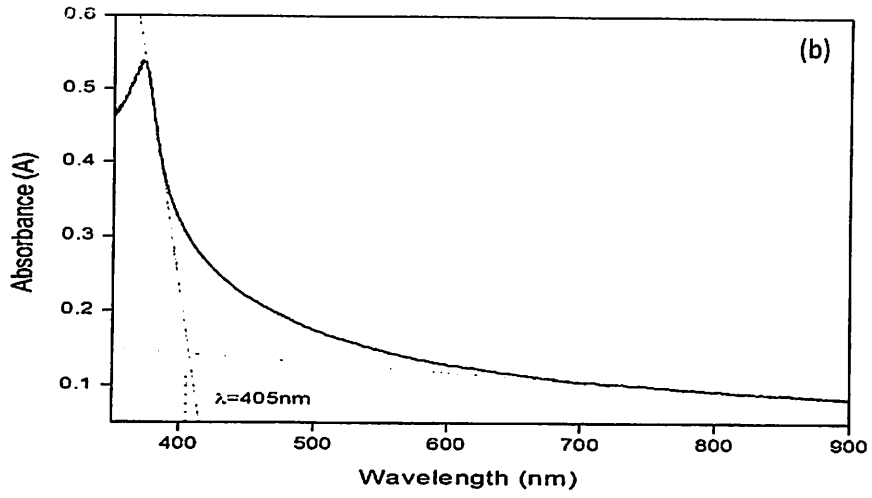

Figure 4.6: UV–vis absorption spectrum of ZnO nanoparticles (a) sample stored for 4 hours (b) sample stored for 12 hours

Extensive study from absorption, the transmittance analysis was performed. Figure 4.7 showed the optical transmission spectra of both ZnO nanoparticles stored at 4 and 12 hours was recorded as a function of wavelength in the range 350-900 nm. From the analysis, it was observed that the value of transmittance decreased from 90 % to 65 % as the storage time was increased. Both samples stored at 4 hours and 12 hours shows transmittance over 60 %. Sample stored for 4 hours showed higher transmittance with 90 %. The sharp decreased in intensity of transmitted light upon prolong the storage time was due to strong absorption at the band edge. The transmittance analysis was important as it measured the amount of light from the original beam passed through the ZnO nanoparticles. Higher transmittance in visible region indicated that ZnO nanoparticles for both sample had less defects and better crystallinity.

From this analysis, it showed that with prolong the storage time, the structural and optical properties of ZnO nanoparticles were improved gradually. The ideal storage time was suggested for 12 hours. The sample stored for 12 hours after calcined provided the optimum storage time as it showed the highest crystallinity, nearly uniform size and shape, and enhancement of E_g (3.06 eV) closer with the reported E_g (3.37 eV) [18] of ZnO nanoparticles. The result obtained from this analysis was used in first-principles calculation for the comparison purpose.

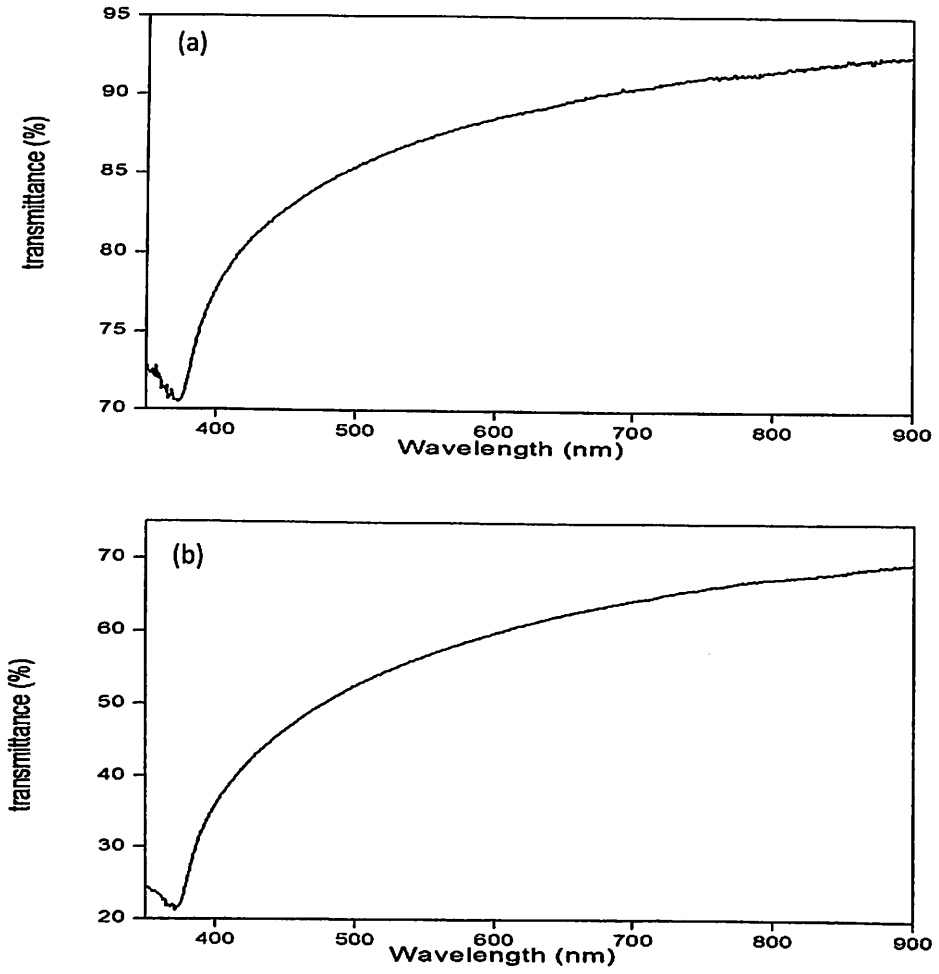

Figure 4.7: The transmission spectra of ZnO nanoparticles (a) stored for 4 hours (b) stored for 12 hours after calcinations

4.2 First-principles calculation of ZnO nanoparticles via CASTEP computer code

In this part, the main data from XRD analysis were used to calculate the electronic and optical properties. Prior to calculation, ZnO was modeled by its structure through geometrical optimization process. From the calculation, the result of electronic structure and optical properties was obtained and analyzed.

4.2.1 Structure modeling

Structure modeling was used to build the model made of compound that resembles ZnO hexagonal structure. To build a model of ZnO structure, Material Studio (MS) Visualizer was used by inserted data obtained from Rietveld-analysis. These data including lattice parameter, space group and atomic position of Zn and O (refer to Table 4.2). Usually, the type of view used for the crystal structure modeling was ball and stick type. The unit cell consist of 5 atoms are built and displayed in Figure 4.8.

The unit cell contains two Zn^{+2} ions were surrounded by an octahedron of three O^{-2} ions. The lattice parameters 'a' and 'c' obtained from the quantitative analysis were used (a = b = 3.2498 Å and c = 5.2068 Å) and inserted into the Cambridge Serial Total Energy Package (CASTEP) computer code. The Rietveld-refinement values were important in first-principles calculation as it provided the information regarding to the height, width and position of the ZnO atom which can be used to determine many aspects of the ZnO crystal structure. After the ZnO model was designed, the primitive cell of ZnO wurtzite-type structure which belongs to $P6_3mc$ space group was later used for structural optimization.

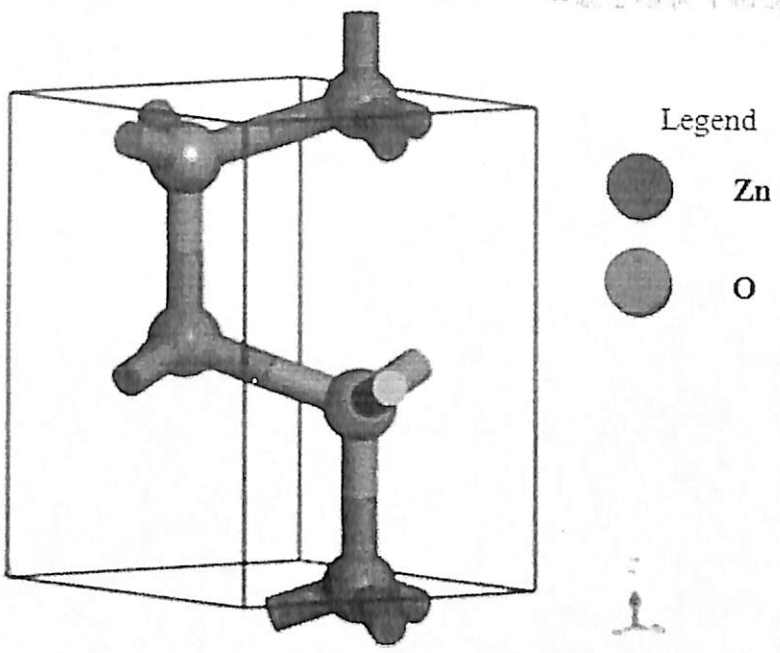

Figure 4.8: The unit cell of ZnO nanoparticles generated from the CASTEP computer code

4.2.2 Geometrical optimization and structural properties

The optimization of the ZnO unit cell was the first step in the calculation. Geometry optimization was performed after the ZnO unit cell was completely built using MS Visualizer. The many-body exchange and correlation effects were described by the LDA functional to calculate ZnO nanoparticles. Then, self-interaction correction by LDA + U approximation was implemented to provide more concise result.

Table 4.3 summarizes the optimized lattice constants and differences in volume, obtained through structural optimization. The relative deviation was calculated by used the experimental value obtained from Rietveld-analysis as a reference calculation. The accuracy of the lattice calculation and atomic position was very important because a

change of 1 % to 2 % in the lattice influenced the stability and structural calculations. The present result showed that LDA functional provided lower deviation which was less than 1 % and 'a' and 'c' value obtained was closed with the value from Rietveld-analysis.

Introducing U into the LDA methods resulted in increasing the lattice parameter which showed values far than experimental. It can be summarize that the lattice parameter (a and c) of ZnO nanoparticles increased substantially as LDA + U functional was adopted, resulting in an expansion of the volumes by 8.78 %. This was due to the fact that it was not possible to get a well balanced energy versus volume in the area of small volumes with localized *d* and *f* electrons. However, this was not a problem for the lattice parameter as for its determination only a few values around the minimum of the energy [60].

Table 4.3: Comparison of lattice constants and volume of ZnO by Rietveld-analysis obtained from XRD and first-principles calculation

Rietveld-analysis (This work)		Functional relative deviation (%)	
		LDA	LDA + U
a (Å)	3.2498	3.1862 **(-1.96)**	3.1460 **(-3.19)**
c (Å)	5.2068	5.1498 **(-1.02)**	5.0679 **(-2.68)**
V (10^6 pm^3)	47.6224	45.2771 **(-4.92)**	43.4402 **(-8.78)**

4.2.3 Electronic properties analysis: band gap by LDA functional

Figure 4.9 illustrated the calculated band structures of pure ZnO unit cell using LDA functional. The Fermi-level had been specified to zero. It can be seen that the bottom of the conduction band and top of the valence band were located at the same k-point (G), which was the representative characteristic for direct gap semiconductors. In the LDA functional theory, neglecting of excitation state during Kohn-Sham function's calculation results in lower energy levels above valence band in calculation energy band than that of experimental results, while, the energy levels below valence band in calculation were consistent with the experimental results. Thus, it showed that the E_g calculated based on LDA functional was lower than that in the experimental.

The calculated E_g of pure ZnO obtained using LDA functional was 0.795 eV, which in good agreement with Chowdhury et al. [52] and Yaakob et al. [5], but obviously lower than experimental values (3.06 eV). This was due to the limitation of the well-known shortcoming of the theory frame of LDA functional. Table 4.4 showed the calculated E_g using LDA functional in this work. Due to underestimation (E_g value smaller than experimental E_g) in the LDA functional, LDA + U method was applied in calculating the electronic properties as it defines the strongly correlated materials of *d* and *f* electron localization.

Table 4.4: The calculated band gap of ZnO nanoparticles using the LDA functional

U_d values for Zn 3*d*	U_p values for O 2*p*	Function	Band gap (eV)	References
0	0	LDA	0.794	[5]
0	0	LDA	0.795	This work

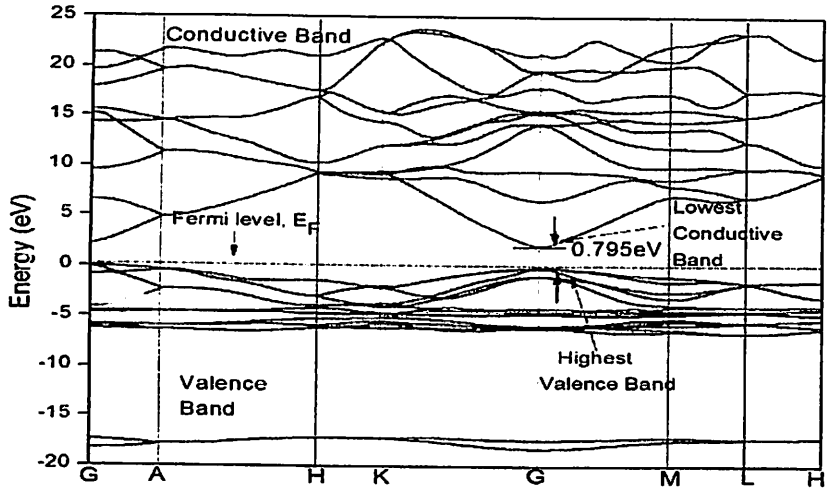

Figure 4.9: Calculated electronic band structure of ZnO nanoparticles using LDA functional with energy states for Zn 3*d* ($U_d = 0$) and O 2*p* ($U_p = 0$)

4.2.4 Electronic properties analysis: band gap by LDA + U functional

Hubbard-U was adopted in the calculation to correct the underestimation that occurred in LDA functional. This approximation was used to study the electronic E_g of pure ZnO. By adopted LDA + U functional, the Zn 3*d* band was shifted to the experimentally identified location. To obtain more accurate representation of the electronic structure of transition-metal oxides, the *p* orbital electrons of oxygen (U_p) also was

corrected due to underestimation in *d*-state of zinc lead to overestimation in *p*-state of oxygen. This can be solved by enhanced p-d coupling. The calculated E_g using LDA + U functional was depends on the energy state of ZnO nanoparticles. The recommended values to calculate the E_g of ZnO nanoparticles were U_d = 5-8 eV and O U_p = 7 eV [44].

To investigate the effect of U for Zn 3*d* and O 2*p* orbitals, several calculations with a range of U_d and U_p values was chosen, as shown in Table 4.5. The calculated E_g increase with the increasing U_d values from 7 eV to 10 eV when U_p values was fixed at 0 eV. However, the calculated E_g was still underestimated compared with the experimental values of 3.06 eV. As the O U_p was modified, the calculated E_g became closer with the experimental E_g. Ma et al. [61] suggested that for oxide materials the O U_p value of 7 eV was suitable for first-principles calculations. It showed that the calculated E_g were still comparable with the reported E_g (3.37 eV) [18] for bulk ZnO when O U_p was fixed at 7 eV. However, as the value of O U_p was rise to 8 eV, the calculated E_g was overestimation.

Figure 4.10 showed the corrected E_g obtained as the addition of the U values for *d* orbitals and U values for *p* orbitals. The corrected E_g can be obtained by the addition to the U values for *d* orbitals as well the U values for *p* orbitals. The electronic E_g using LDA + U functional was presented in Figure 4.11. In this work, the calculated E_g of ZnO nanoparticles with energy state Zn U_d= 5 eV and O U_p= 7 eV showed the most accurate result with 3.08 eV which comparable with the experimental band gap (3.06 eV).

The accuracy of the result obtained using LDA + U functional was due to the location of the Zn 3*d* band shifted toward lower energies and also the changed in the band dispersion. The modification for O 2*p* was also required as the addition of U_p can improve the total energies of systems [40]. Thus, E_g value which in good agreement with the experimental data corresponds to the location of the Zn 3*d* and O 2*p*, spin orbit coupling and crystal-field splitting energies, as well as the order of states at the topmost valence band, can be achieved. From this analysis, it showed that by adopted LDA + U function, the E_g obtained was closed to the experimental E_g.

Table 4.5: The calculated band gap of ZnO nanoparticles using LDA + U functional

U_d values for Zn 3*d*	U_p values for O 2*p*	Functional	Band gap (eV)
7	0	LDA + U	1.19
8	0	LDA + U	1.23
9	0	LDA + U	1.26
10	0	LDA + U	1.29
4	7	LDA + U	2.98
5	7	LDA + U	3.08
6	7	LDA + U	3.17
7	7	LDA + U	3.24
8	7	LDA + U	3.31
8	8	LDA + U	3.59

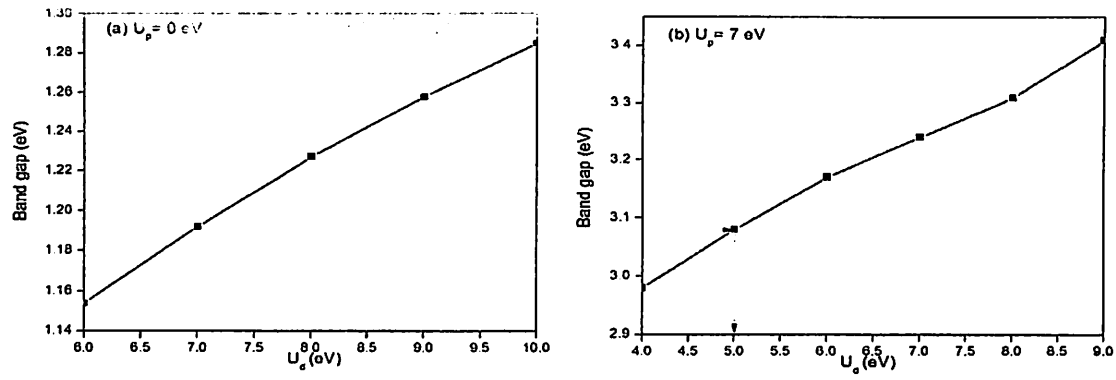

Figure 4.10: The band gap energies of ZnO nanoparticles (a) U_p was fixed as 0 eV and (b) U_p was fixed as 7 eV. The dashed arrows in (b) specify the U parameters corresponding to the experimental band gap

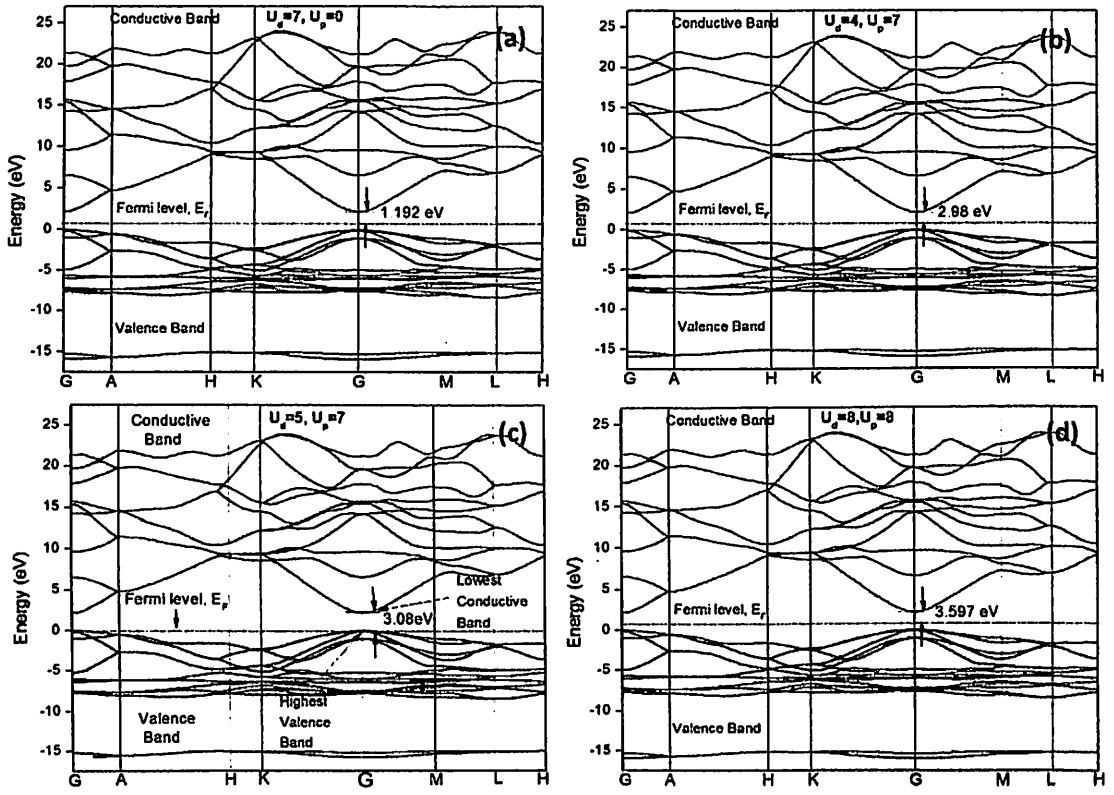

Figure 4.11: Electronic band structure using LDA + U functional with energy states (a) Zn U_d = 7 eV, O U_p = 0 eV (underestimate), (b) Zn U_d = 4 eV, O U_p = 7 eV (underestimate), (c) Zn U_d = 5 eV, O U_p = 7 eV (closed) and (d) Zn U_d = 8 eV, O U_p = 8 eV (overestimate)

4.2.5 Electronic properties analysis: density of states by LDA functional

Figure 4.12 showed the partial DOS (PDOS) and total DOS (TDOS) of pure ZnO nanoparticles using LDA functional. It should be noted that a sharp TDOS peak of ZnO appeared at -7 eV, which was mainly from O-2*s* state. The valence band can be divided into two regions which were from -20 eV to -10 eV and -10 eV to 0 eV. Meanwhile, the conduction band consist one region only.

The lower energy region from -20 eV to -10 eV comprised mainly O 2*s* and partially from Zn 3*d* and Zn 4*p*, meanwhile the upper region from -10 eV to 0 eV comprised mainly the O 2*p* and Zn 3*d* orbital. The conduction band of ZnO was dominated by the state of Zn 4*p*, Zn 4*s* as well as the state of O 2*p*. This indicated that a significant charge transfer was occurred from Zn 4*s* to O 2*p*. The overlapping between the Zn 3*d* and O 2*p* on the valence bands (Figure 4.10c) revealed the strong covalent bond between the first nearest neighbor Zn-O in pure ZnO nanoparticles.

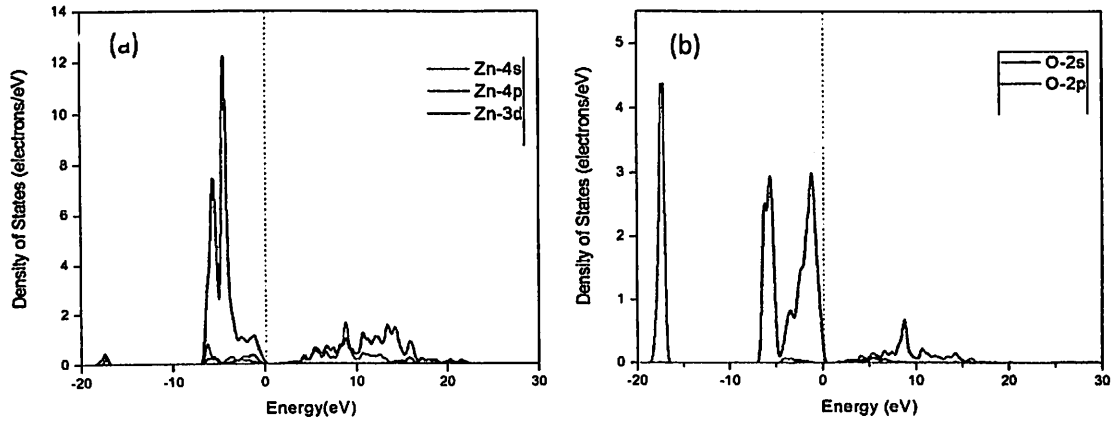

Figure 4.12: (a) PDOS of Zn (b) PDOS of O (c) PDOS of ZnO (d) TDOS of ZnO using LDA functional (continue)

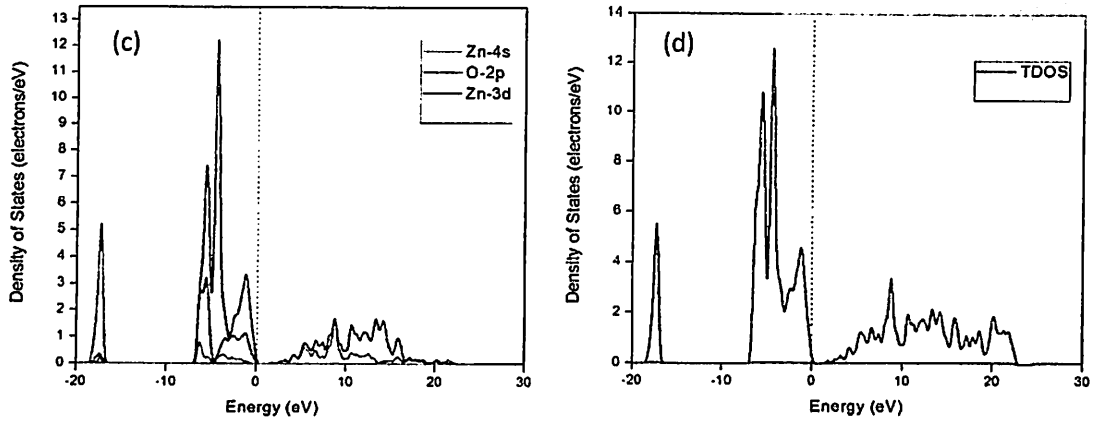

Figure 4.12: (a) PDOS of Zn (b) PDOS of O (c) PDOS of ZnO (d) TDOS of ZnO using LDA functional

4.2.6 Electronic properties analysis: density of states by LDA + U functional

The Zn 3*d* band obtained from the LDA calculations was relatively broader and located close to the top most valence band, which contradicts with the standard data. The large errors in calculated density of state were owing to strong coulomb correlations. This was due to relatively small ionic radii of oxygen and shorter Zn–O bond length, which results in strong interaction of the Zn 3*d* electrons with the valence band [40].

The discrepancy was removed using the LDA + U functional (Figure 4.13). By adopted LDA + U functional, the Zn 3*d* band of ZnO was located closer to the topmost valence band, thus increasing the influence of the coulomb correlation effects on the electronic structure. The Zn 3*d* band becomes more localized and shifted toward lower energies in agreement with experimental data.

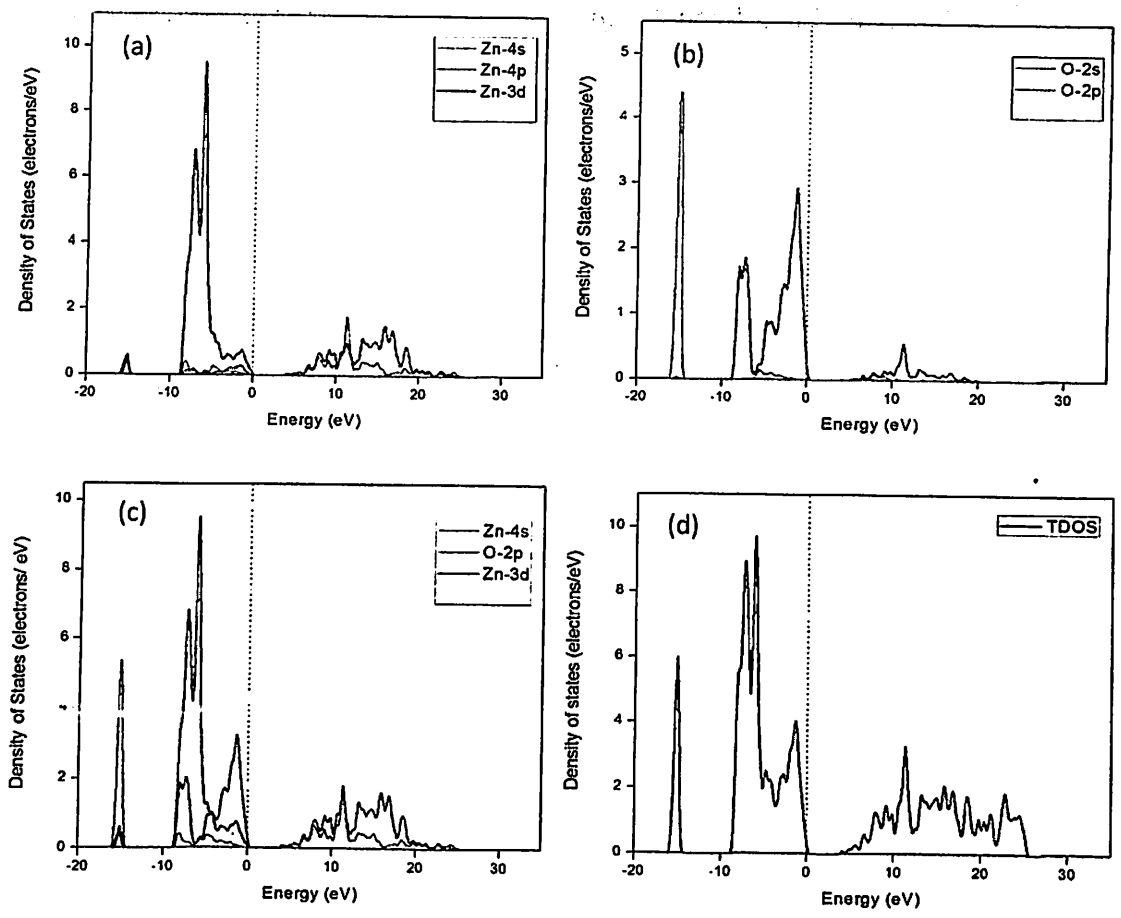

Figure 4.13: (a) PDOS of Zn (b) PDOS of O (c) PDOS of ZnO (d) TDOS of ZnO using LDA + U functional

From this analysis, it showed that the electronic band structure and DOS of ZnO nanoparticles were successfully calculated using LDA functional and corrected by Hubbard-U. This study revealed that the application of Hubbard-U significantly improved the calculation of ZnO nanoparticles electronic properties. The LDA + U functional was employed by modified the energy state of Zn $U_d = 5$ eV and O $U_p = 7$ eV exhibited the best calculated electronic E_g (3.08 eV) of ZnO nanoparticles closer with the experimental E_g (3.06 eV). For calculated electronic DOS, Hubbard-U enhanced the calculation of the

localization of Zn $3d$ and O $2p$ electron. As a result, the calculated data exhibited significantly good agreement with the experimental data.

4.2.4 Optical properties determination

The absorption spectrum of the pure ZnO nanoparticles using LDA + U functional was shown in Figure 4.14. It can be seen that the absorption region was quite wide ranged from 0 eV to 40 eV. The main absorption part still belongs to the ultraviolet (UV) region. The main peak value of absorption spectrum of pure ZnO was located at 17 eV (peak A), which correspond to the charge transfer from Zn $3d$ to O $2p$ orbits. The band gap energy estimated from graph absorption (cm^{-1}) versus energy (eV) was 3.08 eV, corresponding to the experimental band gap of 3.06 eV.

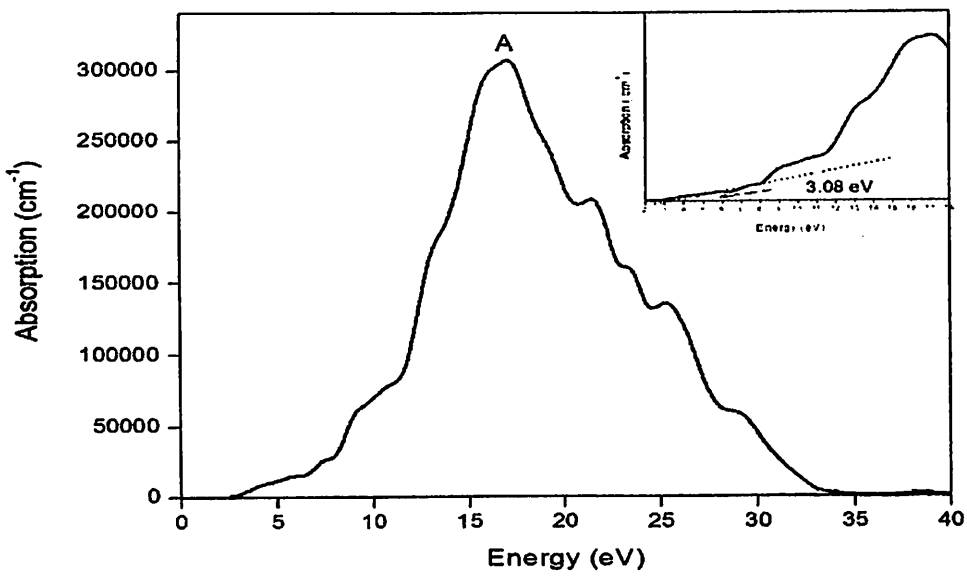

Figure 4.14: Absorption of pure ZnO nanoparticles using LDA + U functional

The optical dielectric functions of ZnO for real (ε_1) and imaginary (ε_2) parts were shown in Figure 4.15a. The dielectric function $\varepsilon(\omega) = \varepsilon_1(\omega) + i\varepsilon_2(\omega)$ can be used to describe the optical properties of a material. The three major peaks of A, B, and C were located approximately at 9, 14, and 16 eV of dielectric function, respectively which corresponded to three intrinsic plasma frequencies. The transition occurred in UV light region which ranged from 3.10 eV to 12.80 eV while no absorption was observed in visible region ranged from 2 eV to 3 eV.

These peaks were consistent with the peaks observed in the DOS calculation. According to the calculated DOS, the A peak at 9 eV originates from the electronic transition between the O 2*p* states in the upper valence band and the Zn 4*s* states in the lowest conduction band. The peak B at 14 eV was due to the transition between Zn 3*d* and O 2*p* states in the valence band. The transition between Zn 3*d* and O 2*s* states resulted in the weak peak C at 16 eV. The real part (ε_1) peaks originates at 2.5 eV while imaginary part (ε_2) was 0 eV.

The refractivity index, n versus energy (eV) graph was shown in Figure 4.15b. The graph described that the refractive index (n) and extinction coefficient (k) of ZnO nanoparticles were change with energy. When the energy was equal to zero, the static refractive index, n was 1.6 eV while, the static extinction, k is 0 eV. The refractive index can be explained based on the basic of the dielectric function. The interception coefficient of ZnO nanoparticles occurred at 16 eV (point A) and 20 eV (point B).

The optical reflectivity, R of ZnO nanoparticles calculated showed the main peak values at 17 eV (Figure 4.15c). The reflectivity peak value obtained indicated that ZnO nanoparticles within the ultraviolet (UV) region. Thus, this material was practical to be used for the optical devices. The reflectivity reduced abruptly at 12 eV and 26 eV, which was due to the peaks of the energy-loss spectrum (Figure 4.15d). The energy-loss function can be described as the energy loss of the electrons traversing the material. The maximum peak observed at 26 eV was related to the existence of plasma oscillations. The peaks of energy-loss spectra also correspond to the trailing edges in the reflection spectrum [51].

From this work, the optical properties of ZnO nanoparticles were successfully calculated using LDA + U functional. The calculated optical dielectric function of ZnO using LDA + U functional was consistent with the experimentally observed spectra. Besides, the absorption, refractive index, reflectivity and energy loss function calculated also comparable with experimental result. From these result, it showed that ZnO nanoparticle was able to utilize the ultraviolet light which make it usable for dye sensitize solar cell (DSCC) application. Overall, this result indicated that by employed LDA + U functional, the calculated electronic and optical properties of synthesized ZnO nanoparticles by sol-gel storage method posses a quality result and consistent with the results obtained from the experimental.

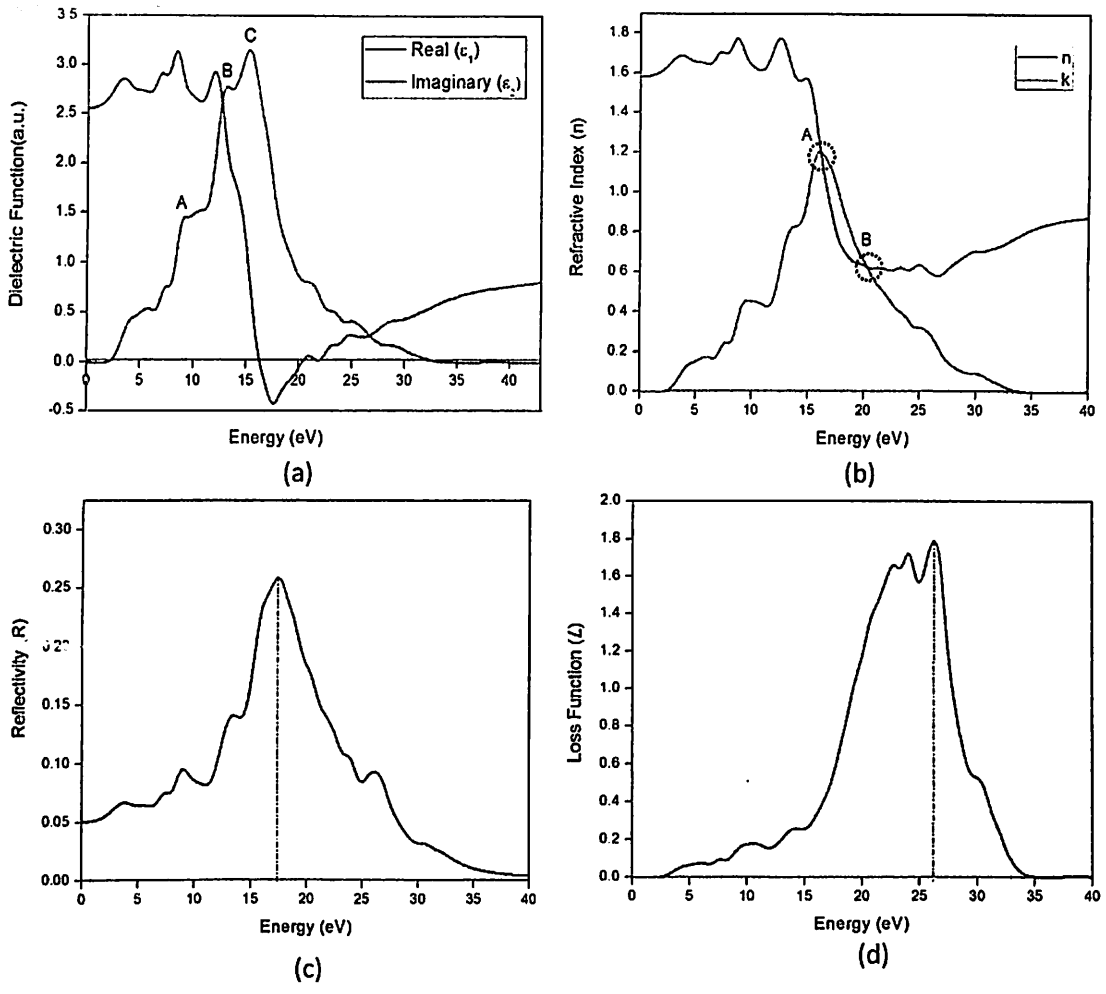

Figure 4.15: (a) Dielectric function, (b) refractivity index, (c) reflectivity, and energy-loss functions of pure ZnO nanoparticles using LDA + U functional

CHAPTER 5

CONCLUSION AND FUTURE WORK

5.0 Conclusion

ZnO nanoparticles were successfully synthesized using sol gel method using different storage time. The synthesized ZnO stored for 12 hours after calcination presented the best structural and optical properties of ZnO nanoparticles. Sample stored for 12 hours after calcined showed the optimum storage time as it provided the highest crystallinity, nearly uniform size and shape, and enhancement of the band gap (E_g) of 3.06 eV. This experimental E_g was used as comparison with E_g obtained from first-principles calculation.

The structural, electronic and optical properties of ZnO nanoparticles were successfully calculated using LDA functional and corrected by Hubbard-U. The calculated E_g using LDA functional was found to be only 0.795 eV, which still underestimate as compared with the experimental E_g. This discrepancy was successfully improved by adopted LDA + U functional.

LDA + U functional exhibited the best calculated electronic and optical properties of ZnO nanoparticles. By adopted LDA + U functional, the calculated E_g (3.08 eV) was comparable with the experimental E_g (3.06 eV) by modified the energy state of Zn $U_d = 5$ eV and O $U_p = 7$ eV. Thus, this study revealed that the application of Hubbard-U significantly improved the calculation of ZnO nanoparticles electronic and optical properties.

5.1 Recommendation for Future Works

For future study and research on the following areas, here are some suggestions as shown below:

i. The effect of pH and different calcinations temperature

   The formation and growth of ZnO nanoparticle can be affected by the different pH and calcinations temperature used

ii. The effects of different precursors used in the synthesized ZnO nanoparticles using sol-gel storage method

   Different precursors used influenced the growth mechanism toward the production of ZnO nanoparticles

iii. Study the first-principles calculations on doping ZnO nanoparticles

   The enhancement of the band gap for ZnO nanoparticles was required to make it suitable for dye sensitize solar cell application

References:

[1] G.-C. Yi, C. Wang, W.I. Park, ZnO nanorods: synthesis, characterization and applications, Semiconductor Science and Technology, 20 (2005), p.22.

[2] A. Arif, O. Belahssen, S. Gareh, S. Benramache, The calculation of band gap energy in zinc oxide films, Journal of Semiconductors, 36 (2015), p.013001.

[3] L. Franklin, C. Ekuma, G. Zhao, D. Bagayoko, Density functional theory description of electronic properties of wurtzite zinc oxide, Journal of Physics and Chemistry of Solids 74 (2013) pp.729-736.

[4] S.S. Alias, A.A. Mohamad, ZnO: Effect of Centrifugation and Storage on Sol–Gel Process, in: Synthesis of Zinc Oxide by Sol–Gel Method for Photoelectrochemical Cells, Springer 2014 pp.27-39

[5] M. Yaakob, N. Hussin, M. Taib, T. Kudin, O. Hassan, A. Ali, M. Yahya, First Principles LDA+ U Calculations for ZnO Materials, Integrated Ferroelectrics, 155 (2014) pp.15-22.

[6] C.-C. Hsiao, L.-S. Luo, A Rapid Process for Fabricating Gas Sensors, Sensors 14 (2014) pp.12219-12232.

[7] A. Kołodziejczak-Radzimska, T. Jesionowski, Zinc Oxide—From Synthesis to Application: A Review, Materials 7 (2014) pp.2833-2881.

[8] A. Moezzi, A.M. McDonagh, M.B. Cortie, Zinc oxide particles: Synthesis, properties and applications, Chemical Engineering Journal 185 (2012) pp.1-22.

[9] J. El Ghoul, M. Kraini, O. Lemine, L. El Mir, Sol–gel synthesis, structural, optical and magnetic properties of Co-doped ZnO nanoparticles, Journal of Materials Science: Materials in Electronics 26 (2015) pp.2614-2621.

[10] Z.-H. Wu, H.-Q. Xie, Y.-B. Zhai, Preparation and Thermoelectric Properties of Co-Doped ZnO Synthesized by Sol–Gel, Journal of Nanoscience and Nanotechnology 15 (2015) pp.3147-3150.

[11] V. Kumar, S. Kumari, P. Kumar, M. Kar, L. Kumar, Structural analysis by rietveld method and its correlation with optical propertis of nanocrystalline zinc oxide, Adv. Mater. Lett. 6 (2015) pp.139-157.

[12] L. Znaidi, Sol–gel-deposited ZnO thin films: A review, Materials Science and Engineering: B 174 (2010) pp.18-30.

[13] S. Talam, S.R. Karumuri, N. Gunnam, Synthesis, characterization, and spectroscopic properties of ZnO nanoparticles, ISRN Nanotechnology (2012) pp.1-6.

[14] M. Wilson, K. Kannangara, G. Smith, M. Simmons, B. Raguse, Nanotechnology: basic science and emerging technologies (2002) p.122

[15] S.S. Alias, A.B. Ismail, A.A. Mohamad, Effect of pH on ZnO nanoparticle properties synthesized by sol–gel centrifugation, Journal of Alloys and Compounds 499 (2010) pp.231-237.

[16] Y. Li, J. Xu, X. Li, X. Shen, A. Wang, Effect of aging time of ZnO sol on the structural and optical properties of ZnO thin films prepared by sol–gel method, Applied Surface Science 256 (2010) pp.4543-4547.

[17] A.K. Zak, M.E. Abrishami, W.H.A. Majid, R. Yousefi, S.M. Hosseini, Effects of annealing temperature on some structural and optical properties of ZnO nanoparticles prepared by a modified sol–gel combustion method, Ceramics International 37 (2011) pp.393-398.

[18] S. Dutta, B.N. Ganguly, Characterization of ZnO nanoparticles grown in presence of Folic acid template, Journal of nanobiotechnology 10 (2012) pp.1-10.

[19] H. Benhebal, M. Chaib, T. Salmon, J. Geens, A. Léonard, S.D. Lambert, M. Crine, B. Heinrichs, Photocatalytic degradation of phenol and benzoic acid using zinc oxide powders prepared by the sol–gel process, Alexandria Engineering Journal 52 (2013) pp.517-523.

[20] M. Ristić, S. Musić, M. Ivanda, S. Popović, Sol–gel synthesis and characterization of nanocrystalline ZnO powders, Journal of Alloys and Compounds 397 (2005) pp.1-4.

[21] A. Moharram, S. Mansour, M. Hussein, M. Rashad, Direct Precipitation and Characterization of ZnO Nanoparticles, Journal of Nanomaterials (2014) pp.1-5.

[22] S. Bagheri, C. KG, S.B.A. Hamid, Facile synthesis of nano-sized ZnO by direct precipitation method, Der Pharma Chemica 5 (2013) pp.265-270.

[23] H. Adly A., S. M.A.Mousa, M.A. Sherief, G. M.Elkomy, Sol – Gel Preparation, Characterization and Electrical Properties of Nanosized Gallium Doped Zinc - Oxide, Journal of American Science 10 (2010) pp.1-6.

[24] S.P. Ghosh, Synthesis and Characterization of Zinc Oxide Nanoparticles by Sol-Gel Process, National Institute of Technology, Rourkela, (2012) pp.1-27.

[25] A. Dumbrava, G. Prodan, A. Georgescu, F. Moscalu, Dependence of ZnO-based dye-sensitized solar cell characteristics on the layer deposition method, Bulletin of Materials Science 38 (2015) pp.65-72.

[26] R. Young, E. Prince, R. Sparks, Suggested guidelines for the publication of Rietveld analyses and pattern decomposition studies, Journal of Applied Crystallography 15 (1982) pp.357-359.

[27] B.H. Toby, R factors in Rietveld analysis: how good is good enough?, Powder diffraction 21 (2006) pp.67-70.

[28] V. Kumar, S. Kumari, P. Kumar, M. Kar, L. Kumar, Structural analysis by rietveld method and its correlation with optical propertis of nanocrystalline zinc oxide, Advanced materials letters 6 (2015) pp.139-147.

[29] J.U. Brehm, M. Winterer, H. Hahn, Synthesis and local structure of doped nanocrystalline zinc oxides, Journal of applied physics 100 (2006) p.064311.

[30] C. Omondi, T. Sakwa, Y. Ayodo, K. Khanna, Synthesis and characterization of ZnO nanoparticles, International journal of application or innovation in engineering and management 9 (2014) pp.57-62.

[31] R.Bhatt, M.Kar, Rashmi, Study of Growth and Characteristics of Pure and Doped Zinc Oxide, Journal of applied physics (2009) pp.1-4.

[32] S.S. Kumar, P. Venkateswarlu, V.R. Rao, G.N. Rao, Synthesis, characterization and optical properties of zinc oxide nanoparticles, International Nano Letters 3 (2013) pp.1-6.

[33] S. Kumar, F. Singh, A. Kapoor, Synthesis and Characterization of Nano-Crystalline ZnO Quantum Dots via Sol–Gel Route for Dye-Sensitized Solar Cells, International Journal of recent trends in electrical and electronic engineering (2014) pp.2231-6612.

[34] A.H. Yuwono, G. Ramahdita, N. Sofyan, The nanocrystallinity enhancement and optical characteristics of pre-hydrothermally treated ZnO nanoparticles, Advanced Materials Research 557 (2012) pp.468-471.

[35] X. Li, G. He, G. Xiao, H. Liu, M. Wang, Synthesis and morphology control of ZnO nanostructures in microemulsions, Journal of colloid and interface science 333 (2009) pp.465-473.

[36] R. Elilarassi, G. Chandrasekaran, Synthesis, structural and optical characterization of Ni-doped ZnO nanoparticles, Journal of Materials Science: Materials in Electronics 22 (2011) pp.751-756.

[37] G. Zheng, S. Clark, S. Brand, R. Abram, First-principles studies of the structural and electronic properties of poly-para-phenylene vinylene, Journal of Physics: Condensed Matter 16 (2004) p.8609.

[38] A. Kohan, G. Ceder, D. Morgan, C.G. Van de Walle, First-principles study of native point defects in ZnO, Physical Review B 61 (2000) p.15019.

[39] M. Segall, P.J. Lindan, M.a. Probert, C. Pickard, P. Hasnip, S. Clark, M. Payne, First-principles simulation: ideas, illustrations and the CASTEP code, Journal of Physics: Condensed Matter 14 (2002) p.2717.

[40] S.Z. Karazhanov, P. Ravindran, U. Grossner, A. Kjekshus, H. Fjellvåg, B. Svensson, Strong Coulomb correlation effects in ZnO, Solid state communications 139 (2006) pp.391-396.

[41] A. Liechtenstein, V. Anisimov, J. Zaanen, Density-functional theory and strong interactions: Orbital ordering in Mott-Hubbard insulators, Physical Review B 52 (1995) p.5467.

[42] G. Friesecke, F. Theil, Geometry optimization, Binding of molecules, Journal of nonlinear Science 12 (2010) pp.1-14.

[43] P. Briddon, Ab Initio Modelling Techniques Applied to Silicon, (1999).

[44] H.-C. Wu, Y.-C. Peng, C.-C. Chen, Effects of Ga concentration on electronic and optical properties of Ga-doped ZnO from first principles calculations, Optical Materials 35 (2013) pp.509-515.

[45] P. Erhart, K. Albe, A. Klein, First-principles study of intrinsic point defects in ZnO: Role of band structure, volume relaxation, and finite-size effects, Physical Review B 73 (2006) p.205203.

[46] S.J. Clark, M.D. Segall, C.J. Pickard, P.J. Hasnip, M.I. Probert, K. Refson, M.C. Payne, First principles methods using CASTEP, Zeitschrift für Kristallographie 220 (2005) pp.567-570.

[47] Z. Fu-Chun, Z. Zhi-Yong, Z. Wei-Hu, Y. Jun-Feng, Y. Jiang-Ni, First-principles calculation of electronic structure and optical properties of Sb-doped ZnO, Chinese Physics Letters 25 (2008) p.3735.

[48] Z.A. Tsegaye, Density Functional Theory Studies of Electronic and Optical Properties of ZnS Alloyed with Mn and Cr, Journal of apllied physics (2012) pp. 37-72.

[49] R. Godby, M. Schlüter, L. Sham, Trends in self-energy operators and their corresponding exchange-correlation potentials, Physical Review B 36 (1987) p.6497.

[50] H.-C. Wu, Y.-C. Peng, T.-P. Shen, Electronic and optical properties of substitutional and interstitial si-doped ZnO, Materials 5 (2012) pp.2088-2100.

[51] L. Li, W. Wang, H. Liu, X. Liu, Q. Song, S. Ren, First principles calculations of electronic band structure and optical properties of Cr-doped ZnO, The Journal of Physical Chemistry C 113 (2009) pp.8460-8464.

[52] R. Chowdhury, P. Rees, S. Adhikari, F. Scarpa, S. Wilks, Electronic structures of silicon doped ZnO, Physica B: Condensed Matter 405 (2010) pp.1980-1985.

[53] M.K. Yaakob, N.H. Hussin, M.F.M. Taib, T.I.T. Kudin, O.H. Hassan, A.M.M. Ali, M.Z.A. Yahya, First Principles LDA+U Calculations for ZnO Materials, Integrated Ferroelectrics 155 (2014) pp.15-22.

[54] Y.-S. Lee, Y.-C. Peng, J.-H. Lu, Y.-R. Zhu, H.-C. Wu, Electronic and optical properties of Ga-doped ZnO, Thin Solid Films 570 (2014) pp.464-470.

[55] L. Honglin, L. Yingbo, L. Jinzhu, Y. Ke, Experimental and first-principles studies of structural and optical properties of rare earth (Re,La,Er,Nd) doped ZnO, Journal of Alloys and Compounds 617 (2014) pp.102-107.

[56] W. Peng, Y. Zeng, C.-B. Zhang, Y.-H. Yan, W. Hu, First-principles study on La-doped ZnO used as transparent electrode for optoelectronic device, International Journal of Physical Sciences 7 (2012) pp.2174-2180.

[57] S. Saha, T. Sinha, A. Mookerjee, Electronic structure, chemical bonding, and optical properties of paraelectric BaTiO 3, Physical Review B 62 (2000) p.8828.

[58] N. Daneshvar, S. Aber, M.S. Dorraji, A. Khataee, M. Rasoulifard, Photocatalytic degradation of the insecticide diazinon in the presence of prepared nanocrystalline

APPENDICES

Appendix I

Determination of band gap (Eg) for ZnO nanoparticles from UV-Vis analysis

By take λ= 405 nm for sample stored 12 hours,

$$E = \frac{hc}{\lambda}$$

where E is energy of photon (J), λ is the wavelength of light (nm), c is the speed of light (3.0×10^8 m/s) and h is the Planck's constant (6.634×10^{-34} J-s).

$$E = \frac{(6.634 \times 10^{-34} \text{ J-s})(3.0 \times 10^8)}{405 \times 10^{-9} \text{ m}}$$

$$= 4.91 \times 10^{-19} \text{ J}$$

$$J = 6.24 \times 10^{18} \text{ eV}$$

$$E_g = (4.91 \times 10^{-19}) \times (6.24 \times 10^{18} \text{ eV})$$

$$= 3.06 \text{ eV}$$

Appendix II

Stoichiometric composition ratio of synthesized ZnO nanoparticles from EDX analysis

	Zn	O
Molecular weight (g mol^{-1})	65.39	15.99
Weight percentage (%)	84.24	15.76
Grams in 100 g sample	84.24	15.76
Moles in 100 g sample	84.24 / 65.39 = 1.29 mol	15.76 / 15.99 = 0.99 mol
Stoichiometric composition ratio	1.29 / 0.99 = 1.3	0.99 / 0.99 = 1
Simplest ratio	1	1

Stoichiometric composition ratio for Zn and O

Zn : O = 1 : 1

= ZnO

Appendix III

A. Example of Rietveld refinement report for ZnO nanoparticles sample stored for 12 hours after calcined at 600 °C

1. Global Parameters

Number of used phases:	1
Number of variables:	9
Number of constraints:	1
Zero shift/ °2Theta:	0.042(2)
Specimen displacement/ mm:	0.000000
Profile function:	Pseudo Voigt
Background:	Polynomial
R (expected)/ %:	9.93207
R (profile)/ %:	12.23475
R (weighted profile)/ %:	15.56702
GOF:	2.45658
d-statistic:	0.26761
U standard:	0.000000
V standard:	0.000000
W standard:	0.010000

2. Relevant parameters of Zinc Oxide

Structure and profile data:	
Formula sum:	$Zn_{2.00}O_{2.00}$
Formula mass/ g/mol:	162.7588
Density (calculated)/ g/cm^3:	5.6744
F(000):	76.0000
Weight fraction/ %:	100.000000
Space group (No.):	P 63 m c (186)
Lattice parameters	
a/ Å:	3.2498(2)
b/ Å:	3.2498(2)
c/ Å:	5.2068(3)
alpha/ °:	90
beta/ °:	90
gamma/ °:	120
V/ 10^6 pm^3 :	47.62239
Overall displacement parameter:	0.81(5)
Extinction:	0.000000
Flat Plate Absorption Correction:	0.000000
Porosity:	0.000000
Roughness:	0.000000
Fitting mode:	Structure Fit

U:	0.201642
V:	0.000000
W:	0.0208(7)
Pref. orientation direction/ hkl:	0.00 0.00 1.00
Pref. orientation parameter:	0.989000
Asymmetry parameter 1:	0.000000
Asymmetry parameter 2:	0.000000
Peak shape:	
parameter 1:	1.078365
parameter 2:	-0.002784
parameter 3:	0.000000
R (Bragg)/ %:	5.14240
Crystallite (rms) Strain/ %:	0.162
Crystallite Size/ Å:	848.4

Occupancy, atomic fract. coordinates and Biso for Zinc Oxide

Atom	Wyck.	s.o.f.	x	y	z	Biso/ 10^4 pm^2
ZN1	2b	1.000000	0.333333	0.666667	0.000000	0.543900
O1	2b	1.000000	0.333333	0.666667	0.375000	0.273700

Appendix IV

The calculated lattice parameter, volume and band gap using LDA + U functional

	LDA + U (This work)									
	$U_d = 0$, $U_p = 0$	$U_d = 7$, $U_p = 0$	$U_d = 8$, $U_p = 0$	$U_d = 9$, $U_p = 0$	$U_d = 10$, $U_p = 0$	$U_d = 4$, $U_p = 7$	$U_d = 5$, $U_p = 7$	$U_d = 6$, $U_p = 7$	$U_d = 8$, $U_p = 7$	$U_d = 8$, $U_p = 8$
a (Å)	3.186	3.188	3.189	3.191	3.193	3.144	3.146	3.147	3.159	3.145
c (Å)	5.149	5.141	5.142	5.143	5.144	5.068	5.068	5.072	5.083	5.064
V (10^6 pm^3)	45.277	45.249	45.309	45.356	45.407	43.396	43.440	43.489	43.944	43.387
E_g	0.795	1.192	1.227	1.258	1.285	2.980	3.08	3.171	3.310	3.597